Theoretical Modelling of Components of a Solar Thermal Power Plant for Performance Enhancement

Hassan Mahmood

PhD

July 2020

Theoretical Modelling of Components of a Solar Thermal Power Plant for Performance Enhancement

Hassan Mahmood

A thesis submitted in partial fulfilment
of the requirements of the
The University of Northumbria at Newcastle
for the degree of
Doctor of Philosophy

Research is undertaken in the
Faculty of Engineering and Environment

July 2020

Abstract

Solar power is a renewable energy source and can meet the growing world demand for electricity. The thermal energy produces by solar is an attractive solution to handle the environmental issues caused by fossil fuels. This research focuses on the theoretical modelling of components of solar thermal power plants for performance enhancement. It involves the modelling of the solar collector and organic Rankine power cycle. The overall solar thermal power plant comprises such components as a collector, evaporator, turbine, condenser, pump, heat exchanger, and thermal storage system. The present research studies the Linear Fresnel Reflector's performance in providing the heat input to the Organic Rankine Cycle and investigate the annual energy production of the power plant, located at the testing site in Almatret, Catalonia, Spain. The work includes step-by-step modification of the actual system design with a performance analysis of the non-concentrating and concentrating power plant systems.

The mathematical model of the ORC was developed based on the thermodynamic equations with simulations performed using MATLAB/Thermolib software. The ORC system performance was investigated for different working fluids at their critical operating conditions. The considered working fluids include the HCFC-245fa, HCFC-134a, Propane, butane, ethanol, and methanol. The ORC model was upgraded by taking into account the heat exchanger to recover the system waste heat, and results were compared to that from a simple ORC model. The recovery of the heat in the cycle increases the thermal efficiency of the ORC, but its benefits depend on the critical parameters of the working fluid. The effect is considerable for R134a and negligible for Ethanol. The Solar Organic Rankine Cycle (SORC) mathematical model was developed, and simulation designed on the MATLAB/Thermolib software. The evacuated tube collector designed for the Almatret latitude position and supplied the power input to the Rankine system. The model based on the water heat transfer fluid of the solar field, and it is transferring the heat to HCFC-134fa, the working fluid of the Rankine cycle via a heat exchanger without a tracking and thermal storage system. The thermal performance of the model investigated base on the day scan results. The solar organic Rankine cycle has an area 600 m^2 to generate peak thermal power 71 kW, and the mechanical output power of the Rankine cycle is 4.274 kW using 30 bar evaporation pressure and 10 bar condensation pressure. The

Generic Algorithm code developed on MATLAB and connected with the Thermolib model to operate the SORC system with optimum variables and thermal efficiency increases from 10.58 % to 11.87 % using the peak value solar irradiance. Fresnel solar reflector model simulated by using the light tools simulation software and have a one-axis tracking system. The actual weather data was imported to the simulation software to investigate the system performance using the day scan results. The theoretical model derived to determine the system thermal energy and conduction, convection, and radiation heat transfer of the receiver tube. The thermal losses of the model investigated and derived solar angles of the specific day. The tracking system based on the incidence angle modifier model (IAM) and calculated the system optical efficiency corresponds to the IAM in terms of the longitudinal and transverse components of the incidence of rays. The analysis performed from ambient conditions to determine the peak value by using the Therminol-62 working fluid. The LFR field produces 106.425 kW thermal energy during peak hour using a high value of IAM, and the reflector area is 214.38 m^2. The thermal losses during the peak time of day at 1:00 PM is 7.872 kW.

The system advisor simulation software used to validate the solar power linear Fresnel system. The complete model simulated with the thermal storage system. The actual weather data and Therminol-62 heat transfer fluid and NOVEC^{TM}649 working fluid import to the simulation model. The simulation model based on the exact power plant is located in the Almatret location and investigated the model thermal performance. The results show that the LFR field with a tracking system and Therminol-62 working fluid increases the system thermal performance. The Therminol-62 have high-temperature ranges at low operating pressure as compare to the steam working fluid. The ORC has a higher value of thermal efficiency NOVEC^{TM}649 than HCFC-134a and produces 7.2 kW output power of the ORC plant during the peak hour of solar irradiance with specific operating conditions. The two-tank thermal storage system extends the Plant four hours of operation and produces the highest power output of 2160 kWh in July.

Table of Contents

List of Figures

List of Tables

Acknowledgement

Thanks to Almighty Allah for his blessing and guidance, determination, and courage during the research work.

I am especially thankful to my supervisor, Professor Khamid Mahkamov, for his kind support, supervision, and guidance at every research study phase.

I am special thanks to my beloved mother for her continuous support and prayers. I am also missing my beloved farther for his continuous support, motivation, and determination during the academic journey. He has passed away. May Almighty Allah bless his soul. I am thankful to my brother and sisters for their support over the years of the study.

I would like to thank my beloved wife for her love, support, and care during the study journey. I have three kids and two born during the study period. I am again thankful to my wife for her continuous support and efforts since the beginning of the study.

Moreover, I would like to thank Dr Carolina Costa and Dr Khaled Hossin for their advice and support during this research.

Many thanks also should go to the colleagues, academic and technical staff at Northumbria University for support, cheerfulness, and encouragement.

Declaration

I declare that the work contained in this thesis has not submitted for any other award and that it is all my work. I also confirm that this work fully acknowledges opinions, ideas, and contributions from others' work.

Name: Hassan Mahmood

Signature:

Date: July 2020

Nomenclature

Symbols

A	Area, m^2
CDP	Conduction heat transfer rate, kW
CVE	Convection heat transfer rate, kW
C	Thermal capacity, kW
C_{loss}	Heat loss coefficient of the tank, $Wm^{-2}K^{-1}$
C_p	Specific heat, kJ $kg^{-1}K^{-1}$
Cr	Specific heat ratio
C_o, C_1, C_2, C_3, C_4	Constants of incidence angle modifier
D	Diameter, m
DHI	Diffuse horizontal irradiance, $W\text{-}m^{-2}$
DNI	direct normal irradiance, $W\text{-}m^{-2}$
F	Focal length, m
GHI	Global horizontal irradiance, $W\text{-}m^{-2}$
h	Enthalpy, $kJ\text{-}kg^{-1}$ or
H_{loss}	Heat losses rate of the tank, W
H_{min}	Minimum height, m
K	Thermal conductivity, $W\text{-}m^{-1}K^{-1}$
L	Length, m

N_p	Chromosome
N_v	Variables
P	Pressure, bar
P_{sr}	The perimeter of the secondary reflector, m
Q	Heat input/rejection rate, kW
R	Radius, m
S	Entropy, JK^{-1}
T	Temperature, K
U	Internal energy, J
UA	Overall heat transfer coefficient, W/m^2K
V	Volume, m^3
W	Width, m
X_{rate}	Selection rate
Z	Height, m
e	Eccentricity
g	Gravittational constant, $m\text{-}sec^{-2}$
h	Heat transfer coefficient, $W\text{-}m^{-2}K^{-1}$
$\dot{m}$	Mass flow rate, $g\text{-}sec^{-1}$
n	Number of days
t	Time, sec
v	Velocity, $m\text{-}sec^{-1}$

w_p	Pump work rate, kW
w_T	Turbine work rate, kW

Greek symbols

α	Solar azimuth angle, degree
α_s	Solar elevation angle, degree
$\alpha_{p,\,abs}$	Absorptance pipe
β	Evacuated Tube Collector absorptance
ϵ	Effectiveness
$\varepsilon_{p,\,abs}$	Emissivity pipe
e	The eccentricity of the earth's orbit
ϕ	Local latitude position angle, degree
θ_i	Incidence angle, degree
ϕ_L	Longitudinal angle, degree
ϕ_T	Transversal angle, degree
θ_z	Zenith angle, degree
σ	Stephan-Boltzmann constant, $W\text{-}m^{-2}K^{-4}$
ρ	Density, kgm^{-3}
δ	Solar declination angle, degree
τ	Transmittance
μ_h	Derates factor

Subscripts

Avg	Average
a, p	Actual pump
a, t	Actual turbine
C	Cold
CDP	Conduction
Des	Design
E, in	Evaporator in
F	Function
H	Hot
h1	Hot fluid inlet
h2	Hot fluid outlet
i	Inner
i, p	Isentropic pump
i, t	Isentropic turbine
L	Longitudinal
Max	Maximum
Min	Minimum
o	Outer
P	Pump
P, in	Pump in

Rc	Receiver
Rd	Radiation
Sc	Solar collector
Sr	Secondary reflector
T	Transversal
T_1	Inner temperature
T_2	Outer temperature
T, out	Turbine out
wf	Working fluid

Abbreviations

CSP	Concentrating solar power
CTC	Cylindrical Trough Collector
DHI	Diffuse horizontal irradiance
DNI	Direct normal irradiance
ETC	Evacuated Tube Collector
FPC	Flat Plate Collectors
GA	Generic Algorithm
Geo	Geothermal
GHI	Global horizontal radiation
GWP	Global Warming Potential
HFC	Heliostat Field Collector

HTF	Heat Transfer Fluid
IAM	Incidince angle modifier
LFR	Linear Fresnel Reflector
NTU	Number Transfer Units
ODP	Ozone Depletion Potential
ORC	Organic Rankine Cycle
PDC	Parabolic Dish Collector
PTC	Parabolic Trough Collector
R-ORC	Regenerative Organic Rankine Cycle
RPM	Revolution Per Minute
SAM	System Advisor Model
WHR	Waste Heat Recovery

Chapter 1: Introduction

1.1. Background

The world population currently is more than 7.7 billion. In 1803, the world population was one billion. It will reach a 10 billion level in 2055. During the 20th century, the people of the world grew from 1.65 billion to 6 billion. The current annual growth rate of the world population is 1.09 %. The annual increase in population is eighty-three million people [1]. China is the most populated country globally, with a population of 1.415 billion (18.5 % of the world population). India is the second most populated country in the world (17.7 % of the world population). The graphical world population growth rate is presented in Appendix A1 [1].

With the rise of the population, people consume more energy and resources. Energy supply plays a dominant role in modern society. There are two types of energy sources: renewable and non-renewable ones. Renewable energy is present in nature in the following forms:

- Sun
- Hydro
- Wind
- Geothermal
- Biomass
- Tidal

In general, almost all of the renewable energy is generated by the sun. Solar energy has a wide range of industrial and commercial applications. It is used to generate electricity, for desalination of water and heating purposes. The solar energy heating results in winds due to the temperature differences in the atmosphere. The sun drives evaporation and condensation of water, and its flow is partially used for hydroelectric power production.

At present, fossil fuels in the form of coal, oil, and gas provide most of the world's energy, but the share of renewable energy forms is growing rapidly.

These sectors include transports, industries, buildings, and non-combustible usage. Fig. 1.1 demonstrates the rise in primary energy demand by sectors, regions, and satisfaction by types of fuels and energies.

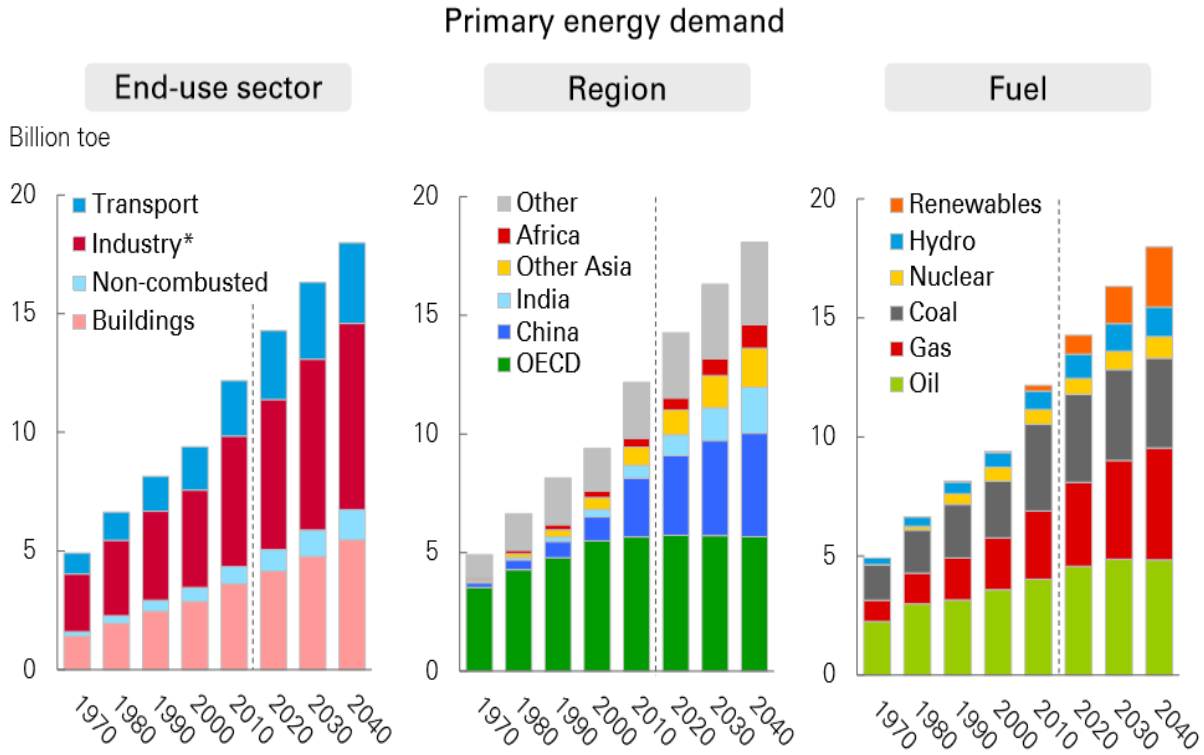

Figure 1.1 BP Energy Economics 2018 [2]

The major portion of the energy is consumed in industry and building sectors. In 2040, the demand of the world energy will increase threefold as compared to 1970. The populated regions have high energy demand, and it is growing rapidly. The coal, oil, and gas are the main fuels for producing power and driving the world economy. Renewable energy is the fastest-growing energy source [2].

Non-Renewable energy resources are fossil and nuclear fuels. Fossil fuels are the hydrocarbons as a major constituent is a carbon. Power is generated by the combustion of fossil fuels, resulting in carbon dioxide production in fuel combustion.

$$C + O_2 \rightarrow CO_2$$

The increasing concentration of carbon oxides in the atmosphere causes global warming, and the combustion of fossil fuels is the main reason for the significant increase in carbon emissions in the environment. It caused the generation of 2.2 gigatons of carbon emissions since 1960. Ten gigatons of carbon emissions were emitted in 2017. Fig. 1.2 shows the global carbon dioxide emissions growth per year due to the combustion of fossil fuels.

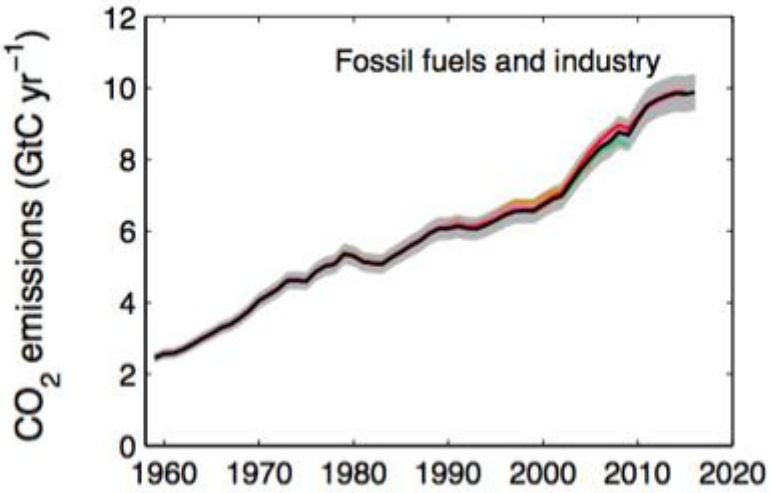

Figure 1.2 Global Carbon Budget 2017 [3]

The carbon dioxide emissions increased the global temperature and sea level, interconnected. It has been predicted that the earth temperature will rise by 1.5 ^{o}C in 2030. As a result, the sea level will increase by 0.1m. The problem is that the earth's temperature is on track to increase by 3 or 4 ^{o}C in 2100. It may cause to raise of the sea level by 0.9 m or more [4]. The relationship between global temperature change and the sea-level increase is presented in Appendices A2 and A3. One solution to prevent irreversible damage to the environment is to cut down carbon emissions and increase energy production using renewable sources. The present work is focused on the generation of power using solar thermal energy.

1.2 Problem Statement

Northumbria University is executing an EU funded project on developing a Small Organic Rankine Cycle (ORC) based solar thermal power plant. In this plant, an ORC turbine is coupled with the solar concentrator and thermal storage.

This research aims to develop a methodology for modelling and designing power plant with the Organic Rankine Cycle turbine, driven by thermal energy generated by the solar thermal collector. The simulation tool will include several modelling levels, including the component thermodynamic modelling of different complexities and modelling of the plant optical part and thermal storage.

The optimisation techniques will be employed to achieve the best plant efficiency. The mathematical model will be calibrated and improved using experimental data acquired from the operating plant over different seasons during the one year. The theoretical part includes developing mathematical models of components of the plant and their integration with an optimisation technique. The validity of the model is based on the System Advisor Model simulation.

1.3 Objectives

The objective of the research is to design a Solar Thermal Power Plant with enhanced performance. The main goal is divided into sub-objectives.

1. To create a mathematical model of the Organic Rankine Cycle (ORC) turbine. To model its operation using thermodynamic principles and calculate its performance. To test the model using different working fluids and various operating conditions.
2. To improve the ORC performance by using the optimised heat exchanger with the calculation of its effectiveness. The working fluid is HCFC-245fa.
3. To create a model of concentrating solar collector field. The collector includes the heater and is attached to the ORC through the intermediate heat exchanger for

transferring heat from the Solar field to the ORC. Such configuration is suitable for small power production and can be upgraded for a higher power production range. The model is realised as a simulation code, and the performance of the Solar Organic Rankine Cycle (SORC) is calculated using the thermodynamic approach and Genetic Algorithm (GA) optimisation to find the optimum values of the design variables.

4. To carry out optical simulations of a Linear Fresnel Collector to evaluate its optical and thermal performance at a specific latitude.
5. Validate the ORC plant with the LFR with actual dimensions and thermal storage in specific locations with the System Advisor Model, developed by the U.S. Department of Energy National Renewable Energy Laboratory.

1.4 Overall Description

The study is focussing on designing the SORC with enhanced performance. The proposed system will be suitable to produce electricity at different temperature ranges. The plant has two main components: the ORC and Solar Collector. The SORC works on using an organic working fluid vapour energy with elevated pressure and temperature for producing mechanical energy. The vapour is generated in the evaporator from the liquid state working fluid by using solar heat. These vapours are causing mechanical work in the turbine. The cooling process is condensing the vapour, and the pump pushes the liquid towards evaporator in a cyclic process.

The selection of the working fluid is essential to design the ORC. There are many working organic fluids available to be used in the Organic Rankine Cycle. The working fluids selection depends on the environmental protection issues, cost, and desired operating temperature ranges since working fluids are organic compounds with different boiling temperatures.

The ORC system is designed using its mathematical model in the MATLAB/Thermolib simulation tool. The model was used to test such fluids as HCFC-245fa, ethanol, Iso-pentane, n-propane, ethanol, HCFC-32, and HCFC-134a at their critical operating conditions. The thermodynamic model calculates the heat added to the system and work output using the energy and mass conservation equations. The results show that the thermal efficiency of the ORC depends on the working fluid selection and the output power of the ORC system depends on the mass flow rate of the working fluid.

The addition of the recovery heat exchanger improves the thermal efficiency of the ORC system. It is used to recover the heat by transferring between high-temperature and low-temperature fluid streams. The parametric analysis was performed to find the best-operating conditions of the system. The effectiveness of the heat exchanger is determined by using the NTU method using energy and mass balances. The results show that using the recovery heat exchanger noticeably improves the efficiency of the ORC.

The SORC plant has two working fluid circuits. The working fluid for the ORC is HCFC-245fa. It has a critical temperature of 154 ^{o}C and water is the heat transfer fluid circulated in the solar collector circuit inside its heating tubes. It has a critical temperature of 374 ^{0}C. The intermediate heat exchanger transfers the heat between HCFC-134a and water. The proposed area of the collector is 600 m^2. The solar collector is also equipped with thermal storage, and its function is to smoothen the influence of irregular solar radiation. If the incoming flow of the fluid is at a higher temperature, it accumulates heat. In the case of the lower temperature, the storage provides additional heating. The developed model was tested at the location of Almatret in Catalonia, Spain (latitude is 41.325^{o}).

During the research, a Linear Fresnel solar collector's design with a one-axis sun-tracking system was modelled using the actual data on its dimensions in Almatret. The surface of the collector is made Fresnel reflector mirrors. These mirrors are mounted in a parallel series. Each mirror has the same width and focal distance to concentrate the solar radiation on a linear receiver. The mirrors change their position with the movement of the sun. The receiver is a hollow tube which contains the heat transfer fluid. The collector simulation is performed using Light Tools software by utilising the database on solar radiation for the collector's actual location. The results from modelling the collector can calculate the exact amount of thermal power produced by the Fresnel field. The results were obtained for one of the days in July month.

The LFR model results were used in the ORC modelling with the SAM software. The actual weather data for the Almatret's position was used. The Therminol-62 thermal oil and NOVEC were considered as heat transfer fluid for the solar field and ORC, respectively. The parametric analysis was performed for the solar field, and the Genetic Algorithm approach was used to optimise the ORC system's design parameters.

1.5 Original Contribution to Knowledge

The research is focused on the generation of power by using solar energy. It deals with the detailed design of the Solar Power Organic Rankine Cycle (SORC) plant. One contribution to knowledge is testing the plant using different working fluids and investigating their properties on the plant's thermodynamic performance. Additionally, the influence of the recovery heat exchanger on the performance of the ORC is studied

There are results from many research works on learning the ORC powered by solar energy. This research considers a solar collector working in the temperature range of 80 – 280 ^{o}C to provide the heat input to the ORC. The developed mathematical model tests two types of solar collectors: Evacuated Tube Collectors (ETC) and Linear Fresnel Reflectors (LFR). Most of the research previously focused on using a single working fluid circulated in the solar collector and Organic Rankine Cycle. The developed SORC model considers two different heat transfer fluids, which was not investigated previously. The present work considers the case in which the heat transfer from the solar collector to Organic Rankine Cycle is carried out using the intermediate heat exchanger. It was demonstrated that it is feasible to generate power at low-temperature conditions using the Evacuated Tube Collectors for domestic or commercial purposes. The SORC modelling created in the simulation software environment was carried out using the accurate solar data database, which depends on the geographical location. The model was used to analyse the plant's performance over a wide range of operating conditions with different working fluids. The SORC model also investigated using the LFR at higher temperature applications and taking into account the sun-tracking system's operation during the daytime. The model was used to model the plant's process with Therminol-62 thermal oil and NOVEC^{TM}649 organic fluid as heat transfer fluids in the plant, which has not been investigated in the literature previously. The modelling also considers the thermal storage system as a part of the SORC plant to extend the plant operation up to four hours in poor solar irradiance.

The proposed mathematical model of the SORC plant is the novelty and contribution to knowledge in this special subject field.

1.6 Thesis Structure

The thesis is structured into seven chapters, which describe the state-of-the-art, scientific methodology deployed to solve problems and obtained results.

Chapter 1: Introduction

This chapter presents a brief description of the Solar Thermal Organic Rankine Cycle concept and problems that should be solved. Objectives of the research work and the results obtained are briefly described.

Chapter 2: Literature Review and Selection of Working Fluid

The relevant publications in the open literature are discussed, and essential results obtained previously on the Solar Organic Rankine Cycle's design analysis and selection of the working fluids are discussed. The study of the design of different Solar Organic Rankine Cycle plant components, such as an evaporator, condenser, solar collectors, pump, and heat exchanger, is conducted.

Chapter 3: Modelling of the Organic Rankine Cycle Plant

The mathematical modelling of the ORC with thermodynamic analysis is performed to calculate the performance of the system. The mass and energy balance equations are applied to individual components of the system. The ORC performance is improved by adding into the configuration a recovery heat exchanger. The impact of different working fluids on the thermal efficiency of the ORC is performed.

Chapter 4: Modelling of the Solar Organic Rankine Cycle (SORC) plant

The mathematical model includes the solar collector, used to supply the thermal input to the ORC. The SORC model uses HCFC-134a as a working fluid. The output power of the plant was calculated using the model. The database with climatic conditions at the specific location was used, and the system performance was investigated. The GA approach was implemented in modelling the power cycle. The turbine output power was used as the objective function to optimise the design variables and define the system optimum parameters.

Chapter 5: Modelling of the LFR Field

The mathematical modelling of the LFR field was conducted using the simulation software Light Tools. The model used the actual weather data and dimensions of the plant located at Almatret. The optical and thermal performance of the solar field was investigated during a particular day. The modelling produced results on the thermal performance of the solar field in terms of thermal power output. The Fresnel field has a one-axis sun-tracking system, and its operation was taken into account during the modelling process.

Chapter 6: Joint Modelling of the LFR and ORC system with thermal storage

The SAM was used to evaluate the solar field's thermal output and mechanical power produced by the Rankine cycle. The characteristics of the LFR field were used to model the ORC system in the actual plant location. The thermal storage was included in the modelling process.

Chapter 7: Conclusions & Recommendations

This chapter summarised all obtained results and findings, and future work recommendations were put forward.

Chapter 2: Literature Review

The Organic Rankine Cycle is one of the technologies used to generate power. The input heat supplied to the Rankine Cycle to evaporate the organic working fluid under controlled operating conditions. The input heat can be geothermal, industrial waste, biomass and solar energy, or different energy types. The organic fluids are hydrocarbons that have different ranges of boiling temperatures. The environmental regulations are the key aspect in the selection of the working fluid. In using solar energy, the ORC is coupled to a solar collector to generate the input heat and such the configuration is also known as the Solar Organic Rankine Cycle (SORC). For the SORC, the solar collector type selection depends on the type of working fluid and the amount of thermal energy necessary for the cycle evaporation process.

2.1 Configuration of the Organic Rankine Cycle

As highlighted above, the Organic Rankine Cycle (ORC) is a Rankine cycle which uses organic working fluids. The general process was suggested by William J.M. Rankine1859. He considered using steam and vapour of ether or alcohols in the cycle [5,6]. Takashisa et al. [7] considered the case with a low-grade heat source for running the ORC. A simulation model of the ORC was developed, and HCFC-123 was used as the working fluid. The ORC model contained four main components, which are the evaporator, turbine, condenser and pump. A heat exchanger was used to transfer the waste heat to the turbine's evaporator. E. Galloni et al. [8] carried out the experimental analysis of a mini ORC power plant that used the R245fa organic fluid. The system was investigated using both the thermodynamic and experimental setup. The proposed source temperature range was 75 – 95 ^{o}C. The maximum vapour pressure up to 10 bar was used with cooling liquid temperature between 20 and 30 ^{o}C. The results showed that the system output power was 1.2 kW, with a thermal efficiency of 9 %. W. Pu et al. [9] performed an experimental study on the ORC for the low-grade energy recovery. The HCFC-245fa and HFE7100 were used as the working fluid. The study considered the effects of the mass flow rate, evaporating pressure, and pressure drop on system performance. Gary et al. [10] proposed an ORC with the HFC-245fa working fluid. The HFC-245fa fluid has a high heat capacity. The heat exchanger deployed in the system improved the overall efficiency of

the cycle. It was suggested that the system could run on solar, geothermal, and waste industrial heat sources.

2.1.1 Temperature-Entropy Diagram

The T-S diagram visualises the cycle and heat transfer in the thermodynamic cycle. As part of the cycle, the evaporator is used for heat input, converting fluid into vapour and then it is condensed in the condense (heat rejection from the cycle) to form the liquid after the turbine expansion process (work produced). The fluids have different values of critical parameters. The T-S diagram for water as the working fluid in the cycle is shown in Fig. 2.1 below and includes the saturation line and a series of constant pressure lines (Pi). The saturation line's left side corresponds to the liquid state, and its right side represents the vapour state. The region below the critical point and limited by the saturation line is the liquid-vapour mixture region.

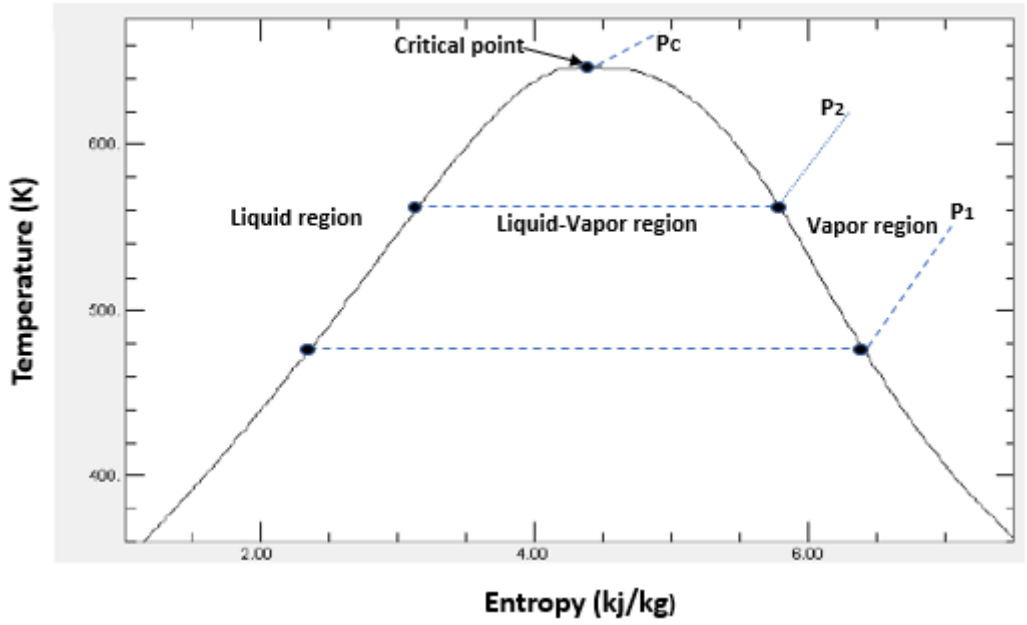

Figure 2.1 T-S Diagram for water using REFPROP 9.1 [11]

The Rankine Cycle is made of processes taking place in the boiler/evaporator, turbine, condenser, and pump. The heat is introduced into the evaporator working fluid, and the liquid is converted into vapour. The generated vapour expands in the turbine to produce the work.

The condenser is used to cool down the working fluid, exiting the turbine, and convert vapour into the liquid phase. The liquid is then circulating back to the evaporator by the pump. Fig. 2.2 shows the schematic diagram of the ideal ORC system and its thermodynamic cycle using a T-S diagram. The ORC operates on the saturated vapour (without superheating). Process 1 – 2 is the isentropic expansion in the turbine, and work ($W_{T, out}$) is produced by the turbine. The end of an expansion is determined by the temperature of the cooling liquid in the condenser. Process 2 – 3 is the isobaric condensation process, during which the heat $Q_{c, out}$ is rejected in the cycle. The working fluid is fully condensed to the liquid state. Process 3 – 4 is the adiabatic compression of the fluid. The pump increases the fluid pressure from that in the condenser to that in the boiler/evaporator and works $W_{p, in}$ is consumed by the pump. Process 4 – 1 involves the isobaric heat $Q_{E, in}$ addition to the system.

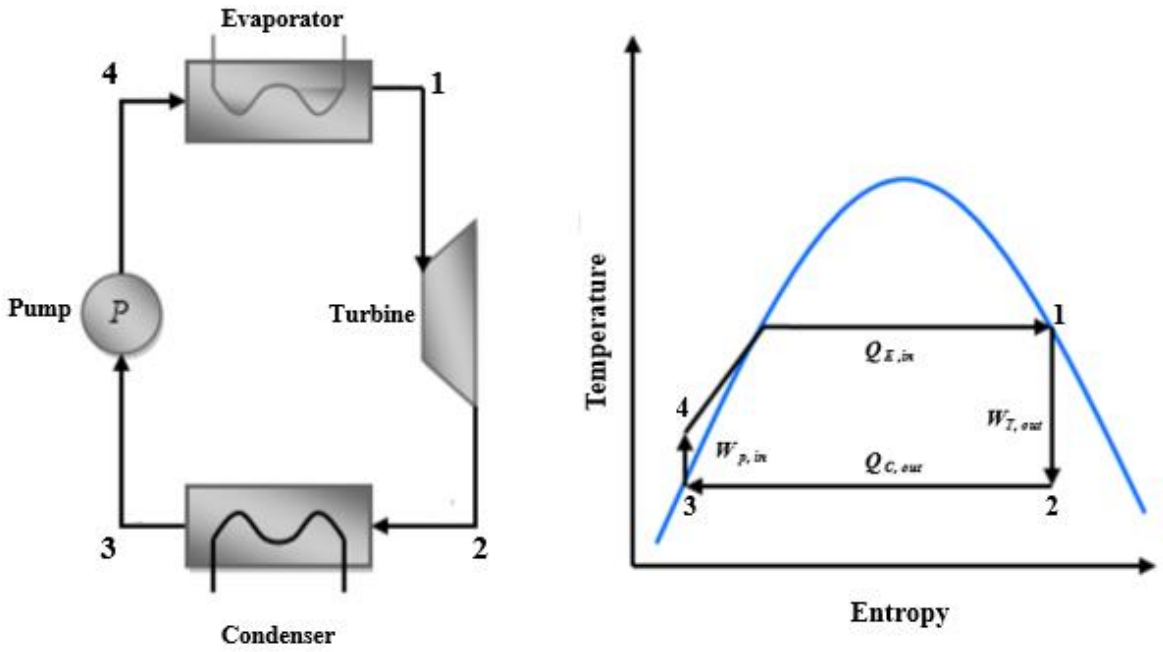

Figure 2.2 Schematic diagram and T-S diagram of the ideal Rankine Cycle [12]

2.1.2 Isentropic Efficiency of the Turbine (Expander)

J. Bhao et al. [13] investigated the selection of expanders for the ORC with different working fluids. The positive displacement devices, such as a scroll, screw, and rotatory expanders and rotary turbine expanders, were considered. O. Badr et al. [14] analysed the different expander types for use in the Rankine cycle and concluded that the positive displacement expanders

provide the higher output power than the turbine. The isentropic efficiency parameter is commonly used to characterise the expansion devices. It relates the actual work generated during the non-adiabatic expansion process to an ideal work generated in the adiabatic expansion process:

$$\boldsymbol{\eta = \frac{h_{in} - h_{out}}{h_{in} - h_{ideal}}}$$

Y. Chen et al. [15] investigated the power cycles used in the automobile industry and proposed the value of the isentropic efficiency of 70 %. M. Bianchi et al. [16] examined the ORC for converting industrial waste heat into electricity and determined its isentropic efficiency to be 75 %. P.J. Mago et al. [17] analysed the ORC system's thermal efficiency and chose its isentropic efficiency to be 80%. Z. Gu et al. [18] investigated the geothermal power generation system using working fluids HCFC-134a, HCFC-125 and propane and used the isentropic efficiency of 75 % for the turbine.

J. Bhao et al. [13] highlighted the following key characteristics of the turbine run using organic working fluids:

- The organic fluids have a higher value of the molar masses compared to water steam. To prevent pressure shock losses in the turbine, it is necessary to avoid the supersonic flow of vapour at the nozzle outlet.
- The turbine system is affected by several losses when the working fluid is used with the high expansion ratio and small enthalpy change over a specific temperature difference range.
- The small dimension of the turbine with reduced flow passage prevents the vapour losses at high densities and low specific volume.
- The turbine must have a compact size and prevent the working fluid escape from the closed cycle.

E. Sauret et al. [19] investigated the ORC system with radial inflow turbines for fluids with a higher value of the density. D. Fiaschi et al. [20] studied the radial flow ORC turbine system with different working fluid flow conditions and achieved the best value of isentropic efficiency of 0.85 when HCFC-134a was deployed. S. Kang [21] investigated the radial ORC

turbine system, which was composed of a two-stage expansion system with an isentropic efficiency of 0.80.

2.1.3 ORC Operating Conditions

H. Wang et al. [22] investigated the ORC with hydrofluoroether as the working fluid and found the cycle's thermodynamic efficiency to increase with the rise of pressure ratio in the cycle and temperature of the fluid in the inlet of the turbine. The very high rate of pressure change in the turbine increases the mechanical load on the system. If the working fluid's boiling temperature is higher compared to the heat input temperature, then the ORC system operation performance is very poor. Dai et al. [23] investigated the optimum parameters of the ORC and suggested reducing the working fluid temperature in the inlet of the turbine to its boiling point to maximise the output power. B. Saleh et al. [24] studied 31 working fluids used in the ORC system to determine thermal properties effect on thermal efficiency. The maximum evaporation pressure was 2.5 MPa, and the minimum condensation pressure was 0.1 MPa. They proposed the evaporator pressure limit of 20 bars. Quoilin et al. [25] found that the high vapour density corresponds to the lower condensing pressure of the ORC system, and low density relates to a high volumetric flow rate. As a result, there would be an increase in the pressure drop across the heat exchanger.

Drescher et al. [26] evaluated the different fluids used in a biomass plant with the ORC system. The selected fluid with a maximum evaporation pressure of 2.0 MPa and minimum condensation pressure of 0.05 MPa. Z. Gu et al. [18] showed that the increased value of the condensing pressure decreased the temperature difference in the cycle leading to the reduction of the thermal efficiency of the ORC. R. Rayegan et al. [27] investigated 117 working fluids, and some of these fluids are listed below in Table 2.1.

Table 2.1 Working fluids with practical pressure limits to be used in the ORC systems [27]

Working fluid	Maximum evaporation pressure P_{evp} (MPa)	Minimum condensation pressure P_{cond} (Kpa)
Acetone	3.4	30.7
Benzene	4.07	12.7
Butane	3.02	234.7
Butene	2.81	297.2
C_4F_{10}	2.06	268.3
C_5F_{12}	1.8	84.7
Cis-butene	3.1	213.7
E-134	2.8	212.8
R218	1.9	867.5
R245fa	2.82	149.1
R-413A	1.84	720.2

E. Cayer et al. [28] conducted a parametric analysis of the ORC system and selected its optimum parameters using the Genetic Algorithm approach. They observed an increase in the power cycle's specific work and thermal efficiency with the rise in heat source temperature. T. C. Hung et al. [29] evaluated the ORC system with the fixed evaporator pressure for low-temperature heat source recovery. The efficiency of the cycle increases with an increase of the heat source temperature for wet organic fluids. For a dry fluid decrease in the condenser,

temperature corresponds to the system pressure ratio rise. As a result, the thermal efficiency of the cycle increases.

Pasetti et al. [30] evaluated the fluids' thermal stability for use in the ORC and observed that the organic fluids become unstable at a higher temperature with decomposition into lighter products. The results in a decrease in the thermal performance of the power unit. U. Drescher et al. [31] conducted the fluid selection for the ORC system in biomass plant and proposed some fluids that are stable up to 600 K. Invernizzi et al. [32] studied the thermal stability of the fluids of the ORC system and recommended to use HCFC-245fa, HCFC-134a, siloxanes, and cyclopentane at temperatures up to 300 ^{o}C.

2.2 Regenerative Organic Rankine Cycle (R-ORC)

A number of authors have studied the recovery heat exchangers impact on the ORC systems performance (Regenerative ORC or R-ORC). The R-ORC system has the heat exchanger used to recover the working fluid's heat energy and preheat the fluid flowing to the evaporator to reduce the heat input into the cycle. F. Heberle et al. [33] investigated the regenerative ORC system to minimise heat input in the evaporator and evaluated the performance of the regenerative ORC using the cost optimisation method, and obtained the efficiency of the system between 14.1 and 18.9 % when the overall recovery heat exchanger area was between 446 and 1079 m^2. Fig. 2.3 shows the schematic diagram of the regenerative ORC system.

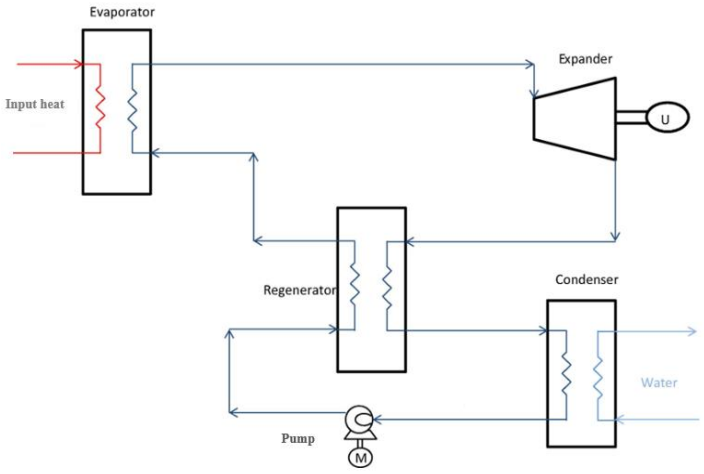

Figure 2.3 Configuration of the R-ORC system [34]

E. Spayde et al. [34] compared the ORC and R-ORC system with a solar energy source. The system performance results in terms of the electric power demonstrate that the R-ORC system achieves noticeably higher thermal efficiency. Xi. Huan et al. [35] performed the parametric analysis of an R-ORC power system. GA optimisation was implemented to define the optimum parameters of the system. The results show that the R-ORC system attains better performance as compared to the basic ORC model. J. Enslin [36] demonstrated that the regenerative heat exchanger increased the efficiency of the ORC for recovering the waste heat energy. A. Mahmoudi et al. [37] also studied the ORC with heat recovery heat exchanger in different design configurations. They observed the performance improvement with the use of regeneration of the heat in the cycle. G. Pikra et al. [38] demonstrated better performance in single and double stage regenerative ORC systems than the conventional ORC plant. Therminol thermal oil was used as a heat transfer fluid.

Peris et al. [39] studied the combined heat and power characteristics of the ORC using the experimental results. The natural gas boiler and thermal oil were used to supply the system with thermal power at about 165 ^{o}C. Under steady conditions, the condenser temperature was between 30 ^{o}C to 70 ^{o}C. The net output power of the ORC was 5.60 kW, with an electrical efficiency being 8.80%. Wang et al.[40] investigated the non-regenerative solar power ORC. The power system's experimental test was performed for a low-temperature application using the HCFC-245fa working fluid with a rolling piston expander. The system's thermal efficiency of the system was 4.2 % and 3.2 % with evacuated and flat plate solar collectors. L. Li et al.[41] performed the experimental test of the low-grade heat recovery ORC using the HCFC-245fa working fluid. The power generation in the cycle was 5.405 kW at the condensation temperature of 23 ^{o}C and with a pressure ratio of 7.3 in the turboexpander. Eunko al. [42] experimentally tested the non-regenerative ORC system with multiple expanders arranged in parallel using the HCFC-245fa working fluid. The turbine's peak output power was 3.4 kW at the pressure ratio of 6.5 and with the thermal efficiency of 7.5%, subject to the amount of the waste heat supplied. Quoilin et al. [43] experimentally investigated the non-regenerative scroll expander ORC using the HCFC-123 working fluid. The ORC generated a 1.8-kW output power with a thermal efficiency of 9.9 % with the heat source temperature of 165 ^{o}C. Navarro et al.[44] experimentally tested the regenerative ORC with the HFO-1336mzz-Z working fluid for low-temperature applications. The heat input to the system was in the temperature range

between 140 ^{o}C to 160 ^{o}C, and the condensation temperature range was between 25 ^{o}C to 40 ^{o}C. The cycle power output is 1.1 kW, and electrical efficiency ranged from 5.5% to 8.3%. Eyerer et al. [45] conducted the experimental comparison of the HCFC-245fa and HCFC-1233zd-E working flids using the non-regenerative ORC. The results showed that thermal efficiency was increased by 6.92 % when using HCFC-1233zd-E compared to HCFC-245fa. The gross output power with HCFC-245fa was 12.17 % higher compared to HCFC-1233zd-E. Bianchi et al.[46] performed experimental analysis of a small ORC power system for low-grade heat recovery applications. The system produced the maximum output power of 1.2 kW with a gross efficiency of 4.4 %. Muhammad et al. [47] experimentally tested the non-regenerative 1-kW ORC. The system was designed for low-grade waste steam with pressure in the range between 1 and 3 bar. The ORC produced 1.016 kW of power with a thermal efficiency of 4.66 % when using the HCFC-245fa working fluid. Table 2.2 shows a comparison of thermal performance of the ORC and R-ORC systems described in the literature.

Table 2.2 Thermal performance of the ORC and R-ORC systems described in the literature

Configuration	**Fluid**	**Heat source temperature °C**	**Power kW**	**Efficiency**	**Author**
Regenerative	R245fa	165°	7.5	8.8%	Peris et al. [37]
Nonregenerative	R245fa	115°	1.73	4.2%	Wang et al. [38]
Nonregenerative	R245fa/ HFE7100	100°	1.979	4.01%	Pu et al [39]
Nonregenerative	R245fa	120°	3.5	7.5%	Yun et al. [40]
Nonregenerative	R123	165°	1.8	9.9%	Quoilin et al. [41]
Regenerative	HFO-1336mzz-Z	160°	1.1	8.3%	Navarro et al. [42]
Nonregenerative	R123	130°	0.4	4.98%	Eyerer et al. [43]
Regenerative	R123	130°	6	7.98%	Li et al. [44]
Nonregenerative	R245fa	135°	1.01	5.75%	Muhammad et al. [45]

2.3 ORC Market Analysis

The ORC market has been rapidly growing since 1980. There are many manufacturers producing ORC products for a wide range of commercial applications. Three suppliers of the ORC technology are leading in terms of the installed units and power capacity. The Turboden company is the primary manufacture of the ORC technology and provided 45% of the installed ORC units with 8.6 % of the world's total cumulative power. The ORMAT group supplied 24 % of installed units and provided 86 % of the world's total cumulate power capacity. The Maxxtec has installed 23% of ORC units and generating 3.4 % of the total cumulative power capacity. Table 2.3 shows the list of the main manufacturers of ORC technology in the world. The main application areas include power generation using geothermal (Geo) energy, waste heat recovery (WHR), biomass and solar energy sources.

Table 2.3 The ORC market analysis [48 – 52]

Manufacturer	Heat source temperature [°C]	Applications	Power range [kWe]
ORMAT, US	150–300	Geo, WHR, solar	200–70,000
Turboden, Italy	100–300	Biomass, Solar, WHR, Geo.	200–2000
Maxxtec, Germany	300	Biomass	315–1600
Opcon, Sweden	<120	WHR	350–800
GMK, Germany	120–350	Geo., Biomass, Solar	50–5000
Bosch KWK, Germany	120–150	WHR	65–325
Turboden Pure Cycle, US	280	WHR, Geo.	91–149
GE Clean Cycle	120	WHR	125
Tri-o-gen, Netherlands	350	WHR	160
Electratherm, US	92	WHR, Solar	50

2.4 Selection of the Working Fluid

Bianchi et al. [53] described the different ORC systems for low-temperature energy conversion plants. As described previously, the main components of the SORC system are the Solar Collector and Organic Rankine Cycle. As part of the Solar Thermal Organic Rankine Cycle's designing process, the Organic Rankine performance is evaluated. The ORC systems are used for power generation from waste heat and a low or medium temperature heat sources such as solar, biomass or geothermal [54]. The fluid selection for the regenerative ORC system was conducted by many authors [55-57]. Raegan et al. [58] investigated 117 organic fluids, which differ in molecular weight and thermo-physical properties (shown in the temperature-entropy diagrams). They analysed the effect of fluid's properties on the net power generated, thermal efficiency, exergy efficiency, and vapour expansion ratio. The results show that the ORC performance strongly depends on the fluid selection and use of the regenerative heat exchanger to reduce the solar ORC irreversibility losses. Several similar studies were conducted on the ORC systems, which used different working fluids [59-61]. Edwin et al. [61] analysed the organic Rankine cycle (ORC) with five various working fluids: HCFC-11, HCFC-12, HCFC-717, benzene and HCFC-113. These fluids have the boiling range between 33.35℃ to 79.85℃. The results show that the higher system thermal efficiency was obtained using HCFC-11 and HCFC-113 working fluids compared to other working fluids. Ferrara et al. [56] compared the cycle with different working fluids for the ORC system with a power of 20 kW. Saleh et al. [57] considered the ORC's operation with working fluids at the subcritical and supercritical values. Lakew et al. [62] analysed the different working fluid's effect on an ORC system's thermal efficiency at the temperature range of 80 – 160 ^{o}C. Drescher et al. [63] carried out the different fluid selection in biomass and heat recovery plants.

Shengjun et al. [64] studied the parametric optimisation of the ORC with the low-temperature source and suggested THAT the fluids HCFC-600a, HCFC-245fa, HCFC-245ca, and HCFC-123 provide the best thermal efficiency. HCFC-41, HCFC-125, and HCFC-218 have good heat recovering ability from a given source of heat, and the lowest heat exchanger area required is when the fluids HCFC-134a, HCFC-152a, HCFC-143a, and HCFC-600 are used. The fluids HCFC-600, HCFC-152a, HCFC-143a, HCFC-600a, HCFC-134a, HCFC-125, and HCFC-41, provide excellent performance at acceptable Levelized cost for considered operating

conditions. A. Lakew et al. [65] also evaluated the working fluid impact on the ORC system performance for the low input temperature source. The analysis was performed for the HCFC-134a, HCFC-123, HCFC-290, HCFC-245fa, HCFC-227ea, and n-pentane working fluids, and it was suggested that the n-pentane ensures the maximum power output at the minimum heat exchanger area. Y. Dai et al. [66] performed parametric optimisation of the ORC system for ten working fluids. The study shows that HCFC236EA provided the highest thermal efficiency for the given operational conditions. Zhang et al. [67] stated that the ORC system with hydrocarbon working fluids generates higher power output as compared to refrigerants.

2.4.1 Classification of Working Fluids

Several authors worked on the classification of the working fluids for the ORC system [65], [68], [69]. The selection of the working fluids depends on the operational temperature range of the system. The efficiency of the system depends upon the entropy drop of the fluid between hot and cold reservoirs. Organic fluids have different properties than water. Bao et al. [13] classified the working fluid as a dry, wet, or isentropic. This classification based on the temperature-entropy diagram curves. Fig. 2.4 shows examples of the curve on the T-S diagram. There are three types of saturation curves. The dry fluids have a positive slope and have $ds/dT > 0$. The wet fluids have a negative slope, which corresponds to $ds/dT < 0$. The isentropic fluids have a zero slope and $ds/dT = 0$.

The dry and isentropic fluids are appropriate for use in the ORC system. In the wet fluids, droplets form during the expansion process, negatively affecting the turbine performance and increasing the system cost. Hung et al. [69] state that the isentropic fluids theoretically provide higher efficiency as compared to other fluids. Bhao et al. [13] highlight that the condensation of wet fluids during the expansion process damage the turbine blades. Dai et al. [66] highlighted the importance of using the superheat cycles to avoid the condensation of the wet fluids. Bhao et al. [13] investigated the dry fluids that positively affect increasing efficiency since the superheat vapour at the turbine outlet eliminates droplets formation. Hung et al. [69] analysed the increase in entropy for dry, wet, and isentropic fluids during the expansion process and suggested that the wet fluids should be used in the non-regenerative ORC systems.

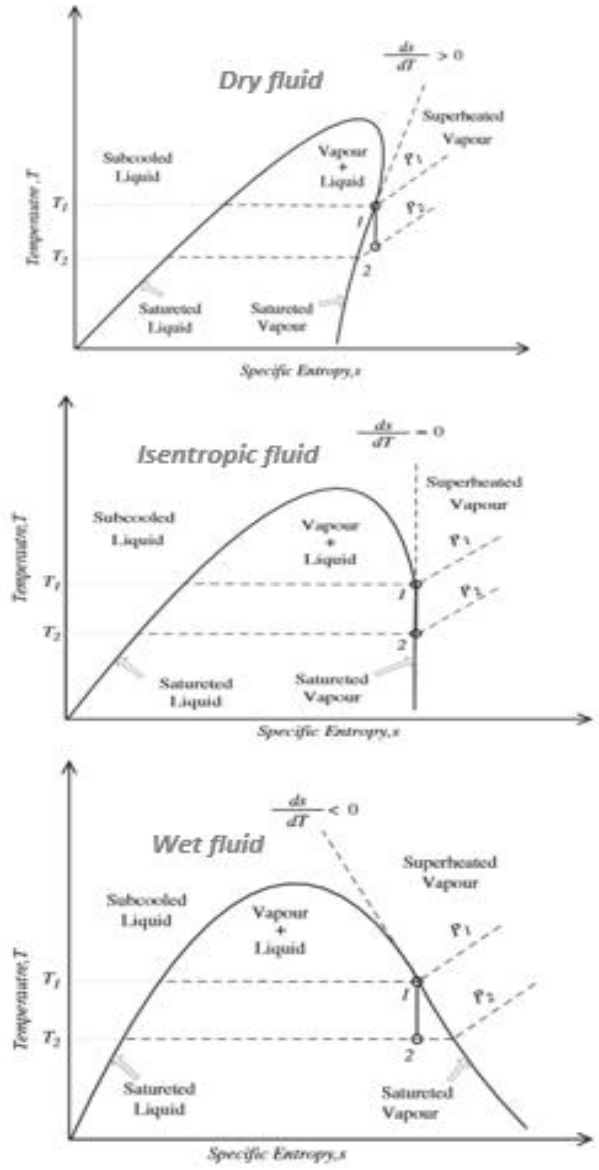

Figure 2.4 T-S Diagram for Working Fluids Classifications [24]

2.4.2 Thermophysical properties of organic fluids

Thermophysical characteristics of organic fluids have a high impact on ORC design and its performance. Saleh et al. [24] noted that the volumetric expansion of the organic fluids is lower as compared to water. As a result, the cheaper expander is suitable in the ORC system with organic fluids, which lowers the system cost. The high latent heat of the working fluid vaporisation leads to an increase in the required energy input in the evaporator, and the authors

suggested that the fluids with low latent heat are more economically suitable. L. Larjola et al. [70] noted that the lower latent heat of the fluid's vaporisation results in a higher temperature difference, lower irreversibility, and higher thermal performance of the ORC system.

Baik et al. [71] highlighted that the low densities of the organic fluids result in the required higher volumetric flows, and it increases the pressure losses in the system and leads to an increase in the size of the turbine. Chen et al. [72] stressed that higher densities of fluids make it possible to have a more compact design of the power unit. A. Papadopoulos et al. [73] noted that the working fluid's low specific heat reduces the pump work and improves the power cycle performance. However, B. Gozdur et al. [74] investigated the ORC system's pumping work and could not confirm the Papadopoulos conclusions.

S. Subbiah [75] conducted the thermodynamic analysis of the binary fluid mixture for the Rankine cycle and concluded that the organic fluids with higher critical temperatures and lower condensing pressures lead to plant components' higher costs. F. Yang et al. [76] pointed out that the condensation pressure lower than atmospheric pressure leads to a risk of fluid leakage. Hung et al. [22] noted that the thermal efficiency of the ORC increases with the increase in the boiling point of organic fluids for a given heat source, and the fluid freezing point must be higher than the system's lowest functional temperature. Z. Gu et al. [18] suggested the molecular weight affects the turbine efficiency, and the use of fluids with heavier molecules require low turbine speeds. Bhao et al. [13] concluded that an increase in the molecular weights of fluids reduces the turbine's isentropic efficiency. Baik et al. [71] stressed that the low viscosity fluids improve the convective heat transfer in the heat exchangers.

Many authors analysed the environmental regulations for the selection of the working fluids. There are three parameters that should be considered, and these are the global warming potential (GWP), ozone depletion potential (ODP) and atmosphere lifetime (ALT) [13], [24], [72], [77]. The ASHRAE list the refrigerant key characteristics such as toxicity, flammability, and corrosivity [13], [18]. There are some fundamentals principles that should be followed in the selection of the working fluid.

- The working fluid should have a low melting temperature to avoid solidification in cold climate conditions.

- The thermal conductivity of the working fluid should be high to maximise the heat transfer rate.
- The working fluid should have low viscosity and coefficient of expansion. It reduces the pump's power consumption and volume variations at different operating conditions.
- Fluids should be environmentally friendly with low corrosion activity, be nontoxic, have low vapour pressure, and have low flammability.
- It should be inexpensive and easily available.

There is a list of organic working fluids with different values of temperature and pressure, presented in Table 2.4. The fluid selection depends upon the concrete heat source, the temperature range of exploitation and the environmental safety parameters.

Table 2.4 Working Fluid Properties NIST Database [78]

Fluid	**Molar Mass (Kg/Kmol)**	**T_{ct} (ºC)**	**P_{ct} (MPa)**	**Type**	**GWP**	**ODP**	**Toxicity**	**Flammability**
RC318	200.3	115.23	2.77	Dry	8200	0	No	No
Butane	58.122	151.98	3.79	Dry	3	0	No	Yes
Isobutane	58.122	134.66	3.62	Dry	3	0	No	Yes
Ammonia	17.03	132.25	11.33	Wet	0	0	Yes	No
R11	137.37	197.96	4.40	Isentropic	4000	1	No	No
R14b	116.95	204.35	4.21	Isentropic	600	0.11	Yes	No
R152a	66.051	113.26	4.51	Wet	140	0	No	Yes
R142b	100.5	137.11	4.05	Isentropic	1800	0.065	Yes	Yes
R134a	102.03	101.06	4.05	Wet	1300	0	No	No
R245fa	134.05	154.01	3.65	Dry	1030	0	No	No

R236ea	152.04	139.29	3.50	Dry	9810	0	No	No
R236fa	152.04	124.92	3.20	Dry	1300	0	No	No
Ethanol	46.068	240.75	6.14	Wet	n.a.	n.a.	No	Yes
Methanol	32.042	239.45	8.10	Wet	n.a.	n.a.	Yes	Yes
R12	120.91	111.97	4.13	Isentropic	10890	1	No	No
Pentane	72.149	196.55	3.37	Dry	5	0	Yes	Yes
R227ea	170.03	101.75	2.92	Dry	3220	0	No	No
R123	152.93	183.68	3.66	Isentropic	77	0.02	Yes	No
R22	86.468	96.145	4.99	Wet	1700	0.05	No	No
R32	52.024	78.105	5.78	Wet	675	0	No	Yes
R113	187.38	214.06	3.39	Dry	6130	1	No	No
Isopentane	72.149	187.2	3.37	Dry	5	0	Yes	Yes
R114	170.92	145.68	3.25	Dry	10.04	1	No	No

2.5 Optimisation of the ORC model

The variables of the ORC system can be optimised to increase the performance of the cycle. Serval authors implemented a Genetic Algorithm (GA) approach to optimise the Rankine cycle [23]. Xu Huan et al. [79] investigated the regenerative ORC system and calculated the thermodynamic system performance using the GA approach. L. Pierobon et al. [80] performed multi-objective optimisation to find the optimum design of the heat recovery ORC system. The net power value, thermal efficiency, and the total volume were used as the objective functions to optimise the operational variables (condensing temperature, turbine outlet pressure, and working fluid) by using the GA approach. Kai et al. [81] effectively used the GA approach to

design the ORC system for low-temperature heat recovery. Sadeghi et al. [82] investigated the ORC system thermodynamic performance operating on the zeotropic mixtures. By using the GA approach, multi-objective optimisation was implemented to achieve the optimum performance of the cycle.

The GA optimisation process is based on the recreation of the natural selection process. The method defines the optimum values of the design variables of a system. These variables are treated as chromosomes, and the evaluation of the chromosome depends on the fitness function. The algorithm generates the population from the chromosomes of high fitness value, and the rest of the results are discarded. There are various types of fitness functions used. Yang et al. [76] have used the cost and thermal efficiency as a fitness function. Kai et al. [81] investigated the cycle with the net power value as a fitness function, and Sadeghi et al. [82] used an objective function for the cycle energy destruction rate and energy efficiency.

2.6 Solar Organic Rankine Cycle

There are different types of heat sources used with the ORC systems and considered in the literature. T. Tartiere et al. [83] studied the world market for ORC technology, and solar application makes 1 % of the total ORC globally installed capacity. The heat source for the ORC can be of a different origin, such as biomass combustion, solar radiation, waste heat from industries, or ground heat source. In the ORC system, refrigerants used as working fluids instead of water, and working fluid conditions and selections greatly affect the SORC energy efficiency. Sprouse et al. [55] analysed the utilisation of various heat sources in the ORC turbines.

Wang et al. [84] analysed low-temperature solar Rankine cycles run on zeotropic mixtures by introducing an internal heat exchanger. The results showed that the zeotropic mixtures significantly affect and increase the Rankine Cycle thermal efficiencies.

Delgado et al. [85] theoretically analysed the solar ORC plant coupled to stationary solar collectors. The twelve working fluids considered to supply heat to the ORC. The four different solar collectors were analysed, including the flat plate collector, evacuated tube collector, compound parabolic collector, and stationary solar collectors. Results produced to determine the operating parameters, aperture area of collectors, and output work of the SORC. Wang et

al. [84] were presented the analysis of the solar ORC performance over the whole day. Quiolin et al. [86] performed the optimisation of the small solar Organic Rankine's heat exchanger.

Different types of solar collectors can be classified following several criteria. These include differentiation based on the absorber/receiver type (Flat, Tubular etc.), concentration ratio (the collector aperture area divided by the receiver surface area), and the indicative temperature. The solar collector can be non-concentrating and concentrating ones. The non-concentrating solar collectors are stationary and have the same area for intercepting the solar radiations as its aperture. Among non-concentrating collectors, there are two main common types: Flat Plate Collectors (FPC) and Evacuated Tube Collectors (ETC).

The earth rotates around its axis within 24 hours. It also rotates around the sun and completes one revolution in 365.25 days. The earth revolves around the sun follows the ellipse path. The mean sun-earth distance (α) has the value of 149.59×10^6 km, and the eccentricity of the earth's orbit (e) has the value of 0.01673. The distance between sun and earth (R) can be calculated as $R = \alpha (1 \pm e)$

Some solar collectors track the position of the sun in the sky. These thermal collectors have lenses or reflecting mirrors to focus the solar radiation beam on the heat absorbing elements. This type of concentrating solar collectors are suitable for higher temperature ranges [55, 86]. The single-axis tracking systems include the Linear Fresnel Reflectors (LFR), Parabolic Troughs (PTC), and Cylindrical Troughs (CTC). The two-axis tracking systems included the Parabolic Dish Collectors (PDC) and Heliostat Field Collectors (HFC).

2.6.1 Non-Concentrating Collector Field

ETC type solar collectors convert the solar energy into heat. Usually, water can be used as the heat transfer fluid, which flows through the manifold to which ECTs are connected. Typically, the number of tubes are 10, 20, 22, or 30. The ETC consist of the following main components [87]:

- Evacuated Tubes;
- Heat Pipes;

- Manifold;
- Mounting Frame.

The internal side of the glass evacuated tubes absorbs solar radiation. There is a vacuum between internal and external glass tubes that eliminates convective heat losses. Inside it has the aluminium fin that transfers the heat from the internal glass to the heat pipe. The heat pipes are also vacuumed and partially filled with heat transfer fluid which boils, and heat is transferred to the condensation zone (the head of the heat pipe located in the manifold socket). Heat is transferred from the vapour to the water in the manifold, condensed and returned in the liquid state to the evaporation zone in the evacuated glass. Fig. 2.5 shows the ETC collector components.

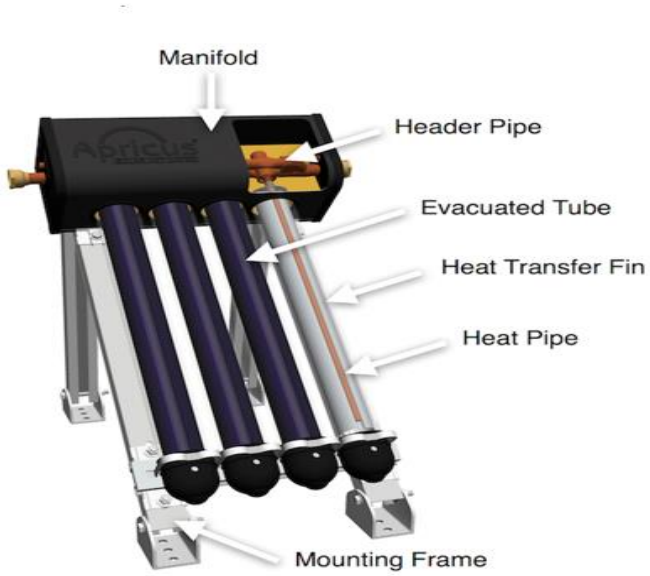

Figure 2.5 The schematic of the ETC [87]

A typical set with ETC has a controller, storage tank, circulation pump, various valves, and piping. It can be of an active or passive flow system. In a passive system, water circulates due to free convection, and the active system contains the circulation pump to circulate water. There are three types of the ETC solar thermal system (Figure 2.6):

- Direct Systems;
- Drain back systems;

- Closed-Loop System/ Indirect System;

The direct open flow system has a built-in electrical element. The tank of the collector has hot (from the collector) and cold water inlets. It is suitable for temperatures below -10 ^{o}C. The direct flow system has an efficient heat transfer mechanism without using a heat exchanger.

The drain system is also suitable for cold climates with winter night temperatures below -10^{o}C. It requires a high head pump to lift the water at the height of the collector. It is a simple drain-back system and has a heat exchanger. It can be either a tank coil or an external heat exchanger. When the pump turned off, the heat flow liquid returned from the collector drain lines. The closed-loop system is suitable for a cold climate condition with winter night temperatures less than -10^{o}C. The poor quality of the coil can cause corrosion or scale in the collector. It has both domestic and commercial applications, the glycol-water mix used to prevent freezing. In a closed-loop system, the liquid circulated within the collector is separated from the primary hot water system through the built-in heat exchanger. Fig. 2.6 shows the schematic diagram of the above types of ETC system.

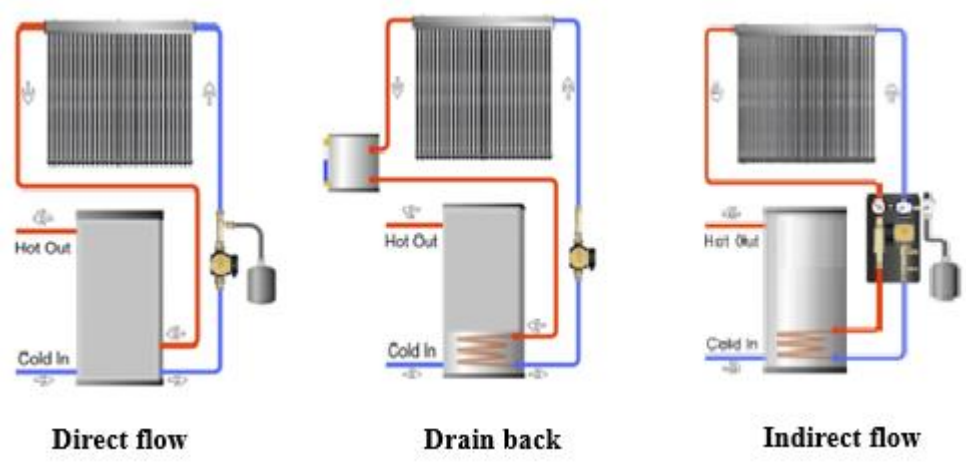

Figure 2.6 Evacuated tube solar collector systems [261]

The ETC systems have a wide range of applications, including water heating, which is used for both domestics and commercial purposes. For example**,** an ETC collector is widely used in China's rural areas for solar water heating as a low-cost technology [88, 89]. The ETCs have a low initial cost and payback period. The Chinese manufacturers dominate the ETC world market [90, 91]. A vacuum tube collector field with an area of 3300 m^2 and a capacity of 2.3

MW was built in China to supply heat to a Lithium production facility in Tibet. Another vacuum tube collector field with an area of 2200 m^2 and a capacity of 1.5 MW was installed in Shandong province for the industrial heat supply in 2017. The Indian Gujarat State Electricity Generation plant is equipped with an evacuated tube collector field with an area of 1575 m^2 and a capacity of 1.102 MW. The Turkish metro shopping centre was equipped in 2009 with a vacuum tube collector with an area of 1200 m^2 and a capacity of 840 kW [92]. The 20 kW ORC with ETC system was tested at Maejo University in Thailand. The ORC efficiency was 8 % when using HCFC-245fa as the working fluid. It was found that the system could generate electricity at 0.547 USD/kWh when the hot water temperature was higher than 100 ^oC.

2.6.2 Concentrating Solar Fields with Single Axis Tracking

The four CSP technologies currently used are Parabolic Dish Systems (PDS), Linear Fresnel Reflectors (LFR), Solar Power Towers (SPT), and Parabolic Trough Collectors (PTC) [93-95]. The LFR is simple in production, has low cost and easy maintenance. It is well developed and widely used in solar thermal systems [96-99]**.** Many published research works present the detailed parameters of the various types of concentrating solar power plants with Organic Rankine Cycle [100-110]. The current research work is focused on the Fresnel Reflectors used with the Organic Rankine Cycle turbine. Construction simplicity and low price of components are advantages of Fresnel technology. The Fresnel collector has the reflecting surfaces (mirrors) to focus the sunbeams onto a linear absorber tube, which is mounted above mirrors, see Fig. 2.7. The LFR mirrors are almost linear (with a very small curvature) in shape and easy to produce. Some such collectors include the secondary reflector mounted over the receiver tube. The design parameters of the collectors are as follows:

- Width of mirrors and their curvature;
- Number of parallel mirror rows;
- Absorber height above the mirror plane;
- Space between the mirror rows;
- Design and optical characteristics of the secondary reflector.

Figure 2.7 Linear Fresnel Reflector of the Power Plant [111]

The main components of the receiver are the secondary reflector and absorber tube itself.

The secondary reflector is placed above mirrors, see Fig. 2.8, and is made of a material with higher reflectivity. The upper side is usually covered with thermal insulation to prevent heat losses. The secondary reflector compensates for the inaccuracy of focusing beams by mirrors upon the receiver tube.

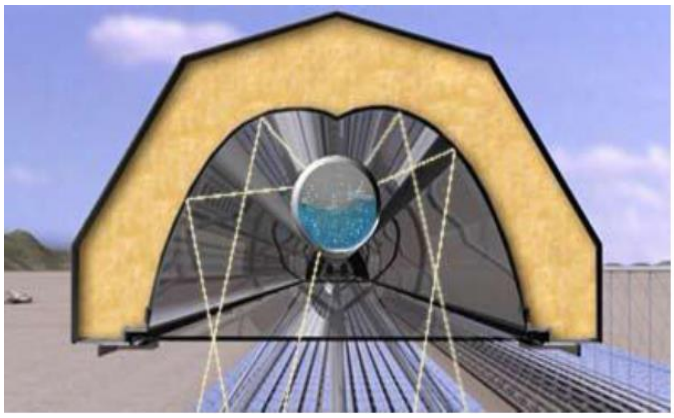

Figure 2.8 Secondary Reflector above the receiving tube of the LFR [112]

Compared to the parabolic trough collectors, the absorber tubes of the LFR are simple in design. The absorber tubes have a selective coating to absorb short wavelengths and block infrared solar re-radiation (see Fig. 2.9). These tubes made of stainless steel. The use of

ceramic materials for such tubes are under investigation to raise the operating temperatures to 450 ^{o}C.

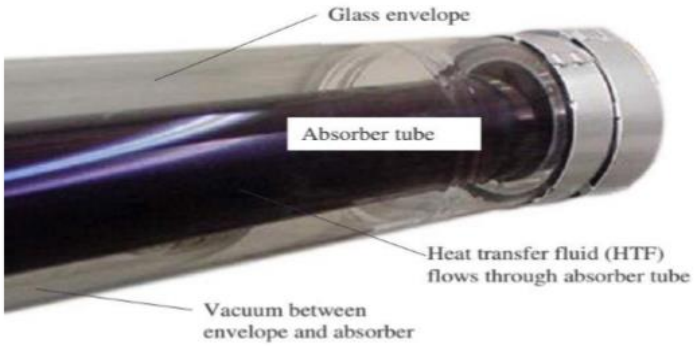

Figure 2.9 LFR absorber tube [113]

The LFR has a single axis sun-tracking system as shown in Fig. 2.10, and different mirror rows will have different angular positions during operation. On which mirrors in a row are mounted, the metallic axis is rotated by an electrical step-motor with a gearbox controlled electronically to focus the receiver solar radiation. The tracking mechanism also returns the mirrors to the initial position after the end of the operational hours.

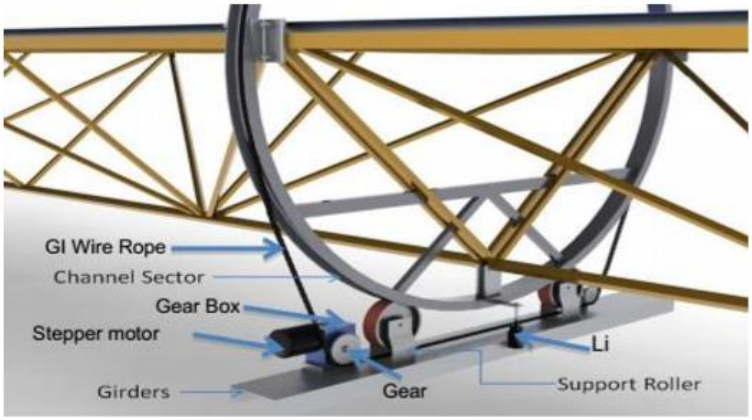

Figure 2.10 A single-axis tracking system of the LFR [114]

2.6.3 Thermal and Optical parameters of LFR Systems

F. Burkholder et al. [115] investigated the heat losses in the PTR70 Schott type collector. The theoretical results were obtained using the System Advisor Software model for a temperature range between 100 ^{o}C and 500 ^{o}C and compared with the experimental results. Sen et al. [116] investigated the thermal performance of the LFR system. The system with a single-track mechanism produced steam at the rate of 2.4 kg/hr and 6.3 kg/hr at pressure 1.5 bar with the reflector area of 5 m^2 and 13 m^2, respectively. Dostucok et al. [117] presented the empirical relation for finding the receiver's thermal efficiency at a Turkey location. Reddy et al. [118] described the numerical analysis conducted to determine the convective and radiative losses from the receiver tube of the LFR system. The reduction of 12.76 % and 54 % of radiative and convective heat losses, respectively, was achieved with the optimum design of the LFR. E. Youssef et al. [119] investigated the LFR-ORC thermal power system in Morocco. The cis-butene was the working fluid for ORC, and the system produced 7.12 kW at the efficiency of 5.32 %. G. Mokhtar et al. [120] investigated the LFR system located in Belinda. The theoretical and experimental efficiency of the system was 29%.

He at al. [121] studied the optical performance of the LFR system using the rays tracing method. Variable parameters were the receiver height, mirrors width. They found that the mirrors close to the central line have higher efficiency, compared to the outer rows. Abbas et al. [122] performed the optimization of the optical design of the LFR system. They investigated the influence of the mirror surface geometry and mirror quality on the system performance. Huang et al. [123] conducted an optical analysis of the LFR with an azimuth tracking system. Results show that optical efficiency was 61%. Song et al. [124] investigated the optical losses of the LFR system suggested the receiver height to be more than 3 m from the Fresnel field to minimize the shading and blocking effects. Val et al. [125] investigated the LFR's annual optical performance by using rays tracing method. Results demonstrated the 0.4 % gain in the thermal energy by using the variable spacing between the adjacent rows and reducing the shading and blocking effects. Benyakhlef et al. [126] studied the mirrors curvature, heat flux distribution of the receiver, and the LFR field's optical efficiency in Morocco. Results showed that the curved mirrors improved the optical efficiency of the system.

Giovanni Francia designed the first LFR field in 1962. The field was made of seven aluminium mirror rows with overall dimensions of 8.2 m x 7.9 m. The receiver's length was 8m, and it was mounted at the height of 6 m above the Fresnel field. The mirrors were rotated with the motor to track the sun position. The system generated 38 kg/hr steam with a temperature of 450 ^{o}C and 100 atm pressure [127]. A pharmaceutical company has installed the LFR system in Jordan. The collector was made of 18 Fresnel modules, each with an area of 22 m^2 and absorber tube set at 4.5 m above the Fresnel field. The system produced 222 kWh of the thermal energy in steam at temperature 166 ^{o}C and pressure 6 bar [128].

One of the LFR fields was installed in the Engineering school at Seville. The field was constructed on the roof of a building. The system produced 174 kWh of energy as the steam. Fig. 2.11 shows the experimental installation of the LFR field, and Table 2.5 presents its parameters.

Figure 2.11 Installation setup of the Seville plant [129]

Table 2.5 Design parameters of the Seville plant [129]

Parameters	**Unit**
Number of mirror rows	11
Number of mirrors in each row	16
Collector area	352 m^2
Row spacing	0.2 m
Mirror profile	Curved
The focal length of mirrors	8.6 – 10.6 m
Receiver	Schott PTR 70
Absorptivity factor	0.95
Receiver height above the primary reflector	4 m
Reflector material	Polished aluminium
Reflectivity factor	0.77
Maximum temperature	200 °C
Peak pressure	13 bars
Mass flow rate	13 m^3/ h

Kimberlina was the first linear Fresnel reflector power system built in the USA. It has a power capacity of up to 5 MW. Similarly, Puerto Errado LFR power system produces 1.4 MW of thermal energy in Spain. The most extensive compact linear Fresnel reflector CSP power system is located in India to produce 125 MW of power [130].

2.6.4 Parabolic Trough Collector (PTC)

Fig. 2.12 shows the schematic diagram of a simple PTC system. A parabolic trough is a line focusing technology, and usually, oil is circulated within the absorber tube and heated up to 400 ^{o}C. The hot fluid is pumped to a heat exchanger to generate steam.

A. Soteris et al. [131] has developed a PTC thermal model with the single-axis tracking system. A. Fahad et al. [132] also investigated the PTC power system's thermal performance integrate with the ORC. The Solar energy generating systems (SEGS) I mainly based on PTC systems. Three operating plants with capacities of 377 MW, 354 MW, and 250 MW were installed in the USA, and twelve plants were built in Spain with capacities between 100 MW and 200 MW.

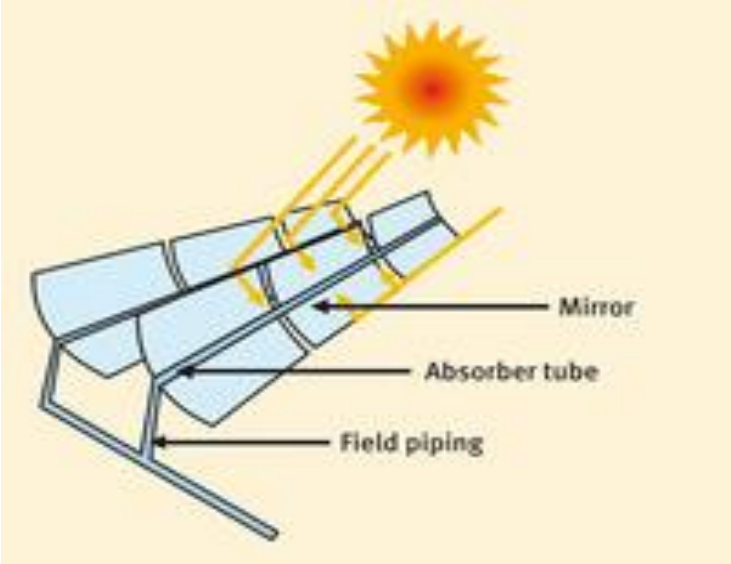

Figure 2.12 PTC system diagram [87]

2.6.5 Central Tower Solar System

Fig. 2.13 presents the schematic diagram of the central tower power system. It is also known as a heliostat power system. It uses large numbers of plane mirrors (heliostats) to concentrate the solar rays from the field upon central receiver located at the top of the central tower. The mirrors have a two-axis sun-tracking system. The receiver absorbs heat used to melt the salt solution, and it transfers the thermal energy to a large hot storage tank. The accumulated thermal energy is used to generate steam and drive a steam turbine. V. Hull et al. [133] investigated the design of the central solar receiver system and studied the different factors that

influence system performance. K. Vignarooban et al. [134] studied the solar tower concentrating system and investigated the molten salt as a heat transfer fluid, which can be heated up to 800 ^{o}C. C. Xu et al. [135] carried out theoretical modelling and energy analysis of the solar tower power system with molten salt. They determined the influence of the concentration ratio and direct normal irradiance (DNI) on the system performance.

The solar tower thermal power systems are a fast-growing technology. It can produce energy on a large scale. Golmud plant, located in China has a thermal capacity of 200 MW. Another plant is under development in China and has a capacity of 995 MW. Jemalong Solar Thermal Station generates 377 MW of thermal power in the USA. Crescent Dunes Solar Energy Project has a capacity of 110 MW of thermal energy in the USA. Copiapo power system is under development in Chile to produce thermal power up to 260 MW. Khi Solar One tower plant has been operational from 2016 in South Africa and has a thermal capacity of 50 MW. There are ten solar power plants under construction in China to generate thermal power from 50 MW to 200 MW [136].

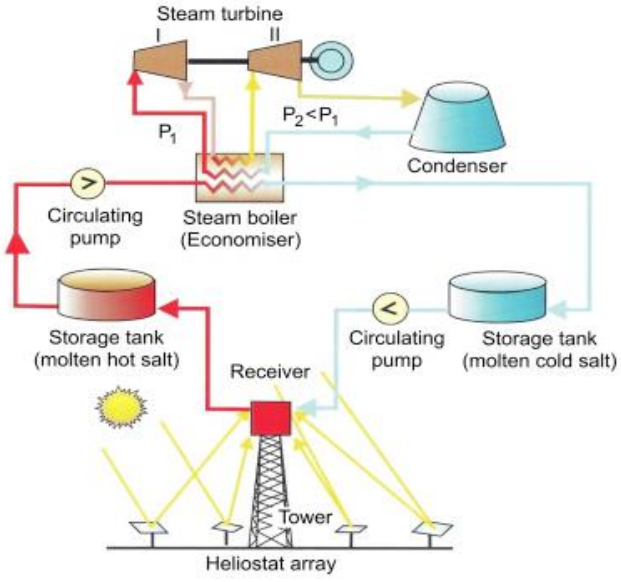

Figure 2.13 Design configuration of a central tower solar system couple with steam turbine [137]

2.6.6 Solar Dish Collector

Fig. 2.14 shows the design configuration of a solar dish collector coupled with the turbine. The Therminol oil absorbs thermal energy in the receiver and transfers heat to the Rankine cycle plant.

The solar dish has a paraboloidal shape and concentrates the solar energy upon a small focal point. It has a dual-axis tracking system. The solar dish may consist of many small reflective mirrors to focus the solar radiation upon a small-area receiver. R. Loni et al. [138] investigated how the dish solar collector was coupled with an ORC system. The system's performance was examined, taking into account the mass flow rate of the thermal oil (the heat transfer working fluid), design parameters of the receiver, and operating parameters of the system. M. Javidmehr et al. [139] studied the parabolic dish collector coupled with an ORC system and the desalination process. The thermodynamic performance was evaluated, and economic analysis of the system was carried out. P. Sasa et al. [140] investigated the dish collector system's daily performance with the aperture area of 10.28 m^2 and with a spiral coil absorber. The results show the thermal efficiency range was between 54.65 % and 67.36 % for the inlet temperatures from 50 ^oC to 350 ^oC.

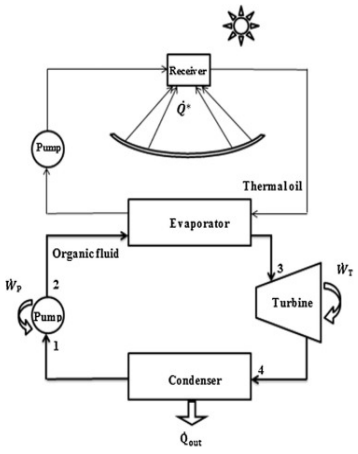

Figure 2.14 Design configuration of solar dish collector coupled with turbine [140]

2.7 Concentration Ratio of Solar Collectors

The concentration ratio is defined as the solar collector aperture area divided by the receiver surface area. Table 2.6 compares the different types of solar collectors. Mwesigye et al. [141]

investigated the PTC system with a concentration ratio of 113 and the working fluid Cu-Therminol VP-1. Tyagi et al. [142] presented the concentrating solar power technology parametric study, demonstrating the thermal efficiency increase with the concentration ratio value. Zhu et al. [143] conducted the theoretical modelling and experimental investigation of the LFR system with a concentration ratio of 15.14. Bellos et al. [144] examined the daily, monthly, and yearly performance of the LFR system with a concentration ratio of 20.46. Rabbani et al. [145] investigated the heliostat solar field for a cogeneration power system. The solar field system has a concentration ratio of 1600. The results showed the receiver's efficiency varying from 71% to 76.3% at the ambient temperature from 260 K to 320 K.

Table 2.6 Solar Collector Parameters [116]

Collector Type	**Shape**	**Concentration Ratio**	**T (ºC)**
Flat Plate Collector (FPC)	Flat	1	30 - 80
Evacuated Tube Collector (ETC)	Flat	1	50 - 200
Compound Parabolic Collector (CPC)	Tubular	1 - 15	60 - 300
Fresnel Reflector (FR)	Tubular	10 - 40	60 - 250
Cylindrical Trough Collector (CTC)	Tubular	15 - 50	60 - 300
Parabolic Trough Collector (PTC)	Tubular	10 - 120	60 - 400
Parabolic Dish Reflector (PDR)	Point	600 - 2000	100 - 1500
Heliostat Field Collector (HFC)	Point	300 - 1600	150 - 2000

2.8 Conclusions

The selection of the working fluid has a substantial impact on the ORC system efficiency. The working fluids have different operating temperature ranges, and the working fluid selection depends on the heat source. If the working fluid has a higher boiling point, then high-temperature energy input is required to convert the liquid into the steam phase, and this, in general, results in the rise of cycle efficiency. The environmental regulations are an essential part of the working fluid selection for the ORC. The turbine output power increases with the working fluid's mass flow rate, and the regenerative heat exchanger addition to the ORC improves its performance.

The ORC modelling is being actively developed and is the area of interest for many investigators. A number of researchers demonstrated that the use of the heat exchanger for the re-use of heat in the cycle considerably improves the thermal performance of the Rankine cycle. The analysis of deploying various working fluids in the cycle and heat exchangers for low to high-range temperature applications helps to select rational design parameters and configuration of ORC systems. The performance of an ORC system using the NOVEC^{TM}649 working fluid has not been studied previously and reported in the literature. The thermodynamic modelling of the Rankine cycle with the NOVEC^{TM}649 working fluid can be considered as a new contribution to the knowledge in this area.

There are different types of solar collectors that can be used to supply energy to the ORC. The solar collector's selection depends on the amount of heat energy required for the ORC operation and the fluid temperature at the exit from the collector. The ETC and LFR are attractive options for coupling to ORC systems operating within a temperature range of 70^{o}C – 250^{o}C. These types of collectors can be connected in series and parallel to increase the energy output. ETC collectors have increased solar radiation receiving capacity all over a day. These are the stationary solar collectors with lower installation costs than Fresnel, parabolic, and heliostat solar collectors. The LFR and parabolic troughs have single-axis sun-tracking systems.

Most authors considered ORC systems with a single type of solar thermal power system with a certain heat transfer fluid for low to medium temperature applications. The thermal performance of the ORC system depends on the selection of the type of solar collectors and on

the geographical location of the plant. The potential of the solar power system located in Almatret (Spain) was investigated in this work, assuming water as a heat transfer fluid in the solar field and HCFC-134a as the working fluid in the ORC. The GA optimisation code was used with the solar thermal power plant simulation model to analyse the system performance for the case in which the evacuated tube collectors were deployed.

The design of the plant with Linear Fresnel Reflector and Therminol-62 as the heat transfer fluid in the solar field and NOVEC^{TM}649 as the working fluid in the ORC cycle was investigated. Such the plant's annual performance was estimated, and results demonstrate that application of the thermal storage system integrated with the LFR field significantly the system overall power output and efficiency.

Chapter 3: Modelling of the Organic Rankine Cycle

This chapter presents the mathematical model and simulation results for the simple Organic Rankine Cycle (ORC) turbine. The ORC performance was evaluated for cases in which HCFC-245fa, HCFC-134a, HCFC-34, n-propane, iso-pentane, methanol, and ethanol were used as working fluids. For steady flow conditions, the energy conservation principle was implemented for the individual components of the ORC to derive the thermodynamic model equations. The ORC model was investigated to calculate the rate of heat added to the cycle, power output and the thermal efficiency of the ORC. The simulation model of ORC was designed on the MATLAB/Thermolib software. The ORC performance improves with a regenerative heat exchanger and recovers heat from the turbine outlet fluid stream. The NTU method was applied to determine the effectiveness of the heat exchanger. The ORC with heat regeneration was analysed, as above, using R245fa, R134a, R34, n-propane, iso-pentane, methanol, and ethanol as working fluids and results were compared that for a simple ORC model. The results show that heat recovery considerably improves thermal efficiency.

3.1 Introduction

The different manufacturers of the ORC systems are working on design improvements using extra components to the original basic cycle. The modifications may include increasing the temperature difference between heat input and rejection to improve the cycle's thermal efficiency. T.C. Hung et al. [146] investigated the ORC efficiencies run on wet and dry working fluids. These fluids included ammonia, benzene, HCFC-11, HCFC-12, HCFC-113, and HCFC-134a. Hung et al. [147] investigated the ORC system's operating conditions run on the HCFC-123, HCFC-113, Benzene, p-Xylene, and Toulene. The results show that p-Xylene provides the highest thermal efficiency. Steven et al. [148] investigated variations of the ORC architecture, and the performance of the ORC was investigated at various operating conditions (evaporation and condensation temperature). Tou et al. [149] investigated the ORC thermal efficiency for several selected working fluids. The results show that the ORC system's thermal efficiency is a weak function of the critical fluid temperature. Ibarra et al. [150] investigated the ORC system thermodynamic performance and suggested that better performance is

achieved when using SES23 as the working fluid compared to HCFC-245fa under the same cycle specifications.

Arnaud et al. [151] proposed the ORC technology for domestic applications with the utilisation of the low-grade heat and carried out the turbine and pump analysis as a part of the parametric optimization. Jinjiang et al. [152] reviewed the working fluid selection and its influence on the ORC expanders and investigated the cycle performance run on the pure and mixed fluids. Lecompte et al. [153] investigated the ORC performance run on the azeotropic mixture using the second law analysis and found that attained maximum power output increases linearly with temperature in the range from 120 ^{o}C to 150 ^{o}C. Kiyarash et al. [154] studied the ORC technology to convert low- and medium temperature heat source into power and presented the literature review results on the ORC fluid selection, its configurations and applications on thermodynamic modelling and experimental results. Wenqiang et al. [155] described the ORC, which used the waste heat in the industrial process and determined its efficiency when HCFC-113 was used as the working fluid. S.H. Kang et al. [156] experimentally investigated the ORC technology run on HCFC-245fa with a low-temperature heat source. The high-speed radial turbine was used in the ORC system, and the thermal efficiency of the cycle and its power output was determined for various operating conditions. I. G. Saez et al. [157] evaluated technically and economically an ORC technology for the solar power system to generate energy for a house. The working fluids considered were HCFC-245fa, HCFC-134a, HCFC-600a, and HCFC-152a. The system power output ranged from 7 to 30 kW at the specific location and climate conditions.

A. Javaanshire et al. [158] carried out the design analysis and optimization of the regenerative ORC with different types of dry fluids and concluded no significant change in turbine output when the regenerative heat exchanger was used in the ORC. T. Tartiere et al. [159] investigated the world ORC technology market based on the installed capacity, economic trends, and historical data. They concluded that there would be growth for the ORCs with regenerative heat exchangers. M. Li et al. [160] described the regenerative ORC for use with a low-grade heat source to generate electricity. The R123 working fluid with a boiling temperature of 27.82 ^{o}C was investigated to utilise the geothermal heat source. The results from the experimental analysis showed an efficiency of 7.98%. T. C. Hung et al. [146] designed the ORC and analyzed

its performance with working fluids which include benzene, toluene, P-xylene, HCFC-113, and HCFC-13 and concluded that P-xylene provides better performance in case of high-temperature heat applications and HCFC-113 and HCFC-13 ensure the better performance for the low-temperature heat recovery.

The schematic of the basic ORC is shown in Fig. 3.1. It has four components, including the pump, evaporator, turbine, and condenser. The liquid vaporizes in the evaporator at elevated temperature and pressure. The pressurized vapour expands in the turbine and produces mechanical power. It is transformed into electricity via a generator. The working fluid is exhausted and cooled down in the condenser back to the liquid state. The pump increases the pressure of the fluid and circulates it back for evaporation. The Pressure – Enthalpy diagram demonstrates the cycle and determines the working fluid properties to evaluate the ORC component thermal performance.

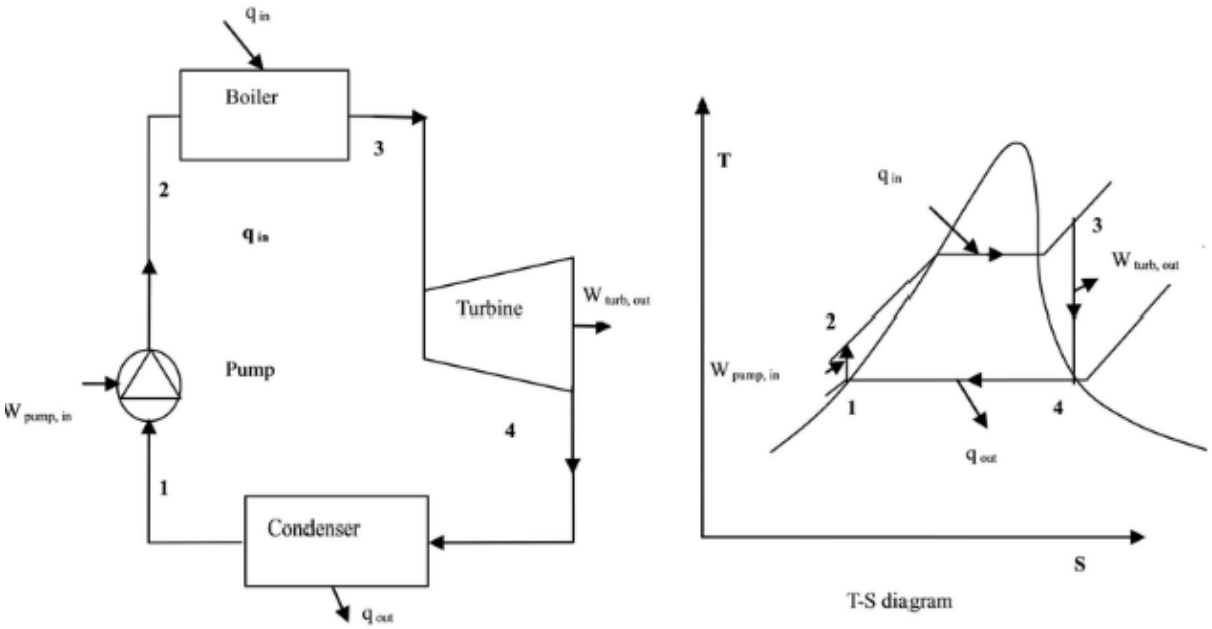

Figure 3.1 Basic ORC system schematic and T-S diagram [161]

The Reheat Organic Rankine Cycle (R-ORC) makes it possible to avoid moisture content during the cycle expansion process. It is a practical solution to improve the thermal efficiency of the basic Rankine Cycle. Turbine blades damage is avoided in the case of the wet working fluid. A schematic and T-s diagram of the R-ORC system is shown in Fig. 3.2. The working fluid here preheated before returning to the evaporator by the working fluid thermal energy

between the exhaust of the turbine and condenser [162-165]. The various authors studied the different configurations of ORC to improve their efficiency using heat regeneration in the systems [166-174].

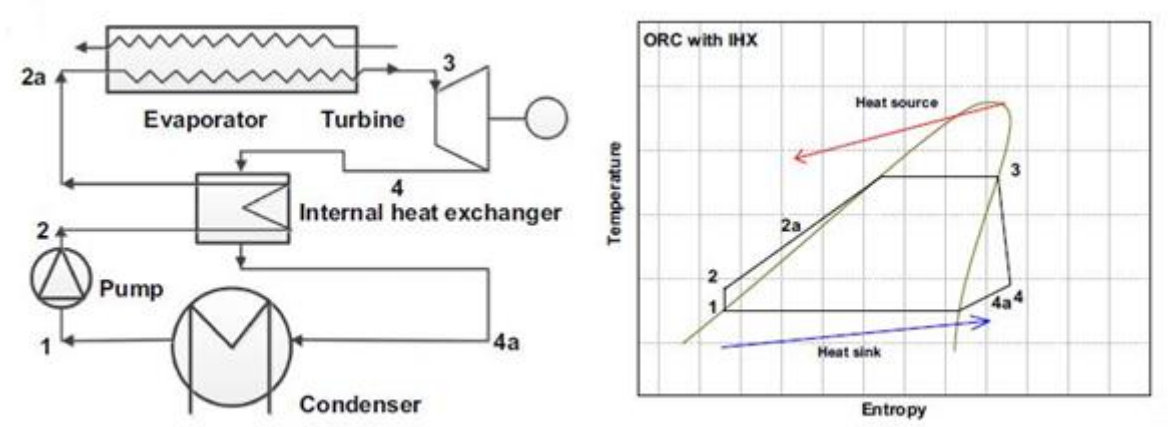

Figure 3.2 R-ORC system schematic and T-s diagram [161]

3.2 Description of the Organic Rankine Cycle (ORC) being investigated

The ORC model consists of the pump, evaporator, turbine, and pump. Each component of the cycle considered as a control volume, and steady-state flow conditions are used to describe its operation. The Kinetic and Potential energy effects are negligible.

The model was tested using different working fluids, including HCFC-245fa, HCFC-134a, HCFC-32, n-propane, iso-pentane, methanol, and ethanol. The analysis was performed using the working fluids at their critical value of the pressure under the same mass flow conditions.

The isentropic pump efficiency is the ratio between the isentropic pump compression work ($w_{i,p}$) and the actual pump compression work ($w_{a,p}$). It can be expressed using the equation below

$$\eta_P = \frac{w_{i,p}}{w_{a,p}} \qquad (3.1)$$

During the simulation process, certain values of the isentropic efficiencies for the turbine and pump were used. The turbine efficiency is the ratio between the actual ($w_{a,t}$) and isentropic ($w_{i,t}$) turbine work. The pump and turbine with a good design have the typical isentropic

efficiency values between 75% and 85%. The turbine and pump isentropic efficiencies were assumed to be 75 % for this ORC model as this value is widely reported in the literature.

The different types of working fluids (hydrocarbons) are the selector for the present model. These hydrocarbons have different evaporating temperatures. The evaporation temperature of the hydrocarbons relates to the input heat added to the ORC. The performance analysis of the ORC with different hydrocarbons determine the application of the ORC corresponds to a low and high input heat source. Hence the operating conditions of the ORC are assumed such that the mass flow rate of the working fluid is equal to 1 kg/sec (for simplicity in comparison). The individual component thermal performance was investigated using the thermodynamic equations based on the enthalpy changes during thermodynamic processes.

The dry (HCFC-245fa, propane and pentane) and wet (HCFC-134a, ethanol, methanol and HCFC-32) working fluids were selected in the ORC modelling. These fluids have an acceptable value of the ozone depletion potential (ODP) and easily available in the market. The ethanol and methanol have higher values of the critical temperature and pressure compared to other fluids. The HCFC-32 has a low value of critical temperature, even at high pressures. The working fluids HCFC-245fa, HCFC-134a and propane have the medium range of the critical temperatures. During the comparison of fluids, the heat input heat added to the cycle was analysed, and the impact of the heat exchanger to recover heat in the cycle was investigated.

Table 3.1 Properties of different working fluids used in the model [NIST]

Property	R245fa	R134a	Propane	Pentane	Ethanol	Methanol	R32
Critical temperature (^{o}C)	154.1	101	96.67	196.6	240.75	239	78.105
Critical pressure (bar)	36.40	40.6	42.47	33.70	61.4	81	57.82
Critical density (kg/m^3)	517	511.9	220	232	280	280	424
Boiling point (^{o}C)	14.90	-26.07	-42.09	36.06	36.06	78.3	51.651

The T-S diagram for HCFC-245fa is shown in Fig. 3.3. The working fluid is heated at the constant pressure in the evaporator to the saturated vapour state. The left side of the saturation liquid line corresponds to the liquid state (in blue), and the curve in red represents the saturated

vapour line. The zone above the red curve represents the superheated vapour region. The intersection of two lines is known as the critical point (Cp). The region below the critical point limited by the saturation lines is the liquid-vapour mixture region.

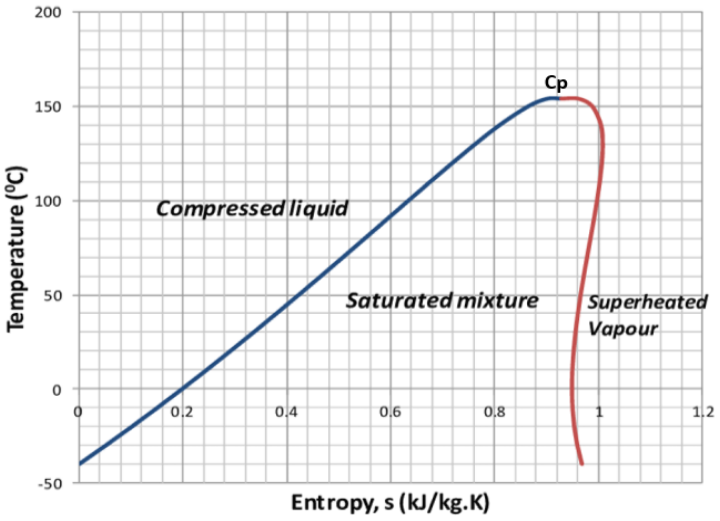

Figure 3.3 T-S diagram for the HCFC-245fa organic fluid [176]

The simulation model of the ORC was developed in the Thermolib toolbox. As mentioned above, such working fluids as HCFC-245fa, HCFC-134a, HCFC-32, n-propane, iso-pentane, methanol, and ethanol were used for the modelling process. Fig. 3.4 shows the Simulink model of the ORC system for the HCFC-245fa working fluid. The circulation pump compresses the saturated liquid from its condensing pressure at state 1 to its critical pressure of the liquid at state 2, and the evaporation of the working liquid take place under the constant pressure followed by the production of the mechanical work in the turbine. The outlet pressure of the turbine is equal to the condensation pressure. The isobaric condensation of the working fluid completes the cycle. The model is integrated by the flow buses to visualize the change in the working liquid properties during the cycle. The enthalpy variation between two states determines the thermodynamic performance of the separate component. The thermal efficiency of the ORC is the ratio of the difference between the turbine and pump works and input heat.

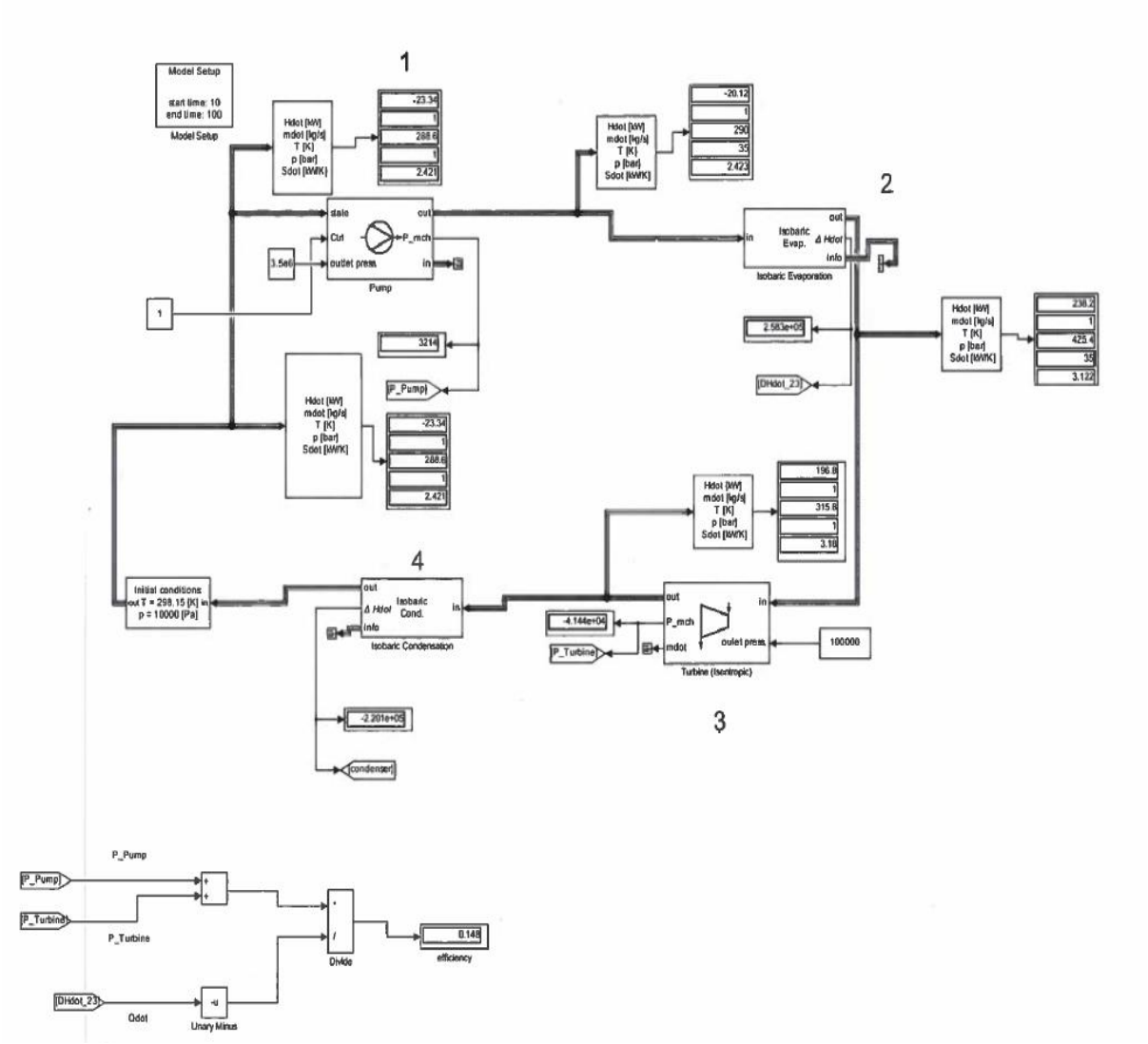

Figure 3.4 Simulation model of a simple ORC

3.2.1 Thermodynamic Modelling of the Organic Rankine Cycle (ORC)

The energy balance equation at steady flow conditions is used to find the individual component and system performance of the ORC:

- The rate of heat added to the evaporator;
- The rate of heat rejected by the condenser;
- The turbine's work;
- The work consumed by the pump;
- The thermal efficiency of the model.

The energy balance equation for the control volume in a general form is written as

$$\mathbf{dEcv/dt = Q - W + \dot{m}_{wf}i\,(Ui + V_i^2/2 + gZi) - \dot{m}_{wf}e\,(U_e + Ve^2/2 + gZ_e)} \quad \mathbf{(3.2)}$$

Here dEcv/dt = Rate of energy change within the control volume; Q = heat; W = work; $\dot{m}_{wf}$ = mass flow at the inlet and exit; U = internal energy at the inlet and exist; $V^2/2$ = kinetic energy at the inlet and exist; gZ = gravitational potential energy at the inlet and exist

The sum of the mass flow rate entering the turbine within the control volume is equal to the sum of the mass flow rate at the exit ($\sum$mi = $\sum$me)

The kinetic and potential energy effects across the boundaries of each ORC component are small and can be neglected. For the steady-state process (3.1) is modified as

$$\mathbf{Q + \sum \dot{m}_{wf}i\,(hi) = W + \sum \dot{m}_{wf}e(he)} \quad \mathbf{(3.3)}$$

The working fluid thermophysical properties were determined using the National Institute of Standards and Technology (NIST) database (the U.S. Department of the Commerce). This database provides data for a wide list of inorganic and organic compounds and produces precise results for thermodynamic properties of working fluids in the wide range of the operating parameters under different conditions [177]. The thermodynamic model calculations of the ORC system were performed using the enthalpy change chart of the working fluids for specific temperature and pressure values using the NIST database.

The following sections demonstrate how the above equations were used in the computational code to calculate the performance of the simple ORC system components.

3.2.2 The Pump in the ORC system

The pump increases the pressure of the incoming fluid (from the condensation pressure) to a target pressure (in the evaporator up to the working fluid critical value pressure value). The enthalpy values were determined using the standard NIST database. The operating conditions for the pump of the modelled ORC are listed in Table 3.2.

The pressure rise in the pump is from 1 bar to 36 bar. The working fluid temperature slightly changes during the pumping process, and therefore, it is considered an isothermal process.

Table 3.2 Operating conditions in the pump

Parameter	Value
Inlet Pressure	1 bar
Outlet pressure	36 bars
Inlet temperature	288.6 K
Outlet temperature	290 K
Mass flow rate	1 kg/sec
Pump power input	3.243 kW

Fig. 3.5 shows the enthalpy change of the liquid for a pressure rise between 1 and 35 bar. According to the pump energy balance condition, the pump input power is 2.481 kW. The enthalpy change of the refrigerant HCFC-245fa is determined using the Nation Institute of Standard and Technology (NIST) US database. The trend is plotted using the excel sheet, and results are showing the enthalpy variation at different values of pressure under adiabatic isentropic compression of the working fluid.

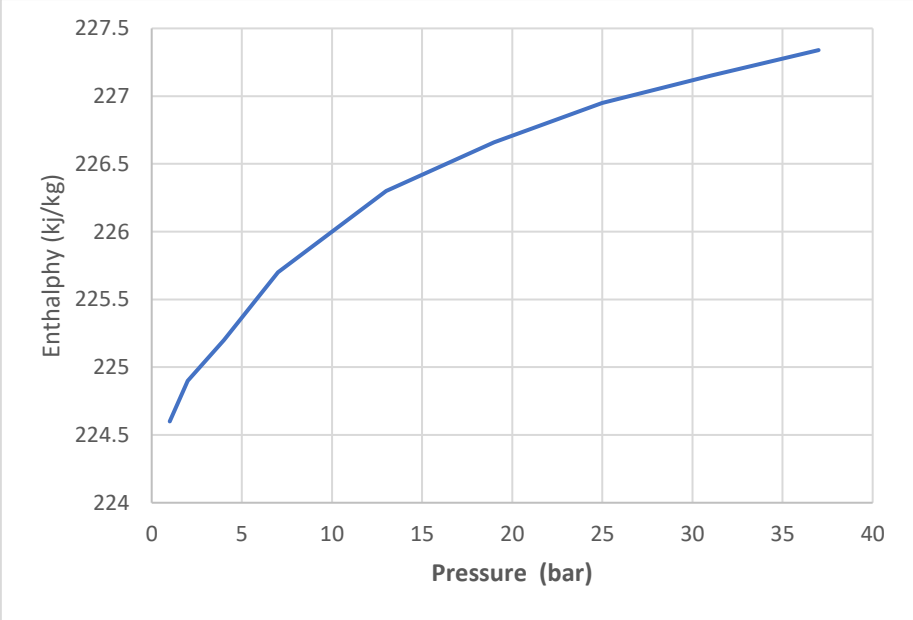

Figure 3.5 Enthalpy variation in the pump as a function of a pressure rise

Fig. 3.6 shows the calculation scheme for the pumping process. Q = 0 correspond to the adiabatic compression.

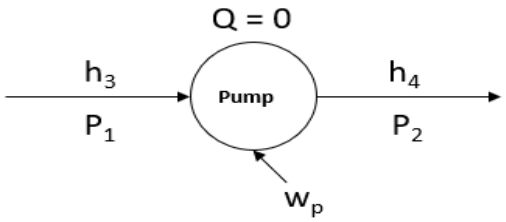

Figure 3.6 Calculation scheme for the pumping process

According to the first law of the thermodynamic, the work input rate for the pump can be calculated as

$$\mathbf{W_P} = \dot{m}_{wf}(\mathbf{h_4} - \mathbf{h_3}) \quad \textbf{(3.4)}$$

The expression (3.4) can be further modified and expressed in terms of the fluid's specific volume and change in pressure:

$$\mathbf{W_P} = \mathbf{v}(\mathbf{P_2} - \mathbf{P_1}) \quad \textbf{(3.5)}$$

3.2.3 Evaporator

The evaporation process is an isobaric/isothermic process. The pump raises the pressure of R245fa at the evaporator close to 36 bar. The heat added to the working fluid in the evaporator converts the liquid into vapour. Fig. 3.7 shows the enthalpy change of the working fluid R245fa during the evaporation process. The enthalpy values were determined using the NIST standard database. Appendix A4 shows the thermophysical properties of the refrigerant HCFC-245fa for the 36-bar pressure.

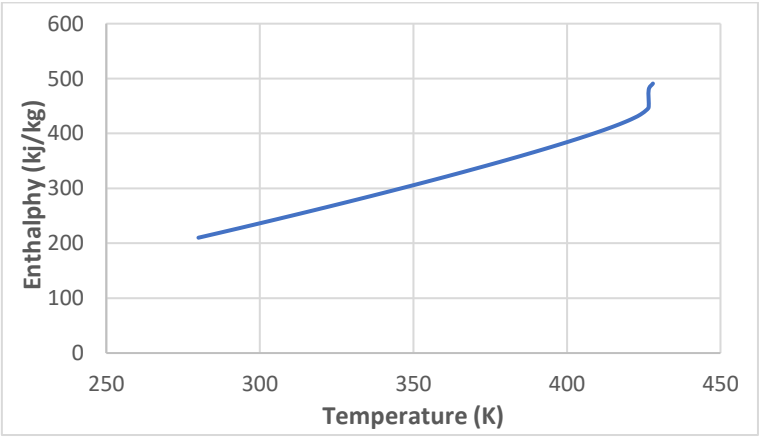

Figure 3.7 The working fluid enthalpy change in the evaporator

The operating conditions in the evaporator are shown in Table 3.3 below.

Table 3.3 Operating parameters in the evaporator

Parameter	**Value**
Pressure	36 bars
Inlet temperature	290 K
Outlet temperature	427.1 K
Mass flow rate	1 kg/sec
Evaporator heat input rate	258.32 kW

The rate of the heat necessary to vaporize R245fa is 258.32 kW, which is calculated as

$$\frac{\boldsymbol{Q_{in}}}{\dot{\boldsymbol{m}}_{\boldsymbol{wf}}} = (\boldsymbol{h_1} - \boldsymbol{h_4}) \qquad \textbf{(3.6)}$$

3.2.4 Turbine

The working fluid expands in the turbine, and its pressure reduces to the condenser' pressure value. The expansion of the working fluid results in the generation of mechanical work. The enthalpy changes in the turbine for the HCFC-245fa were calculated using the NIST standard database for the specific temperature and pressure values of the fluid. The operating parameters of the working fluid in the expansion process are listed below in Table 3.4.

Table 3.4 Operating parameters in the turbine

Parameter	**Value**
Inlet pressure	36 bars
Outlet pressure	1 bar
Inlet temperature	425.4 K
Outlet temperature	315.8 K
Mass flow rate	1 kg/sec
Turbine output power	41.847 kW

The turbine generates 41.847 kW of mechanical power, calculated as

$$\frac{W_T}{\dot{m}_{wf}} = (h_1 - h_2) \quad \textbf{(3.7)}$$

3.2.5 Condenser

The heat is rejected in the condenser, and the vapour of the working fluid R245fa is converted to the liquid state. The enthalpy values are determined using the NIST standard database. These values are related to the fluid temperature at the condenser inlet and outlet, and the condensation process takes place in isobaric/isothermic conditions. The operating parameters in the condensation are shown in Table 3.5 below.

Table 3.5 Operating parameters in the condenser

Parameters	**Value**
Pressure	1 bar
Inlet temperature	315.8 K
Outlet temperature	288.6 K
Mass flow rate	1 kg/sec
Heat rejection rate	220.14 kW

For the above parameters, the heat rejection rate of 220.14 kW is calculated as

$$\frac{Q_{out}}{\dot{m}_{wf}} = (h_2 - h_3) \quad \textbf{(3.8)}$$

The thermal efficiency (η) of ORC is 14.8 %, which is defined as

$$\eta = \frac{w_T - w_p}{Q_{in}} \quad \textbf{(3.9)}$$

The expression (3.8) can be modified as

$$\eta = \frac{(h_1 - h_2) - (h_4 - h_3)}{Q_{in}} \quad \textbf{(3.10)}$$

3.3 Energy and Mass Balance in the simulation process

The energy and mass balance are checked during the simulations using the Thermolib model of the ORC. The commands used are listed in Appendix A5. The energy balance for some components in the model is not equal to zero due to the inaccuracies resulting from the integration procedures but is within acceptable accuracy. The mass balance is achieved throughout the system automatically since this is the input parameter.

Table 3.6 shows the energy balance analysis results for the simulation model of the ORC (computational time is 1,000 seconds).

Table 3.6 Energy balance in the components of the ORC system with R245fa as the working fluid

Components	**Port Name**	**Energy (kJ)**
Pump	Flow in	-23.564
	Flow out	20.319
	P_el	3.243
Balance		-0.002
Turbine	Flow in	240.512
	Flow out	-198.665
	P_mch	-41.847
Balance		0.00

The results of the mass balance check are shown in Table 3.7

Table 3.7 Mass Balance of the ORC as results of Simulink/Thermolib simulations in case of R245fa

Components	Port Name	Flow Direction	R245fa (kg/s)
Pump	Flow in	in	1
	Flow out	out	1
Balance			0
Turbine			
	Flow in	in	1
			1
Balance			0

3.4 Discussion of simulation results for the simple ORC with HCFC-245fa as the working fluid

In this section, the modelling results from Simulink/Thermolib simulations demonstrate that the selected approach produces correct results. As expected, the computational results show an increase in thermal efficiency with the evaporator pressure. At the critical pressure of HCFC-245fa, the thermal efficiency has the maximum value. The thermal efficiency of the modelled ORC system with operating parameters indicated in Tables 3.2-3.5. The power consumed by the pump is (W_p) 3.243 kW. The amount of heat rate (Q_{in}) added to the evaporator working fluid is 258.32 kW. The mechanical power of the turbine (W_t) is 41.847 kW. The rate of heat rejected in the condenser (Q_{out}) is 220.14 kW. The net power output of the cycle (W_C) is 38.604 kW. Table 3.8a is showing the thermal efficiency of the cycle.

Table 3.8a Thermal performance of the ORC model using R245fa working fluid

Working Fluid	**R245fa**
Pump input work rate (W_p)	3.243 kW
Evaporator heat input rate (Q_{in})	258.32 kW
Turbine output work rate (W_t)	41.847 kW
Heat rejection rate in the condenser (Q_{out})	220.14 kW
Thermal efficiency of the cycle (η)	14.944%

The simulation model of the ORC is shown in Fig. 3.4. The simulation model calculates the thermal state and properties (temperature, pressure, enthalpy, entropy, heat capacity etc.) of the working fluid. The mass flow rate of the working fluid is given as 1000 g/sec, and the turbine's outlet pressure is taken as 1 bar. Table 3.8b shows the calculation of the output power of the turbine for different values of pressure in the evaporator. The evaporator input heat (Q_{in}) increases with the rise in pressure up to 26 bars and decreases with a further increase in the evaporation pressure. The pump work input rate (W_p) continuously increases with a higher value of the pressure. As a result, the cycle efficiency rises with an increase in the evaporator pressure for the R245fa working fluid.

Table 3.8b Effect of vapor pressure of R245fa on thermal efficiency

Evaporation Pressure (bar)	Evaporation Temperature (K)	Pump input work rate (W_p) kW	Evaporator heat input rate (Q_{in}) kW	Turbine output work rate (W_t) kW	Condenser heat rejection rate (Q_{out}) kW	Thermal Efficiency (%)
15	380.7	1.323	260	35.33	226.1	13.07
18	389.4	1.607	264.1	37.62	228	13.64
22	399.6	2.20	267.4	39.92	229.5	14.19
26	408.5	2.363	268.8	41.51	229.6	14.57
29	414	2.647	268.2	42.23	228.6	14.71
35	421.9	3.214	258.3	41.44	220.1	14.87

Fig. 3.8 shows that higher pressures in the evaporator correspond to the elevated operating temperatures in the evaporator. These values are determined using the NIST database.

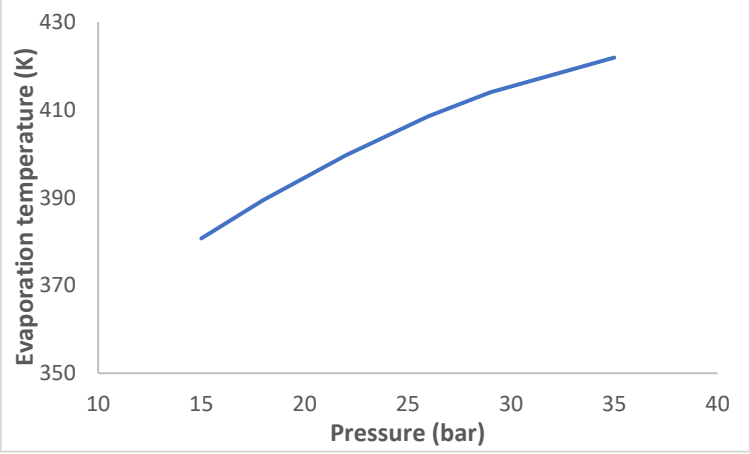

Figure 3.8 Relation between temperature & pressure for HCFC-245fa

Fig. 3.9 demonstrates that after exceeding the pressure level of 25 bar, the rise in the cycle efficiency slows down.

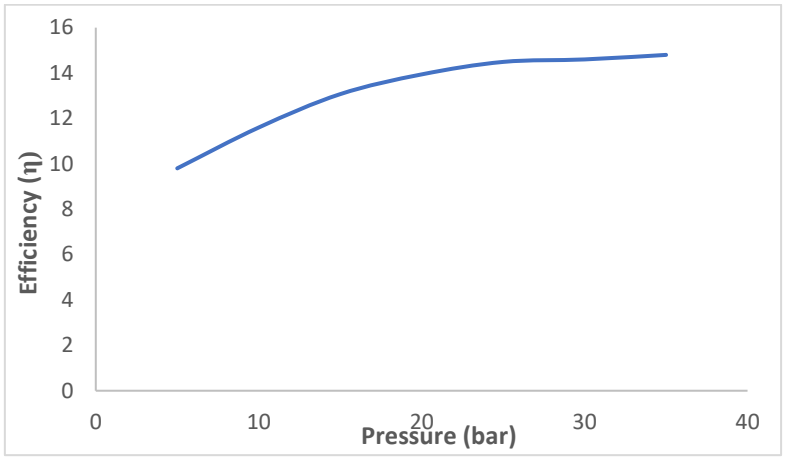

Figure 3.9 Relation between pressure & efficiency in case of R245fa

The kinetic and potential energy losses are assumed to be negligible at the inlet and outlet of the turbine. The isentropic efficiency of the turbine was considered to be 75 %. The mechanical work generated by a turbine system has a linear dependency on the working fluid mass flow rate (as shown in Fig. 3.10).

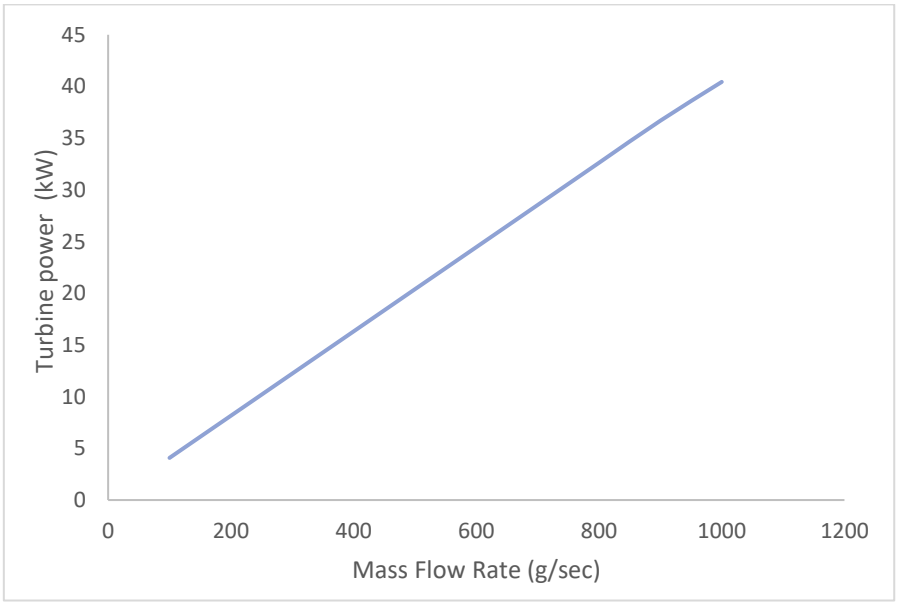

Figure 3.10 Relation between mass flow rate of the working fluid and turbine power in case of R245fa

The above results demonstrate the correctness of the developed modelling method, which now can be used for other types of working fluids.

3.5 Performance Analysis of the ORC system run on different Organic Working Fluids

The developed model of the simple ORC was used to simulate its operation on different organic working fluids. These fluids have different critical temperature and pressure values and other physical and chemical properties. The modelling was performed using equations 3.1-3.12 for ethanol, iso-pentane, n-propane, methanol, HCFC-32, and HCFC-134a. Table 3.9a shows the properties of the working fluids. As mentioned above, for simplicity of comparison, the working fluid mass flow rate was assumed to be 1 kg/sec for all fluids, with condensing pressure being 1 bar. Some of the considered fluids cannot be used in practice at the condensing pressure of 1 bar due to condensation temperatures significantly below the ambient one.

The isentropic turbine efficiency is the ratio between the turbine real work output to the turbine work output under ideal conditions. It can be expressed using the expression below in the enthalpy change during the compression process.

$$\boldsymbol{\eta = \frac{h_{in} - h_{out}}{h_{in} - h_{ideal}}} \qquad \textbf{(3.11)}$$

The turbine typical isentropic efficiency value is between 0.7 and 0.9 (70%-90 %). In calculations, the isentropic turbine efficiency is assumed to be 75 %, as reported by a number of researchers in the literature, e.g. [14, 16]. The real power output of the turbine is determined as the product of isentropic power and isentropic efficiency.

Table 3.9b shows the operating conditions used in modelling with different working fluids Table 3.9c presents information on the individual component performance of the ORC system.

Table 3.9a Characteristics of investigated working fluids [178-182]

Working fluid	Chemical Formula	Molar mass (g/mol)	Boiling point at 1 atm (°C)
R245fa	$C_3H_3F_5$	134.05	40.0
Ethanol	C_2H_5OH	46.07	78.24
iso-Pentane	$CH_3(CH_2)_3CH_3$	72.15	27.83
n-Propane	$CH_3CH_2CH_3$	44.1	-42.1
Methanol	CH_3OH	32.04	64.7
R32	CH_2F_2	52.02	-51.65
R134a	CH_2FCF_3	102.03	-26.5

Table 3.9b Operating conditions with the different working fluids

Working fluid	Mass flow rate (g/sec)	Evaporation pressure P_c (bar)	Evaporation temperature T_c (K)	Condensation pressure P_{cd} (bar)
R245fa	1000	36.5	427.16	1
Ethanol	1000	61.4	514	1
iso-Pentane	1000	33.7	460.35	1
n-Propane	1000	42.3	370	1
Methanol	1000	81	513	1
R32	1000	57.8	351.11	1
R134a	1000	40.5	374.23	1

Table 3.9c Performance of the ORC system with different working fluids

Working fluid	**Q_{in} rate kW**	**W_T rate kW**	**Q_{out} rate kW**	**η**	**W_{cycle} rate kW**
R245fa	258.32	41.4	220.14	14.8	38.180
Ethanol	693	146.4	733	17.04	99
iso-Pentane	542	88	461	14.9	81
n-Propane	482	92	400	17.23	82
Methanol	939	180	773	17.61	166
R32	327	65	268	18.17	59
R134a	236.96	40.1	200.61	15.33	36.349

The selection of working fluid depends on the available heat source and sink temperatures. The working fluids such as HCFC-32 and HCFC-134a are suitable for the low-temperature application of the ORC system. Methanol requires a large value of the input heat energy for evaporation and provides a higher value of the thermal efficiency as compared to the HCFC-245fa. The application of such a working fluid usually requires higher values of the heat source temperature.

3.6 Evaluation of the ORC System with regenerative heating (heat recovery)

The regenerative ORC system was studied by numerous authors, e.g. [167-169]. As it was described in previous sections, in the regenerative ORC cycle, the part of the thermal energy of the working fluid exiting the turbine is used to preheat the working fluid flowing to the evaporator. The preheating takes place in the special heat exchanger, which is called the heat recovery heat exchanger.

The operating conditions and working fluids used in the regenerative ORC system are the same as used in the modelling of the simple ORC system, and the cycle results are compared to the thermal performance of the simple ORC. Such comparison helps to understand the recovery heat exchanger impact on the ORC system performance. Fig. 3.11 shows the calculation scheme of such regenerative ORC cycle. The same assumptions are in the modelling of the regenerative ORC system.

3.6.1 Thermodynamic Modelling of ORC system with heat recovery

This section presents the results of the modelling of the ORC system with heat recovery (regeneration). The power (W_p) required to circulate the R245fa by the pump is 3.02 kW. The inlet pressure of the working fluid to the turbine is 35 bar, and its corresponding temperature is 425.4 K. The target temperature in the condenser is 315.8 K at pressure one bar. The power output (Wp) in the turbine is 41.4 kW. The net power output is defined as

$$\mathbf{W_C = W_T - W_P} \qquad \mathbf{(3.12)}$$

and is 38.38 kW.

The heat recovery exchanger increases the working fluid temperature from 288.6 K to 300.6 K. The temperature of the working fluid then rises to 425.4 K in the evaporator. Due to the heat added to the cycle from an external source, the heat is added at the rate of 243.3 kW, which results in the efficiency of the cycle being 15.8%.

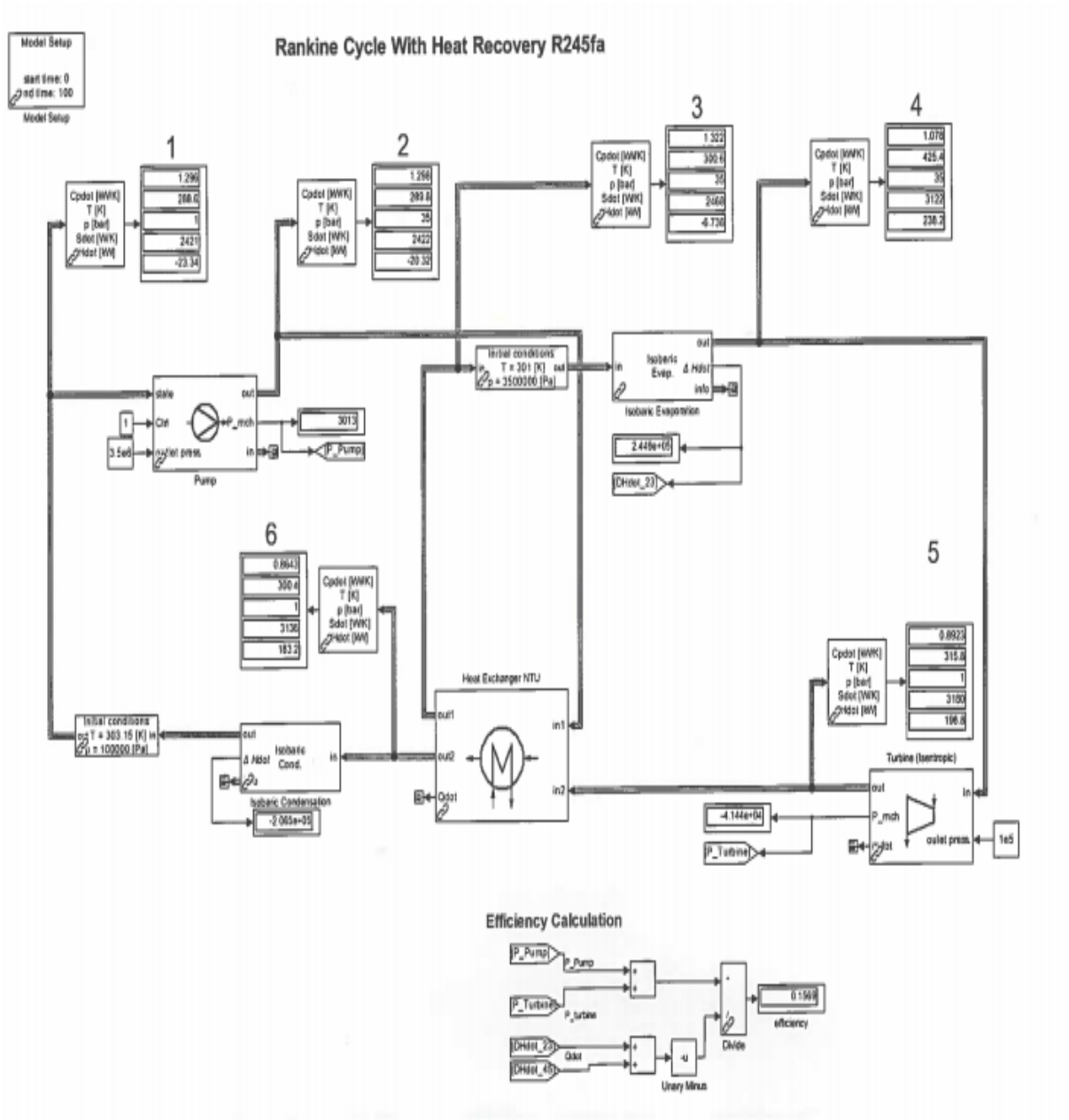

Figure 3.11 Schematic diagram of the regenerative ORC cycle in the Simulink/Thermolib environment

3.6.2 Design Considerations for Heat Exchanger

The number of transfer units (NTU) method is applied to calculate the heat exchanger effectiveness and calculate the overall heat transfer coefficient under steady-state conditions. The heat exchanger transfers the heat from the outlet fluid stream of the turbine to the

evaporator input fluid stream. It is recovering the part of the heat energy before the condensation of the HCFC-245fa fluid stream. The heat exchanger model is based on the counterflow fluid streams pattern, as shown in Fig. 3.12. The area of the heat exchanger assumed to be 20 m^2. The heat losses to the environment considered to be zero.

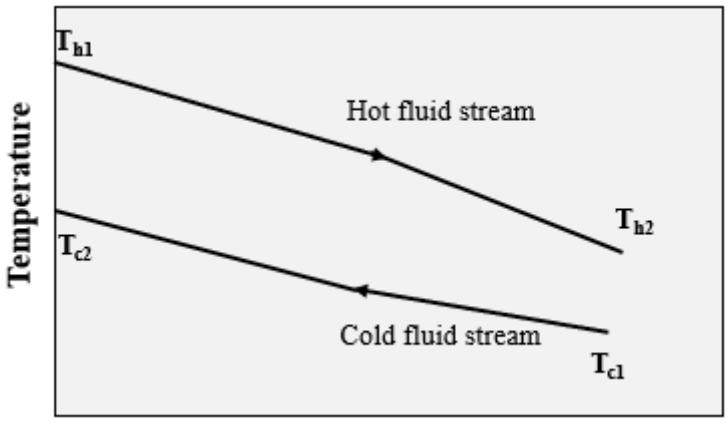

Figure 3.12 Counterflow fluid streams of the heat exchanger

The thermophysical properties of the R245fa working fluid were determined using the NIST database for the hot and cold fluid temperatures (T_{h1} and T_{c1}) at the inlets of the heat exchanger. The hot and cold fluid temperatures (T_{h2} and T_{c2}) in the outlets of the heat exchanger are determined using the NTU method. Table 3.10 shows the operating parameters of the HCFC-245fa flow in the heat exchanger used in the calculations.

Table 3.10 Operating parameters in the recovery heat exchanger

Property	**Value**
Hot Fluid Temperature at Inlet (T_{h1})	315.8 K
Hot Fluid Temperature at Outlet (T_{h2})	303.97 K
Specific Heat of Hot Fluid ($C_{p,\,hot}$)	0.892 kJ/K kg
Cold Fluid Temperature at Inlet (T_{c1})	289.6 K
Cold Fluid Temperature at Outlet (T_{c2})	297.72 K
Specific Heat of Cold Fluid ($C_{p,\,cold}$)	1.298 kJ/K kg

To find the heat exchanger effectiveness (ϵ), it is necessary to find the maximum heat transfer (Q_{max}) of the heat exchanger. The maximum heat depends on the heat capacity rate and the difference between the hot fluid temperature at the inlet (T_{h1}) and cold fluid temperature at the inlet (T_{c1}) of the heat exchanger. The mass flow rate of the R245fa is 1 kg/sec in both flow streams. The hot fluid capacity (C_h) rate is 0.892 kW/K, and the cold fluid heat capacity rate (C_c) is 1.298 kW/K and is calculated as

$$C_h = \dot{m}\, C_{p,\,hot} \tag{3.13}$$

$$C_c = \dot{m}\, C_{p,\,cold} \tag{3.14}$$

Here the specific heat ratio $\mathbf{Cr = C_{phot}/\ C_{pcold} = 0.69}$

The maximum heat exchange rate (Q_{max}) between hot and cold fluid streams is 15.706 kW and is calculated as

$$Q_{max} = C_{min}\,(T_{h1} - T_{c1}) \tag{3.15}$$

The hot fluid temperature (T_{h2}) and cold fluid temperature (T_{c2}) at the outlets of the heat exchanger are 303.97 K and 297.72 K, respectively and are determined from

$$T_{h2} = T_{h1} - \frac{Q_{max}}{\dot{m}c_{P,hot}} \tag{3.16}$$

$$T_{c2} = T_{c1} - \frac{Q_{max}}{\dot{m}c_{P,cold}} \tag{3.17}$$

The effectiveness (ϵ) of the heat exchanger is 0.45 for the above parameters of HCFC-245fa and is calculated as

$$\epsilon = \frac{C_{p,cold}\left(T_{c_2} - T_{C_1}\right)}{C_{p,min}\left(T_{h_1} - T_{C_1}\right)} \tag{3.18}$$

The actual heat exchange rate between fluid streams is 7.086 kW and is calculated as

$$Q_{\,actual} = \epsilon\, C_{p,\,min}\,(T_{h1} - T_{c1}) \tag{3.19}$$

In the case of the counterflow concentric tube heat exchanger and Cr < 1, the number of transfer units (NTU) is 0.7277 and is calculated as

$$NTU = \frac{1}{C_r - 1} \ln \frac{\epsilon - 1}{\epsilon C_r - 1} \tag{3.20}$$

The overall heat transfer coefficient (U) is 25.11 W/m^{2}K and is calculated as

$$U = (NTU \times Cr) / A \tag{3.21}$$

3.7 The Energy and Mass Balance in Reheat ORC

Tables 3.11a and 3.11b present the results of energy and mass balance checks for the recovery heat exchanger, turbine and pump obtained during simulations of the regenerative ORC with HCFC-245fa as a working fluid. The results show that energy and mass balances are observed in the simulation process.

Table 3.11a Energy Balance in regenerative Organic Rankine Cycle

Components	**Port Name**	**Flow Direction**	**Energy (kJ)** (1.541)
Heat Exchanger (NTU)			
	Qdot environment	-	0
	In1	Flow in	-19.62
	In2	Flow in	18.801
	Out1	Flow out	0.680
	Out2	Flow out	-17.478
	Thermal mass-energy stored at the start		2.491
	Thermal mass-energy stored at the end		2.531
Balance	-	-	0.0006
Pump			
	In	Flow in	-22.521
	Out	Flow out	19.511
	P_el	-	3.008
Balance	-	-	0.000973
Turbine (Isentropic)			
	In		227.610
	Out		-186.001
	P_mch		-41.609
Balance	-	-	0

Table 3.11b Mass Balance in regenerative Organic Rankine Cycle

Component	Port Name	Port Direction	R245fa (kg/s)
Heat Exchanger (NTU)			
	In1	Flow in	1
	In2	Flow in	1
	Out1	Flow out	1
	Out2	Flow out	1
Balance			0
Pump	In	Flow in	1
	Out	Flow out	1
Balance			0
Turbine (Isentropic)			
	In	Flow in	1
	Out	Flow out	1
Balance			0

3.8 Results of the simulations of the regenerative ORC with different working fluids

Table 312 present results of simulation of the regenerative ORC cycle run on various working fluids. There is an increase in efficiency for all considered working fluids when using the heat recovery heat exchanger.

Table 3.12 Results of simulations of the regenerative ORC with different working fluids

Parameters	n-propane	iso-pentane	R134a	R32	Methanol	Ethanol
Heat added rate (Q_{in}) (kW)	443	530	212	316.1	935	685
Heat rejected rate (Q_{out}) (kW)	382	432	182	240	770	725
Turbine work rate (T_w) (kW)	92	88	40	65	180	146.4
Thermal efficiency (η)	18.83	15.24	17.22	18.94	17.68	17.11

3.9 Conclusions

The mathematical models of the simple and regenerative ORC cycles were developed in Simulink/Thermolib environment. Results obtained in simulations compared to thermodynamic calculations of the cycle performance and accuracy of the developed models were confirmed.

The effect of the cycle heat recovery heat exchanger depends on its effectiveness which is determined by the temperature difference between the hot and cold fluids at the heat exchanger inlets. For considered operational conditions in the cycle, the heat exchanger effectiveness was determined to be 0.53, 0.395, 0.36 and 0.529 for n-propane, iso-pentane, R134a and R32, respectively. The methanol and ethanol have a small temperature difference between the hot and cold fluid flow, and the heat exchanger effectiveness value was below 0.20, which means that heat recovery is low. Table 3.13 shows a comparison of efficiencies of simple and regenerative ORC cycles for different working fluids. Results demonstrate an increase in efficiency when the recovery heat exchanger is used, but the magnitude of the increase depends on the critical parameters of the working fluid and may vary from being considerable (R134a) to negligible (Ethanol). Since the additional heat recovery exchanger makes the system more complex in design and increases its capital cost, the decision on the application of such cycles should be made as a result of the careful technical-economic analysis in each type of application.

Table 3.13 Comparison of efficiencies of simple and regenerative ORC cycles for different working fluids

Working fluid	Regenerative ORC Efficiency	Simple ORC Efficiency
R245fa	15.76	14.8
n-propane	18.83	17.23
iso-pentane	15.24	14.9
R134a	17.22	15.33
R32	18.94	18.17
Methanol	17.68	17.61
Ethanol	17.11	17.04

Chapter 4: A Small Solar Thermal Power Generation System

This chapter presents the results of the small ORC simulations, coupled with the solar field made of non-concentrating solar collectors, to supply heat input. The energy transfer between the collector and ORC takes place via an intermediate heat exchanger. The thermodynamic modelling was performed for the case in which HCFC-134a was used as the working fluid in the ORC. The model calculates the heat energy generated by the solar collector field, the number of transfer units of the heat exchanger and thermal energy input to the ORC's evaporator. The simulation model was developed in MATLAB/Thermolib 5.2 environment, and the day-long performance of the Solar Organic Rankine Cycle (SORC) was determined. The water is the heat transfer fluid for the solar collector field. The total solar irradiance value was determined using the Meteonorm database at the latitude angle of 41.305^{o}, which corresponds to Almatret (Spain). The GA approach was implemented in the Simulink model of the SORC to determine the turbine optimized design variables.

4.1 Introduction

Solar thermal power systems are widely used in different applications, including space heating and domestic hot water [183,184]. The ORC plants are coupled to a wide range of concentrating and non-concentrating solar collector types [185,186]. Several works were published with studies on ORC plants powered by solar energy. Wang et al. [187] presented results on the ORC performance running on 245fa and powered by solar energy to demonstrate that it was a feasible way of generating power. Declaye et al. [188] proposed a small-scale solar power plant with an ORC with a capacity of up to 3 kW. The ORC worked in the temperature range of 140 ^{o}C and 35 ^{o}C in the evaporator and condenser. The thermal efficiency of the ORC was determined to be 14 %. The mass flow rate of the working fluid was 64.3 g/sec. Yamamoto et al. [189] proposed an ORC plant powered by a low-grade heat source. A simulation model of the ORC was developed in which the HCFC-123 working fluid was used. A heat exchanger was used to transfer the waste heat to the evaporator of the ORC. F. Velez et al. [190] performed the Organic Rankine Cycle thermodynamic analysis with a maximum of 150 ^{o}C by using HCFC-134a as the working fluid. The simple Rankine cycle thermal efficiency was 11%, and

it was increased to 14 % with the deployment of the internal regenerative heat exchanger. Suresh et al. [191] presented results of the analysis of the SORC, considering the area of the collector, solar heat input, and thermal efficiency by using HCFC-245fa, HCFC-123, HCFC-114b and ethanol as working fluids. The simulation was carried out, and economic modelling was performed for SORC with the power of 1 kW. E. Spayde et al. [192] evaluated the SORC performance, running on HCFC-218, HCFC-227ea, HCFC-236ea, HCFC-236fa, and HCFC-318 as working fluids. A. Odhiambo et al. [193] investigated the performance of the SORC with HCFC-245fa as the working fluid. The temperature in the exit from the solar field was 163.5 ^{o}C, and the turbine output power was determined to be 33.34 kW. The system's thermal efficiency was found to be 14.55 %. Z. Jesko et al. [194] considered the non-concentrating solar collector with a maximum efficiency of 50% and a temperature range of up to 200 ^{o}C. C. Kraphan et al. [195] described a solar ORC coupled with evacuated tube solar collectors and operate in Thailand's climate conditions. The ORC generates the power of 280 kW by using HCFC-245fa as the working fluid, and the estimated electricity generation cost of the system varied between 0.37 and 0.43 USD/kWh. Idrus et al. [196] experimentally determined an ETC system thermal performance based on the water as the working fluid at pressure 6 bar. The aperture area of the collector was 240 $m^{2,}$ and this generated 70 kW of thermal energy in the peak hour of a day.

Tchanche et al. [197] investigated the different types of working fluids for a low-temperature solar ORC. Rayegan et al. [198] investigated 117 organic fluids, considering their temperature-entropy diagrams, and analyzed the cycle's net power, thermal efficiency, exergy efficiency, and vapour expansion ratio. Y. He et al. [199] investigated the influence of the selection of the working fluid, evaporation temperature, and flow rates on the efficiency of the SORC using the developed simulation model in TRNSYS. Santiago et al. [200] analyzed a simple organic Rankine cycle (ORC) using five different working fluids that include two isentropic fluids (HCFC-11 and HCFC-12), one wet fluid (HCFC-717), and two dry fluids (benzene and HCFC-113). These fluids have boiling temperatures in the range from 33.35℃ to 79.85℃. The results show that higher system thermal efficiency was achieved when the HCFC-11 and HCFC-113 working fluids were used. Tchanche et al. [201] also investigated different fluids and suggested that HCFC-134a was the most suitable working fluid for a low-temperature solar ORC. The schematic of the ORC and its T-s diagram are shown in Fig. 4.1.

The heat is added to the working fluid in the evaporator. The heat source is the heat transfer fluid flowing from solar collectors. The working fluid is converted into vapour during isobaric heating. The high-pressure vapour expands in the turbine to produce mechanical work and is discharged to the condenser. The cooling water or coolant is used for heat rejection during the condensation process, and vapour turns to liquid. The pump circulates the liquid to the evaporator by increasing its pressure to the level in the evaporator. The thermodynamics cycle can be presented using a T-s diagram.

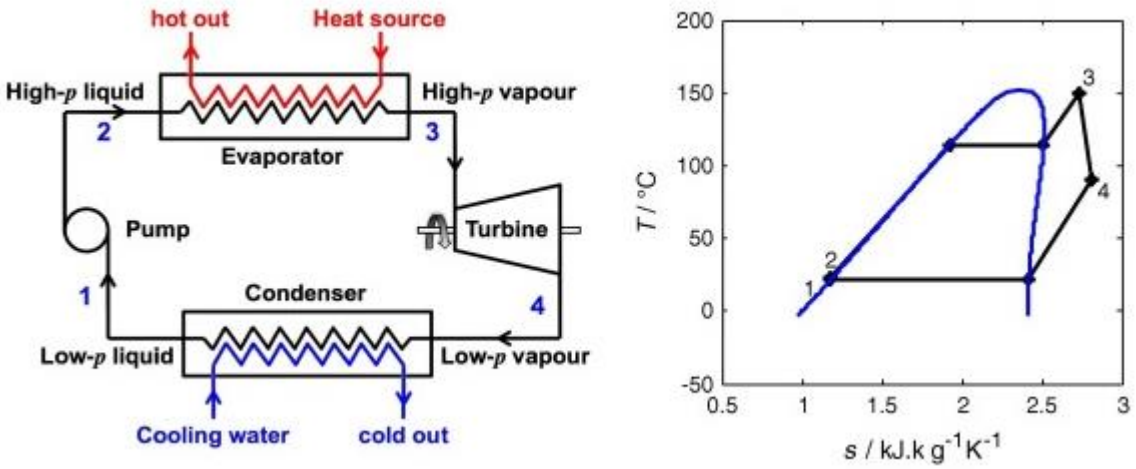

Figure 4.1 Schematic of the ORC system and T-s diagram of the cycle [202]

4.2 Description of the simulation scheme of the SORC plant under investigation

Fig. 4.2 shows the simulation scheme of the Solar Power Organic Rankine Cycle under investigation. The SORC plant contains the solar field, pump, evaporator, turbine and condenser of the ORC. Thermal energy is delivered to the ORC from the solar collector via a heat exchanger. A PI controller used, which maintains the desired pressure of the vapour in the evaporator. A liquid tank stores the heat transfer fluid that is circulated within the solar field. The heat exchanger block transfers the heat from the heat transfer fluid of the solar field to the working fluid of the ORC. The HCFC-134a working fluid is evaporated at 30 bar pressure within the evaporator. The condenser pressure is one bar. The circulating pump of the ORC returns the liquid HCFC-134a to the evaporator.

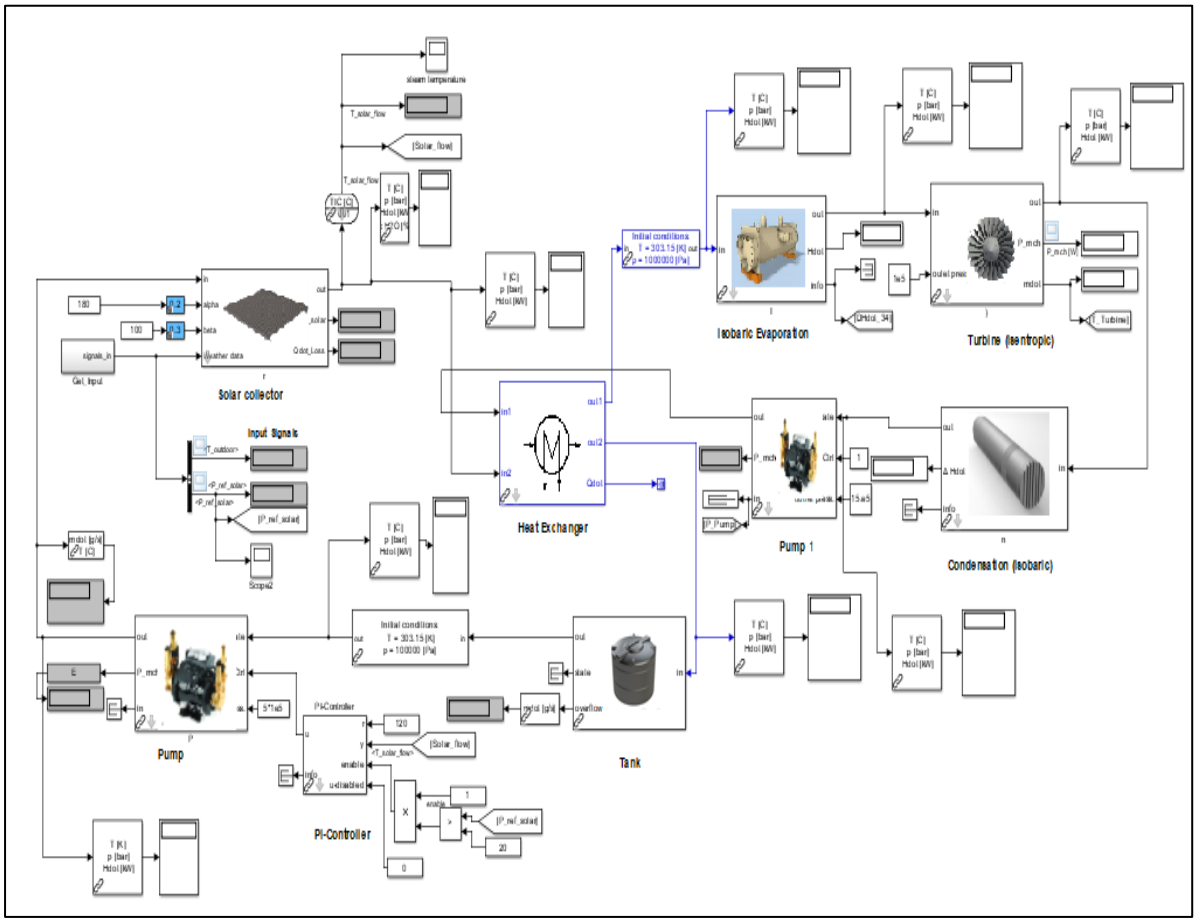

Figure 4.2 Simulation scheme of the Solar Power Organic Rankine Cycle

The mass and energy balance equations are solved for each control volume, considering some assumptions. All processes in the plant components are assumed to be steady-state, and changes in the kinetic and potential energies are neglected. The heat losses in the system components are not considered. The main parameters of the plant are presented in Table 4.1. The proposed system is suitable for small to medium power generation applications. The thermodynamic modelling of ORC carried out using the HCFC-134a as a working fluid in the cycle and water as the heat transfer fluid in the solar field. In July-month, the global horizontal radiation is 243 kWh/m^2 at Almatret's location. The parametric analysis of the plant was performed using the simulation model of the SORC. To generate the thermal output of the solar collector equal to 71 kW, it is necessary to provide the mass flow rate of circulating water equal to 300 g/sec at 2 bar pressure for the size of the collector equal to 600 m^2. The Simulink model of SORC determines the water temperature at the collector's inlet and outlet.

Table 4.1 The key parameters of the SORC plant

Parameter	**Value**
Isentropic pump and turbine efficiency	75%
ECT aperture area	600 m^2
Collector inlet temperature, T_{sc1}	400 K
Collector outlet temperature, T_{sc2}	353 K
HCFC-134a inlet temperature of the heat exchanger, T_{htf1}	312.16 K
HCFC-134a outlet temperature of the heat exchanger, T_{htf2}	359.26 K
The water pressure within the collector	2 bars
The mass flow rate of water	300 g/sec
The mass flow rate of HCFC-134a	200 g/sec

The important step in the modelling process was the selection of the working fluid for the given heat input, determined by the size of the collectors and climatic conditions and the ORC configuration. Table 3.9c presents results on the thermodynamic performance analysis of an ORC system using different types of working fluids, used at the critical pressure value, condensing pressure of 1 bar and mass flow rate of 1000 g/s. The comparison shows that the HCFC-134a working fluid is suited for low to medium temperature heat sources, compared to HCFC-245fa, Ethanol, iso-pentane, n-propane, methanol, and HCFC-32 at their critical states. Additionally, HCFC-134a has a zero ozone depletion potential (ODP) and a lower global warming potential (GWP) value of 1430. It is also non-toxic and non-flammable, and it is commonly used in commercial refrigeration systems. Therefore, HCFC-134a was selected as the working fluids for the proposed SORC system. The ORC using HCFC-134a provides a higher value of thermal efficiency compared to HCFC-245fa and Iso-butane. Some key parameters of HCFC-134a are shown in Table 4.2. The proposed system is suitable for small to medium power generation applications.

Table 4.2 Main characteristics of HCFC-134a and H_2O [78]

Fluid properties	**R134a**	**Water**
Chemical Formula	CH_2FCF_3	H_2O
Molar mass	102.03 g/mol	18 g/mol
Critical temperature (T_c)	101.06 ^oC	373.946 C
Critical pressure (P_c)	40.5928 bar	220.640 bar
Critical density (D_c)	511.90 kg/m^3	322 kg/m^3
Melting point	-103.3 ^oC	0 ^oC
Normal boiling point	-26.074 ^oC	100 ^oC

The solar collector absorptance coefficient β depends on the surface material. The optical efficiency *(η_{opt})* of the ETC depends on the outer tube transmittance, inner tube absorptance, and incidence angle modifier coefficient *(IAM)*. Table 4.3 shows the specification of the Apricus type ETC used in this work. It has high values of the collector tube absorptance and transmittance.

Table 4.3 Specification of Apricus type ECTs [203]

Property	**Value**
Length of each absorber tube (mm)	513±5
Inner tube diameter (mm)	46.99
Outer tube diameter (mm)	57.912
Coating material	Cu-Al/N-SS
Glass material	Borosilicate glass
Absorptance	>93%
Emittance	<8%
Transmittance	>90%

Below the simulation schemes of each plant component are presented, which are based on conservation of energy and mass principles. During the simulation, parameters in the inlet and outlet (mass flows, energy) are indicated.

Fig. 4.3 shows the simulation scheme for the Solar Collector. Here α is the azimuth angle which varies during the day. The sunshine duration of the specified location (Almatret) is approximately 11 hours in July. The simulation model is designed to run 86400 seconds to evaluate the day performance of the plant. The weather conditions may also affect the solar collector performance by reducing solar irradiance under cloudy conditions. During the modelling, first, the value of the solar zenith angle is determined. It depends on the Latitude; Month, Day and Time. Using the solar radiation database for the fixed location, the amount of solar radiation on the collector and thermal energy produced by the solar collector is calculated. It is assumed that heat losses to the environment are zero. The collector fluid passes through the thermal mass component, which regulates the solar collector target temperature. A PI controller is used to control the target temperature of the collector fluid. The target temperature is 400 K at pressure 2 bar, and the mass flow rate of water is 300 g/sec.

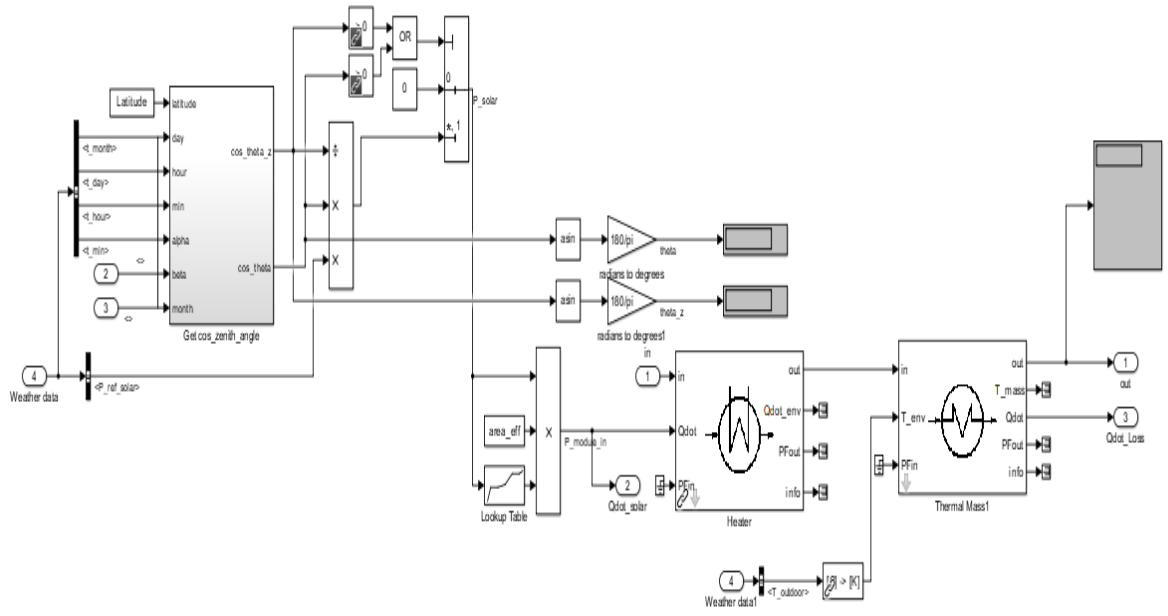

Figure 4.3 Simulation scheme for the Solar Collector

Fig. 4.4 shows the Simulink scheme of the heat exchanger to calculate the heat transfer between the water and HCFC-134a. The overall heat transfer coefficient (UA) is calculated using the NTU method. The energy stored is defined as the thermal energy accumulated by the heat exchanger material overall mass. It is assumed that there are no heat losses in the heat exchanger.

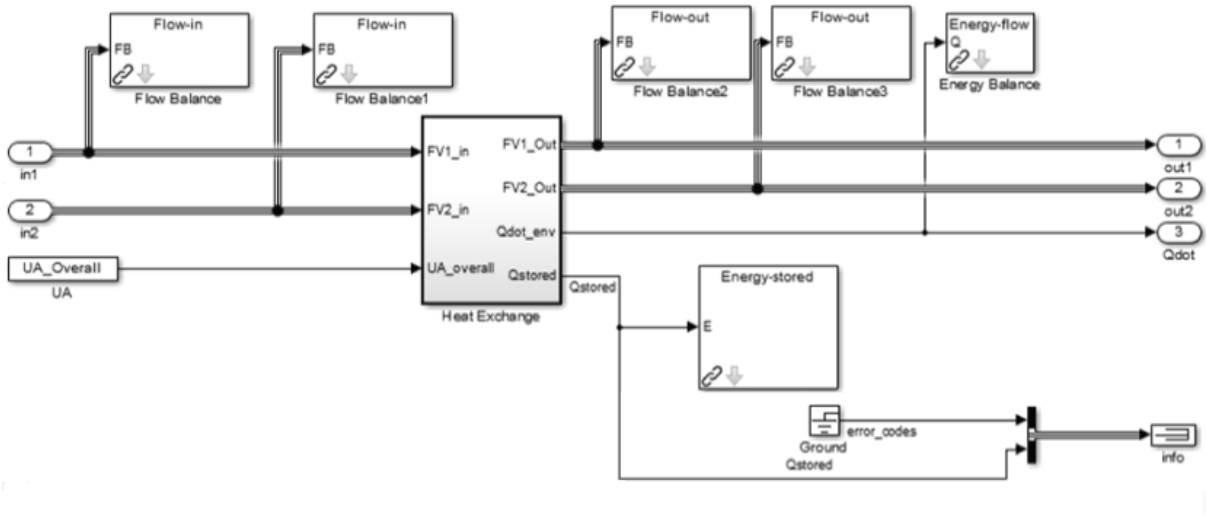

Figure 4.4 Simulation scheme of the Heat Exchanger

The heat exchanger's thermal mass is defined by the mass of the heat exchanger (kg) and heat capacity of the material (J/kg-K), and it is measure in J/K. Fig. 4.5 shows the schematic for the thermal mass of the heat exchanger. The two flow streams enter the heat exchanger, and some heat is stored as the thermal mass of the heat exchanger. The amount of heat exchange is calculated as

$$\mathbf{Q_{stored} = mCp\ \Delta T} \qquad \mathbf{(4.1)}$$

Here m is the mass of the heat exchanger, Cp is the heat capacity of the materials of the heat exchanger, and ΔT is the temperature difference between the fluid and the material of the heat exchanger.

The total energy stored is equal to the sum of the heat transferred from two fluid streams ($\dot{Q}_{TM1}$ and $\dot{Q}_{TM2}$).

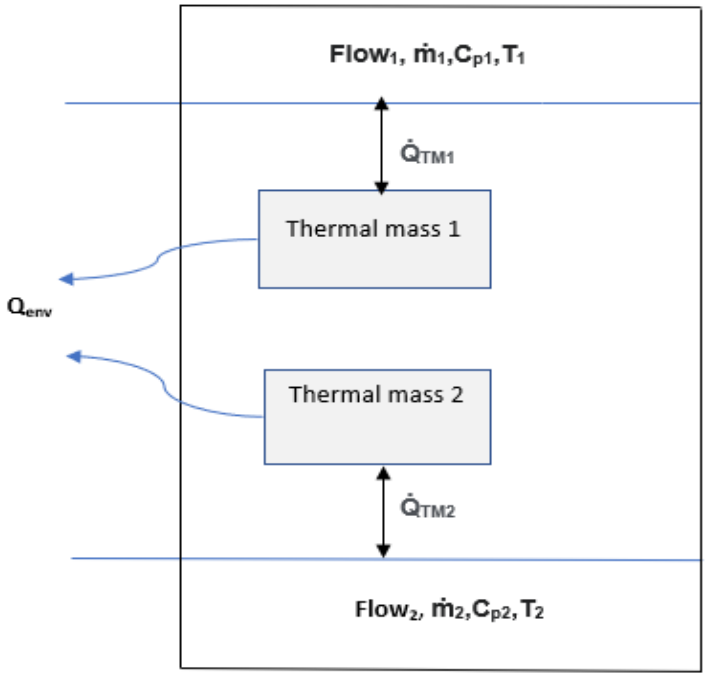

Figure 4.5 Thermal mass of the heat exchanger

Fig. 4.6 shows the calculation scheme of the evaporator and condenser of the ORC. The flow bus (FB) indicates the flow between blocks and contains the fluid thermodynamic properties. The saturation temperature of the fluid is calculated using the Antoine equation as

$$\mathbf{T} = \frac{\mathbf{B}}{\mathbf{A} - \mathbf{Log}(\mathbf{P})} - \mathbf{c} \qquad \textbf{(4.2)}$$

where A, B, and C are the Antoine coefficients equal to 4.02877, 686.188, and -26.945, respectively, and p is the pressure (bar) [204].

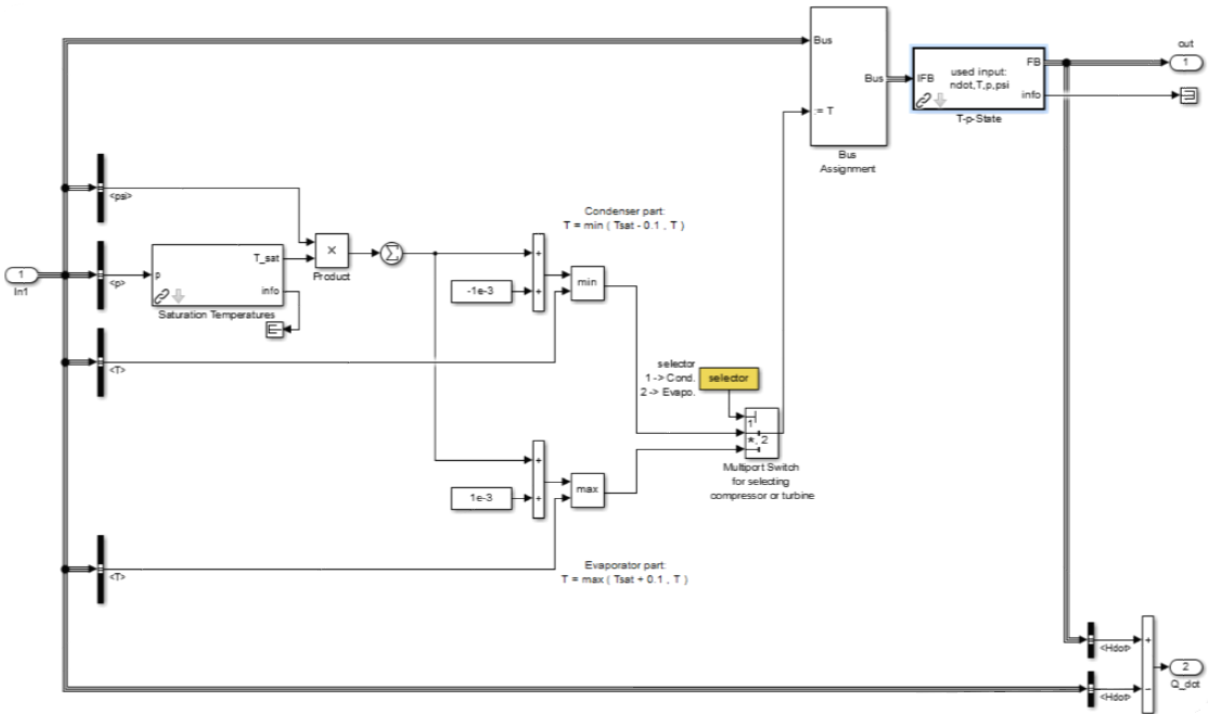

Figure 4.6 Simulation scheme of the Evaporator or Condenser in the ORC

Fig. 4.7 and 4.8 show the schematics of the turbine and pump for simulations. The power output from the turbine is defined as

$$\boldsymbol{P_{tis}} = \dot{m}(\boldsymbol{h_{tin}} - \boldsymbol{h_{tout}}) \qquad \textbf{(4.3)}$$

The isentropic efficiency (η_s) of the turbine should be used to take into account losses during the expansion process:

$$\boldsymbol{\eta_s} = \frac{\boldsymbol{\Delta h}}{\boldsymbol{\Delta h_s}} \qquad \textbf{(4.4)}$$

The real power output of the turbine (P) of the turbine is modified as

$$\mathbf{P_t = \dot{m}\ x\ \eta_s\ x\ \Delta h_s} \qquad \textbf{(4.5)}$$

The isentropic power input to pump is

$$\boldsymbol{\dot{m}_p}\left(\boldsymbol{h_{pin}} - \boldsymbol{h_{pout}}\right) = (\mathbf{P_{pout} - P_{pin}})/\boldsymbol{\rho} \qquad \textbf{(4.6)}$$

where ρ is the fluid density.

The real pump power input is

$$\boldsymbol{P_p} = \frac{\dot{m}\boldsymbol{\Delta P}}{\boldsymbol{\eta\rho}} \qquad \textbf{(4.7)}$$

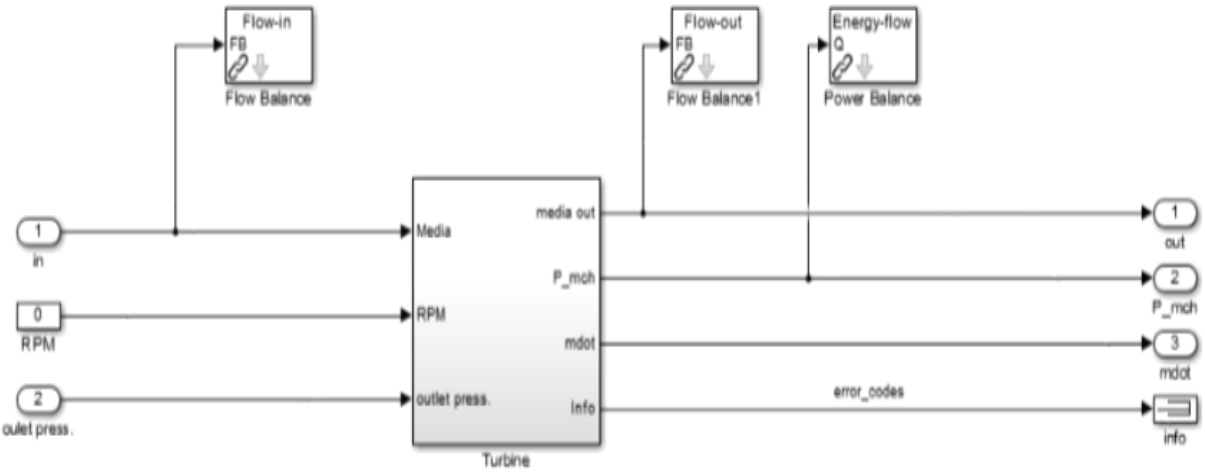

Figure 4.7 Simulation scheme of the Turbine

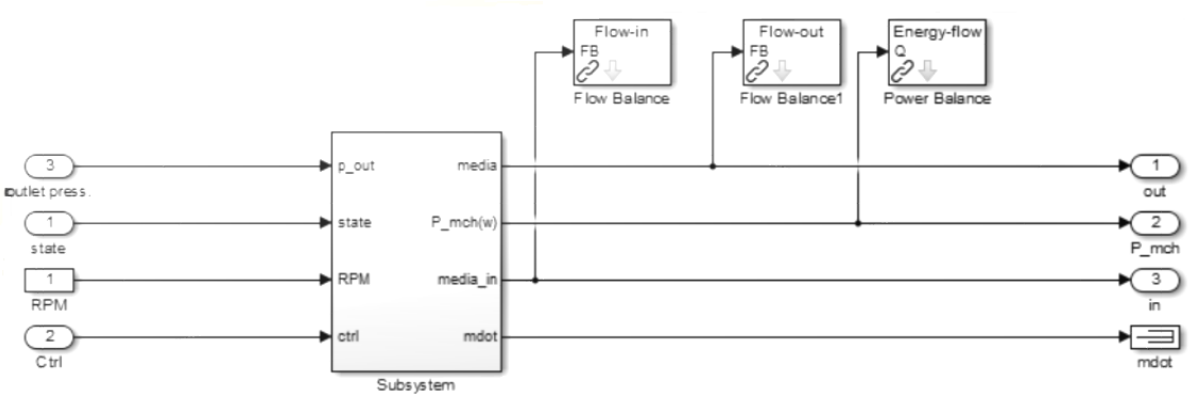

Figure 4.8 Simulation scheme of the Pump

4.3 Determination of the total Irradiance value

The performance of the SORC is directly proportional to the solar irradiance. As mentioned above, it is necessary to calculate the total solar irradiance at the plant location during the simulation process. This is the variable parameter, which also depends on the time of the year. This parameter was determined using Meteonorm, which is a software tool and provides the standard global solar data for engineer, education and planners. Meteonorm has the built-in library with the Global Energy Balance Archive (GEBA). Meteonorm calculates the yearly, monthly, hourly and minute values of the global, direct and diffuse solar irradiance on the horizontal and inclined surfaces of any geographical location [205]. The SORC is modelled

using the Meteonorm solar irradiance data for Almatret. The data for total global irradiance is presented in Table 4.4. It can be seen that the peak values of the solar irradiance are observed during the summer period in June and July. Table 4.4 shows the average monthly values of the Global horizontal radiations (GHI), air temperature (Ta), dewpoint temperature (Td), and wind speed (FF).

Fig. 4.9 shows the GHI variation during each month of a year with the maximum values in the summer period and a minimum value in December and January.

Fig. 4.10 shows the average sunshine duration for Almatret, which influences the performance of the solar collector. The sunshine duration is approximately 4.5 hours during January and 11 hours in July. The average daily GHI in July reaches to 9 kWh/m^2.

Table 4.4 Meteonorm Radiation interpolation data for Almatret [205]

Month	**GHI** kWh/m^2	**Ta** ^{o}C	**Td** ^{o}C	**FF** m/sec
January	63	7.9	2.3	3.2
February	88	9.4	2.5	3.5
March	138	12.2	4.1	3.6
April	172	14.5	6.3	3.6
May	208	18.4	9.6	3.3
June	226	23.2	12.9	3.2
July	243	25.1	14.8	3.4
August	205	25	14.7	3.2
September	155	21.3	12.9	3
October	108	17.3	10.7	2.8
November	74	11.7	5.2	3.2
December	55	8.1	2.8	3.2
Annual	1732	16.2	8.2	3.3

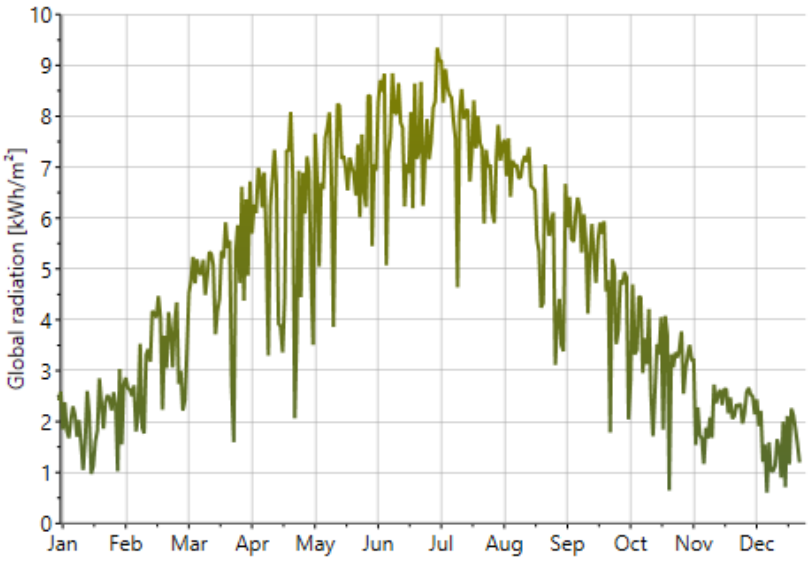

Figure 4.9 Meteonorm GHI Interpolation Data (Almatret) [205]

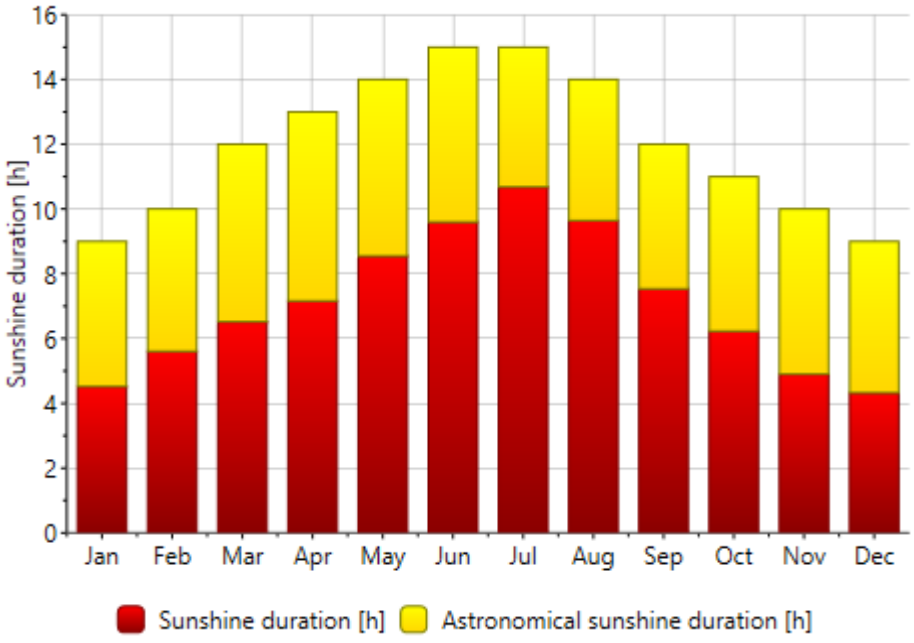

Figure 4.10 Meteonorm Sunshine Duration Data (Almatret) [205]

Solar Declination Angle

Solar declination angle δ is the angle between the sun rays and earth equator. It depends on the number of days and varies within a range of ±23.45°. This variation causes the seasonal change on earth and has a maximum value of 23.45° in summer on June 21. The minimum value is -

23.45° on 20 December. The graphical representation of the declination angle is shown in Appendix 6.

The value of this angle is defined as

$$\boldsymbol{\delta = 23 \cdot 45 sin\left[360\left(\frac{284+n}{365}\right)\right]} \quad \textbf{(4.8)}$$

where 'n' is the number of the day of the year. For example, for the 2nd July, n is 183; therefore, $\delta = 23.04^{o}$. The solar declination angles for some days in the year are shown in Table 4.5.

Table 4.5 Solar Declination angles

Month	Day	Year	Solar Declination
Jan.	17	17	-20.19
Feb.	16	47	-13
March	16	75	-2.4
April	15	105	9.4
May	15	135	18.8
June	11	162	23.1
July	2	183	23.04
Aug.	16	228	13.5
Sep.	15	258	2.2
Oct.	15	288	-9.6
Nov.	14	318	-18.9
Dec.	10	344	-23

The solar altitude or zenith is the angle *h* between the zenith and the centre of the sun. It determined by using the following expression.

$$\textbf{sinh = sin}\delta\textbf{sin}\phi\textbf{ + cos}\delta\textbf{cos}\phi\textbf{cosw} \quad \textbf{(4.9)}$$

where ϕ is a local latitude angle.

The solar azimuth angle α determines the position of the sun on the sky is

$$\sin\alpha = \frac{\cos\delta\sin w}{\cos h} \quad (4.10)$$

The angle of incidence for the horizontal solar thermal collector θ_i is calculated as

$$\cos\theta_i = \sin\delta\sin\phi + \cos\delta\cos w\cos\phi \quad (4.11)$$

If the surface faces the south and have a 45° tilted angle *(β)*from the horizontal position, then the incidence angle is

$$\cos\theta_i = \sin\delta\sin(\phi - \beta) + \cos\delta\cos w\cos(\phi - \beta) \quad (4.12)$$

4.4 Results and Discussion

The set of equations used for thermodynamic modelling of the operation of the plant. The amount of solar energy absorbed by the surface of the collector *(Q_c)* depends on the inlet *(T_{sc1})* and outlet temperature *(T_{sc2}),* specific heat and steady flow mass flow rate of the fluid circulated within the collector

$$Q_c = \dot{m}c_p(T_{sc2} - T_{sc1}) \quad (4.13)$$

The ETC is mounted with a fixed orientation and tilt angle of 45°. The collector's cylindrical tube surface absorbs the maximum amount of solar irradiance all over the day**.** The efficiency (η) of the collector can be defined as

$$\eta = \eta_{opt} - a\frac{(T_m - T_a)}{G_h} - b\frac{(T_m - T_a)^2}{G_h} \quad (4.14)$$

The ambient temperature T_a=25 °C, the mean temperature *(T_m)* is the average value of the tube inlet and outlet temperatures and constants a and b are the heat loss coefficients. The heat loss coefficients of the collector vary with the temperature. European Solar Thermal Industry Federation (ESTIF) produced the heat loss coefficients values for the ETCs system, shown in Table 4.6.

Table 4.6 Heat loss coefficients of the ETCs [206]

Parameter	Value
a - first-order heat loss coefficient	1.2 Wm^{-2}
b - second-order heat loss coefficient	0.008 $Wm^{-2}K^{-2}$

The effectiveness (ϵ) of the intermediate counterflow heat exchanger depends on the ratio of the temperature difference of heat transfer fluid and working fluid and the specific heat capacity of fluids:

$$\boldsymbol{\epsilon = \frac{C_{p,hot}(T_{sc2} - T_{sc1})}{C_{p,cold}(T_{sc2} - T_{htf1})}} \quad \textbf{(4.15)}$$

The number of transfer units (*NTU*) of the counterflow heat exchanger depends on the specific heat capacity ratio of hot and cold fluid streams and the effectiveness of the heat exchanger:

$$\boldsymbol{NTU = \frac{1}{C_r - 1} \ln \frac{\epsilon - 1}{\epsilon C_r - 1}} \quad \textbf{(4.16)}$$

The overall heat transfer coefficient *(U)* of the heat exchanger depends on the number of transfer units (*NTU*) and specific heat capacity ratio and area of the heat exchanger (A_{HE}):

$$\boldsymbol{U = (NTU \times Cr) / A_{HE}} \quad \textbf{(4.17)}$$

The equations for calculating the ORC performance are presented in Chapter 3 (Eq. 3.4-3.10). Table 4.7 shows the plant calculated performance parameters for maximum mass flow rates of the HFT in the solar field and working fluid of the ORC.

Table 4.7 ORC operating parameters

Parameter	Value
Net output power (kW)	4.274 kW
Isobaric evaporator operating temperature at 30 bar	359.26 K
Isentropic turbine outlet temperature (K) at 10 bar	334.17 K
Isobaric condensation outlet temperature (K) at 10 bar	312.16 K
Adiabatic pump outlet temperature (K)	310.88 K

The results show that the plant site declination angle is 23.04^{o} for the 2nd of July. The zenith angle *(h)* is 67.66^{o} at 1:00 PM of local time. The position of the sun in the sky is 32.78^{o}. In the case of the solar collector horizontal surface, the incident angle (θ_i) of solar radiation is 22.27^{o}. If the collector is tilted towards the southwest at 45^{o} (β), the incidence angle (θ_i) is 30.46^{o}. Fig. 4.11 shows variations of the global horizontal irradiance *(GHI)* and direct normal irradiance *(DNI)*, and diffuse horizontal irradiance *(DHI)* during the day. Results show the average values of the solar irradiance during the July month at the Almatret's geographical position. Fig. 4.12 shows the variation in the collector field thermal power output during the day-time in July. The results were calculated using the MATLAB/Thermolib 5.2 simulations for the specific design consideration (as discussed above) and Almatret's geographical position. The simulations of the SORC took 86400 seconds. The collector field produces the maximum thermal power at the level of 71 kW at 1:00 PM. The power output of the plant will have the same trend of variation during the day.

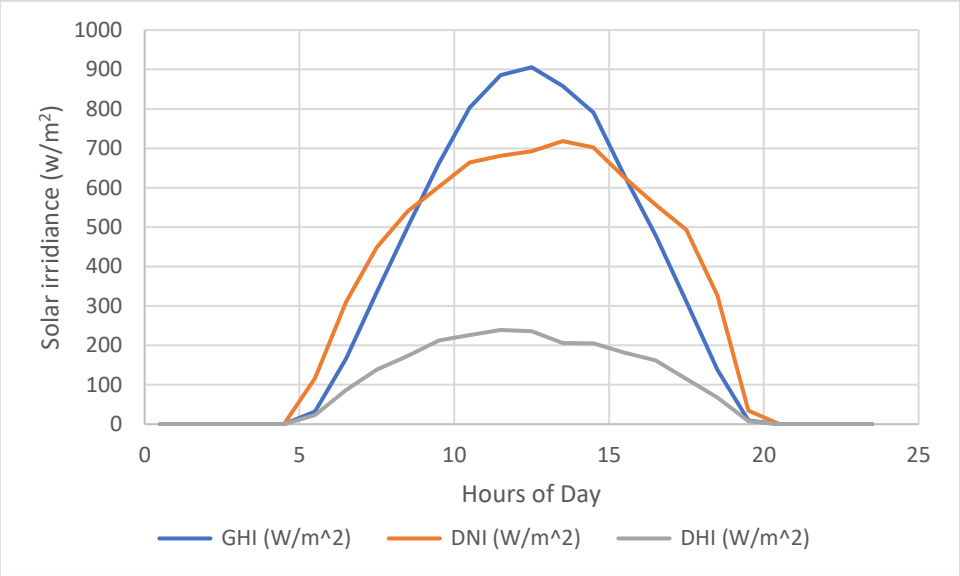

Figure 4.11 Solar irradiance variation on 2 July

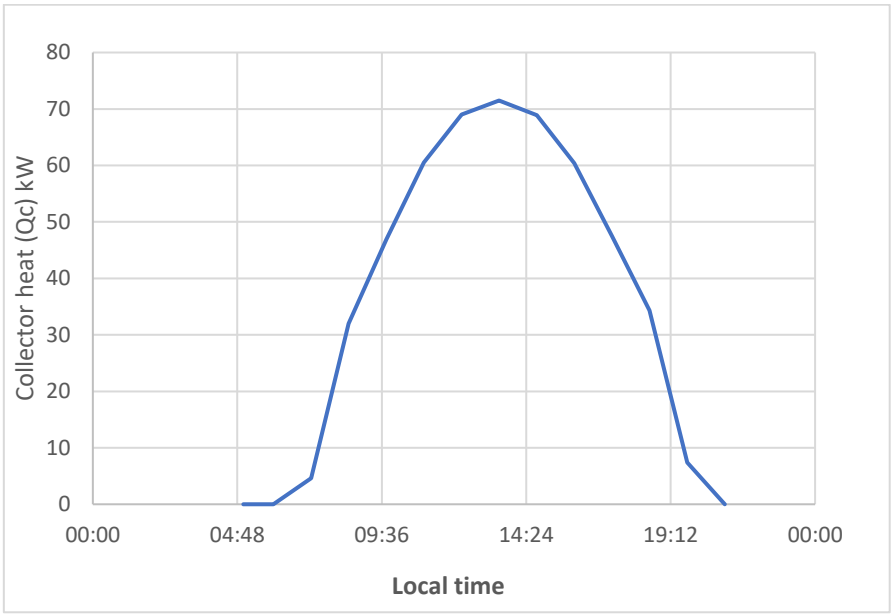

Figure 4.12 Thermal power generated by the solar field during the day

Fig. 4.13 shows the variation in the input energy required by an HCFC-134fa in an evaporator to generate a corresponding power by the turbine as a function of the working fluid mass flow rate. The evaporator input energy of 39.94 kW provides 4.274 kW of the turbine power at the mass flow of the working fluid equal to 200 g/sec.

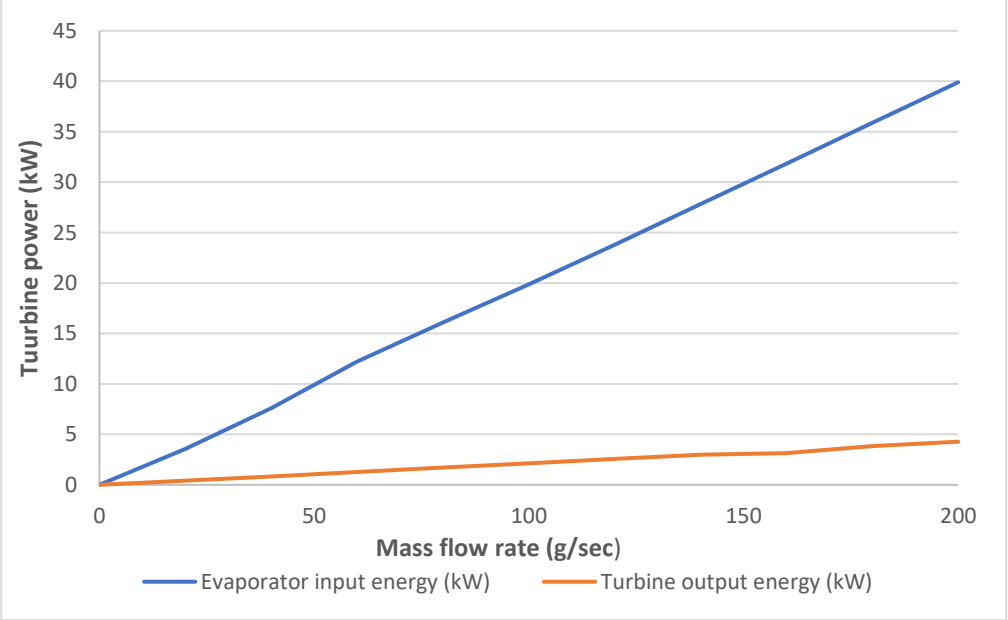

Figure 4.13 Effect of mass flow rate in the evaporator and turbine output

The thermal efficiency of the ORC depends on the power output of the turbine. Fig. 4.14 shows the influence of the turbines outlet pressure (pressure in the condenser) on the turbine power output for the evaporator's pressure of 30 bar and mass flow rate of the working fluid R134a equal to 200 g/sec. The turbine produces the maximum power of 11.9 kW at the outlet pressure of one bar. But at this pressure, the working fluid temperature after condensation is 252.6 K (not practical). At the higher values of the outlet pressure, the output power decreases, and the turbine produces 6 and 4.274 kW of power at the outlet pressure of 6 and 10 bar.

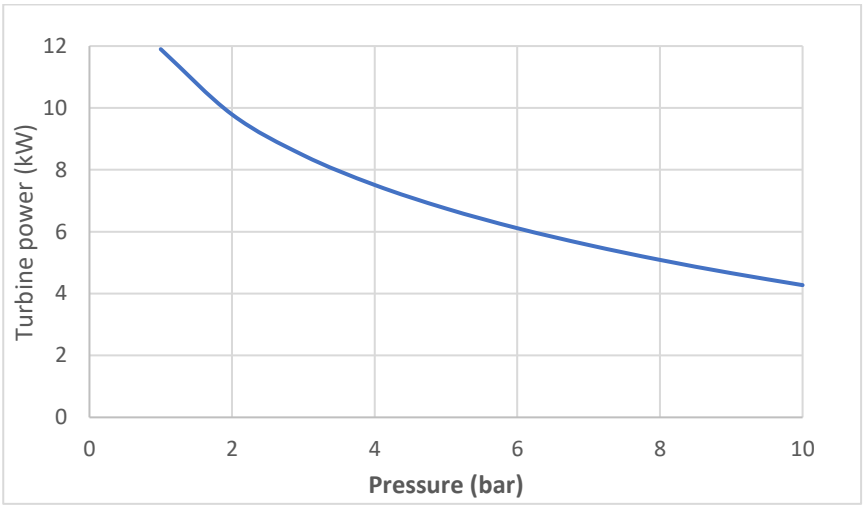

Figure 4.14 Effect of the turbine outlet pressure on the power generated by the turbine

The specific heat capacity ratio (C_r) of heat transfer fluid and working fluid is 0.684, and the effectiveness (ϵ) of the intermediate heat exchanger is 0.7829 at 1:00 PM. The number of transfer units *(NTU)* is 2.386, and the overall heat transfer coefficient *(U)* is 108.52 W/m^{2}K for the area of the heat exchanger (A_{HE}) equal to 15 m^2. The thermal energy input (Q_{in}) of 39.94 kW is required to vaporize the R134a working fluid at the 30-bar pressure and generate the output power (w_t) of 4.274 kW. The pump requires 0.4347 kW of input power to raise the fluid pressure from 10 to 30 bar. The thermal efficiency of the ORC system is 10.58 %.

Table 4.8 shows the thermal performance of the SORC model using 30 bar evaporation pressure and 10 bar turbine output pressure of the working fluid for various mass flow rates of the working fluid in the cycle. As expected, there is a linear correlation between an increase in the turbine output power and an increase in the mass flow rate of the working fluid. The thermal

efficiency of the ORC insignificantly decreases due to a more rapid increase of the pump power input.

Table 4.8 Performance of the ORC using the variation of the mass flow rate of R134fa fluid

$\dot{m}$ (g/sec)	$Q_{in,\ evp}$ (kW)	$W_{in,\ p}$ (kW)	$W_{out,\ T}$ (kW)	$Q_{out,\ C}$ (kW)	Efficiency (η)
50	9.597	0.1067	1.069	9.22	11.01 %
75	14.76	0.163	1.603	13.68	10.742 %
100	20.02	0.2168	2.167	18.24	10.708 %
125	24.79	0.217	2.671	22.6	10.681 %
150	29.85	0.326	3.206	27.36	10.62 %
175	34.87	0.380	3.740	31.93	10.609 %
200	39.94	0.4347	4.274	36.49	10.58 %

4.5 Genetic Algorithm Optimization of the SORC

The optimization is used to achieve the best performance of the plant under given operational conditions. The goal function is the minimized energy input or maximised output work. The optimization results in finding the set of different design and operational parameters (variables) to reach the goal function minimum or maximum value. There are a large number of optimization techniques. The Genetic Algorithm (GA) approach is an example of a global optimization solution [207] and is widely used in the engineering models. M. Feidt et al. [208] developed an analytical approach to optimize solar ORC. The objective function was the maximum power output as a function of the temperatures, the effectiveness of the heat exchanger, heat transfer and mass flow rates. J. Sun et al. [209] investigated the optimization of the SORC system running on HCFC-134a as the working fluid. ROSEN algorithm optimization was implemented to maximize the net output power generations base by varying a number of parameters, including the mass flow rates and heat source temperature. J. Wang et al. [210] carried out the thermodynamic analysis of the ORC operating on the low-grade heat source. The GA was implemented to optimize the Rankine cycle output power. Y Feng et al. [211] compared the results of the basic ORC and regenerative ORC. The GA was applied to optimize the Levelized energy cost by varying the evaporator and condenser temperatures and degree of superheat. L. Zhai et al. [212] investigated the thermodynamic performance of the ORC based on the radial-inflow turbine system. The flow rate of the working fluid in the

turbine was optimized by using the GA approach and varying the rotational speed, loading coefficient, degree of reaction, and velocities ratio.

The optimization of the SORC based on the GA approach [213]. R. L. Haupt et al. [214] described the MATLAB code for the GA optimization. K. Kraitong [215] modified this code to optimize the operating parameters of a Stirling engine. B. Belgasim [216] implement the code to optimize the theoretical and experimental model of the solar desalination unit. K. Hossin [217] optimized the hybrid solar/biomass ORC using GA optimization. The similar approach and code used in this work. The system generates 4.274 kW of output power by using HCFC-134a as the working fluid. The optimization process requires an objective function to maximize system performance. The SORC system performance is defined by the turbine output power, evaporator input heat, and fluid mass flow rate. These factors also determine the economic characteristics of the ORC. The power produced by the turbine is the main parameter of the SORC system and is used as an objective function. The GA optimization changes variable parameters between upper and lower limits and finds the best values of variable parameters within range to maximize the system performance. The SORC system variable parameters are listed in Table 4.9 below, with their upper and lower values (for the previously modelled ORC with the evaporator pressure 30 bar and condensation pressure 10 bar,).

Table 4.9 Upper and lower limits of the ORC variables for GA optimization

Parameter	**Lower bound**	**Upper bound**
Mass flow rate of R134a, M_R	150 g/sec	200 g/sec
Evaporation Temperature, Tc	300 K	400 K
Evaporator input heat, Q_{in}	30 kW	80 kW
Turbine outlet pressure, P_{out}	9.5 bar	11 bar

The combination of the above parameters is the chromosome in the GA procedure:

$$\textbf{chromosome} = (M_R, Tc, Q_{in}, P_{out}) \qquad (4.18)$$

The chromosome is defined in the Thermolib model of the SORC. The GA method maximises the turbine output work, which is achieved with a certain chromosome:

$$\mathbf{Q_{mech,\,T} = f\,(chromosome) = (M_R, Tc, Q_{in}, P_{out})} \qquad \mathbf{(4.19)}$$

The initialization of the population is the first step of the GA process. The population is the set of the chromosome, and genes are the variable parameters to reproduce the generation. The population has N_p chromosomes and N_v variables. The matrix N_p x N_v is used to generate random values for each generation. The evaluation of each chromosome is carried out using the fitness function. An individual chromosome can compete further if it has a certain fitness score. The chromosome with a higher fitness value is selected for the next generation, and the rest are discarded. The selection rate parameter is also used with recommended value of 50 %. For two-parent chromosomes selected for a pairing process, a crossover-point random selection process is used to form new offsprings, as shown in Fig. 4.15 and 4.16.

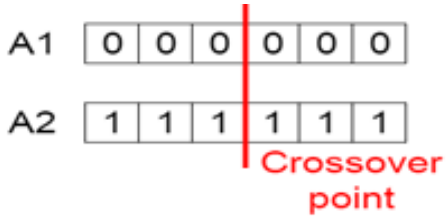

Figure 4.15 Crossover of two offsprings

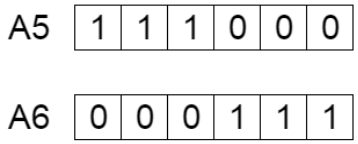

Figure 4.16 Formation of new offsprings

The mutation operation is also used to increase the genetic diversity of the new offsprings. The simplest method is to flip a part of the offspring, and the recommended size of this part is 20% [214]. Fig. 4.17 shows the mutation process of the offspring.

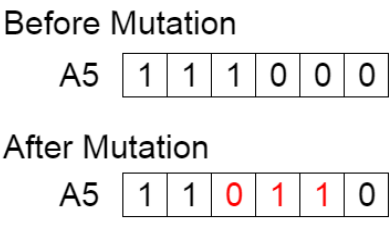

Figure 4.17 Mutation of the offspring

The GA approach continues the change of chromosomes until it produces the optimum one, maximising the objective function. If there is no change in the value of offspring compared to the previous generation, then GA terminates the process. The above GA algorithm was implemented as a code in MATLAB to optimize the SORC. The optimized variable parameter maximizes the output power of the turbine. The flow chart of the GA approach for the SORC optimisation is shown in Fig. 4.18. The GA procedure is linked with the MATLAB/Thermolib model of the SORC and works between the upper and lower limits of the selected variables. Table 4.8 shows the control parameters of the GA algorithm for the optimisation of the SORC.

Table 4.10 Control parameters of GA optimization

Control parameters	Value
Population size	30
Maximum generations	80
Selection rate	0.5
Mutation rate	0.2

The variation in the value of the variable parameter increases with the number of generations. In a case, if no variation in the variable value takes place for at least twenty generations, the optimization process has achieved the best value of the variable. Fig. 4.19 shows the variation of the mass flow rate of the working fluid over several generations. It can be seen that the constant value of 665 Kg/hr is achieved after forty generations. It indicates that the optimal value of the mass flow rate of the working fluid R134a is 184.72 g/s.

In the optimisation process, the evaporator pressure initial value is 15 bar with a corresponding saturation temperature of R134a. Fig. 4.20 shows the variation in the evaporation temperature of the fluid with the number of generations. The variation range used is between 300 K and 400 K. The evaporator temperature optimised value is 352 K (the constant value after forty generations).

Fig. 4.21 shows the optimum value of the heat input in the evaporator. The input heat value becomes constant after forty generations. The optimal input required by the working fluid is 37.634 kW.

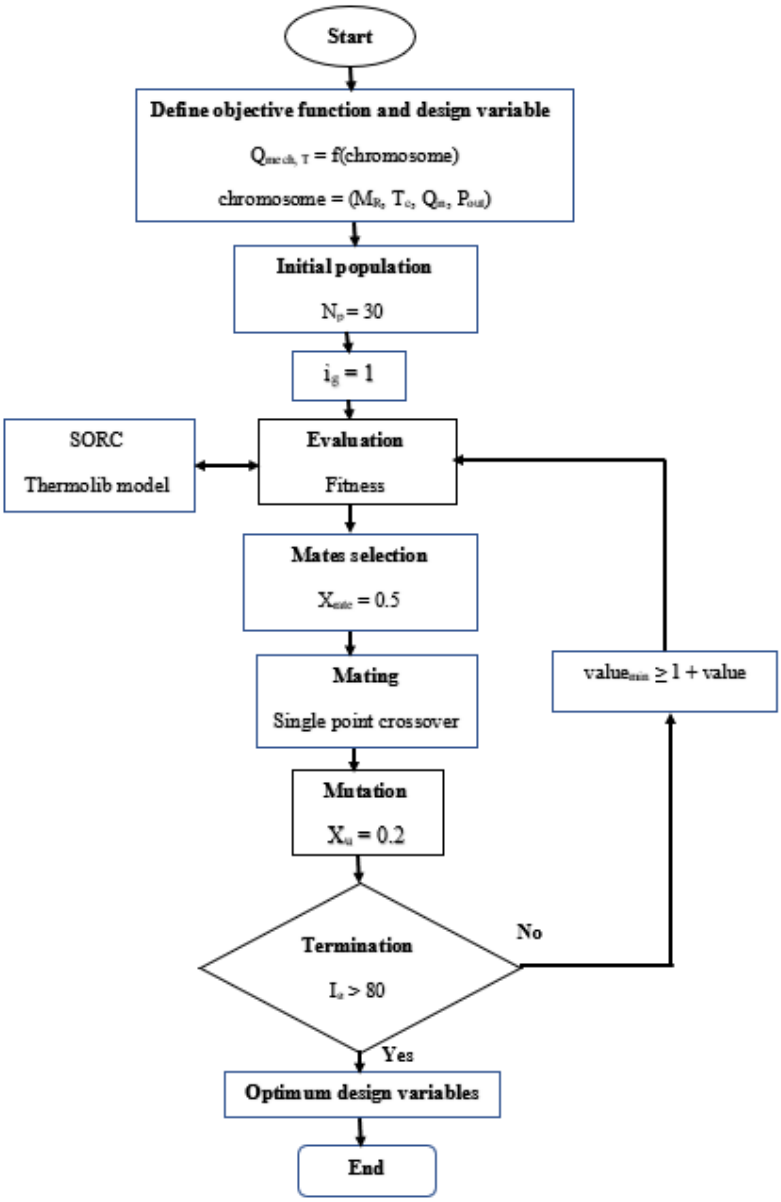

Figure 4.18 Flow chart for GA optimisation to be used with Simulink SORC model

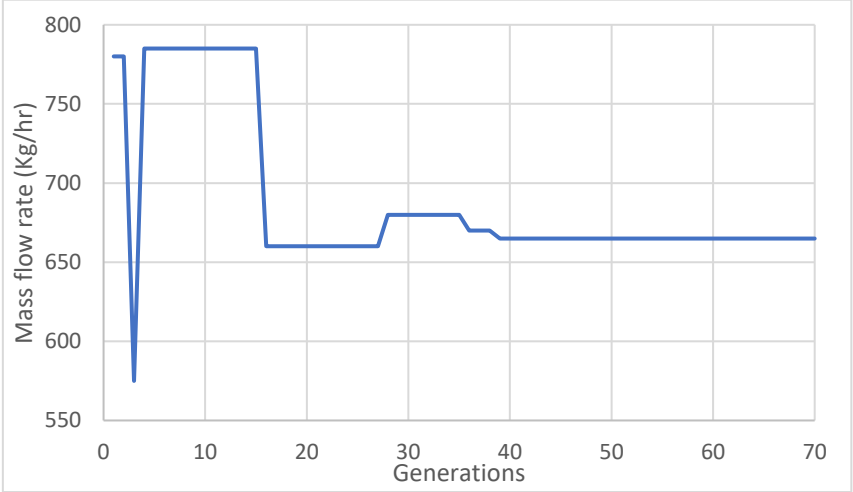

Figure 4.19 Variation of the mass flow rate of the working fluid with an increase in the number of generations

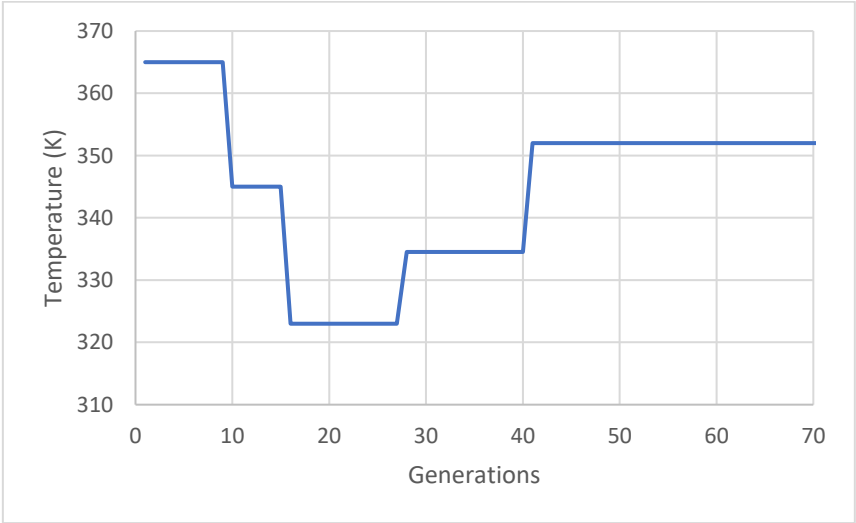

Figure 4.20 Variation of the evaporator temperature with an increase in the number of generations

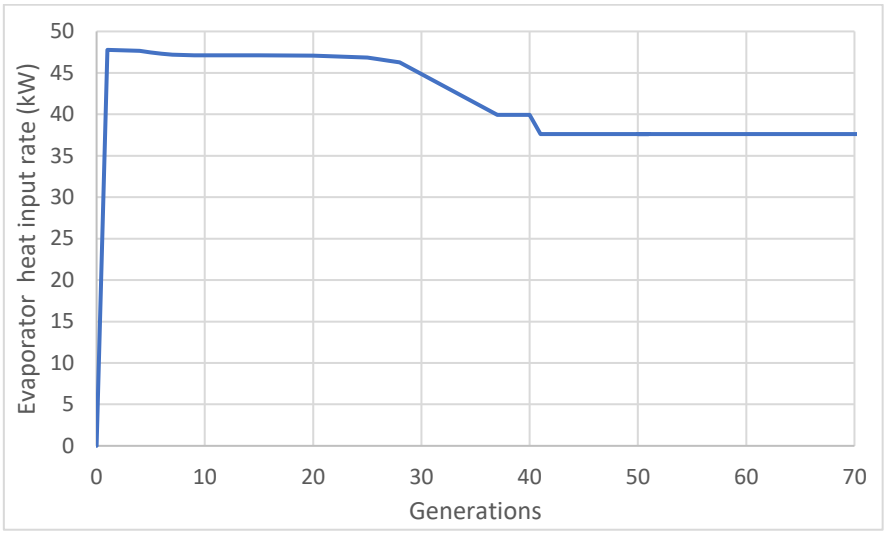

Figure 4.21 Variation of heat input rate with an increase in the number of generations

The performance of the turbine also depends on the condenser pressure value. Fig. 4.22 shows the variation of the condenser pressure with the number of generations. The optimized value of the condenser pressure is 9.92 bar.

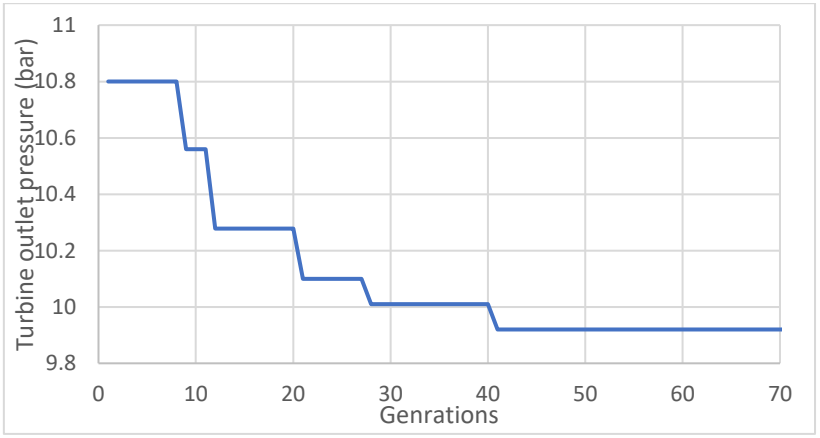

Figure 4.22 Variation of condenser pressure with an increase in the number of generations

As a result of variations of the above variable parameters, the objective function (turbine power output) also changes with generations. Fig. 4.23 shows the variation in the objective function with the number of generations. The turbine power of 4.52 kW is achieved for the optimum values of the variable parameters.

Table 4.11 shows the resulting optimal values of variable parameters and the value of objective function obtained from the GA optimisation process.

Table 4.11 Optimum value of the design variable

Optimum parameters	**Value**
Mass flow rate, M_R	184.72 g/sec
Evaporation Temperature, T_c	352 K
Evaporator input heat, Q_{in}	37.634 kW
Turbine outlet pressure, P_{out}	9.92 bar
Turbine output work, $Q_{mech,\ T}$	4.52 kW

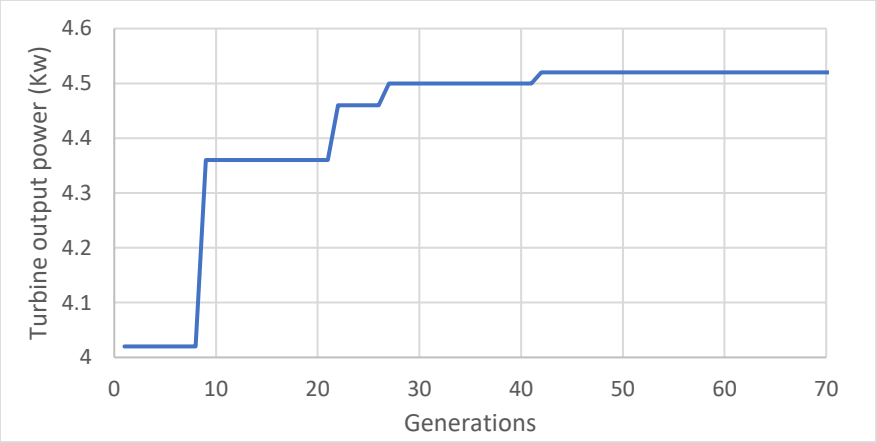

Figure 4.23 Variation of turbine output power with an increase in the number of generations

4.6 Conclusions

The Simulink/Thremolib model of the solar ORC was developed and linked to GA optimisation code in MATLAB. The model of the SORC includes a non-concentrating solar collector field with water as the transfer fluid and a simple ORC plant with HCFC-134a as the working fluid. The model also consists of an intermediate heat exchanger for passing the thermal energy from the solar field to the ORC. The developed model makes it possible to simulate the solar collector operation during the day, and its operation on the 2nd of July was simulated (between 10:30 to 19:00 - sunlight hours). As an example, the SORC plant operation parameters were determined using the solar collector thermal performance at 1:00 PM, and the turbine is producing 4.274 kW mechanical output power. The solar collector performance depends on

the value of the solar irradiance, which changes during a day. There is a linear increase of the turbine power output with the rise of the mass flow rate of the working fluid in the cycle, but the efficiency of the cycle slightly reduces due to a more rapid increase in power required to drive the pump. The GA optimisation for the ORC with the given specification produced that the power plant generates 4.52 kW of peak power with the thermal efficiency increased from 10.58 % to 11.87 %.

CHAPTER 5: Modelling of Linear Fresnel Reflector Collector of the SORC

This chapter describes the Linear Fresnel Reflector (LFR) Model of the SORC plant in Almatret. The numerical modelling developed base on the heat transfer analysis of the solar irradiance to the receiver tube. The optical modelling of the LFR field was carried out using the collector modified design parameters at the plant site with the deployment of the LightTools simulation software based on the Monte-Carlo ray-tracing method. The software calculates the optical performance of the collector field, taking into account the local data on solar irradiance and evaluating the daily performance of the LFR in terms of the total solar thermal energy generated by the system.

5.1 Introduction

Several authors carried out investigations on LFR solar thermal power systems. G. Xu et al. [218] studied the supercritical direct steam generation SORC driven by the LFR. The analysis shows that the operating temperature range of the LFR power system is from 150 ^{o}C to 350 ^{o}C, and cyclohexane is the best working fluid with an efficiency of 19.65 %. J. He et al. [219] presented the geometrical analysis and ray-tracing result in the Fresnel mirror system of equal and varying width and absorber height. The mirrors had the north-south orientation, and the system was modelled with a 5-degree variation in the sun's position. G. Zhu et al. [220] summarized state-of-the-art in the LFR technology and overviewed the design concepts, technical challenges, and performance parameters for intermediate temperature range cases. R. Abbas et al. [221] investigated the effect of the design variables of the LFR system using ray-tracing modelling. R. Grena et al. [222] presented the LFR model for using the molten nitrates as a heat transfer fluid. The thermal and optical analysis of the model was performed and summarised the system advantages and disadvantages. F. Yung et al. [223] investigated the possibility of direct steam generation by the LFR system and proposed using the IAM coefficients to calculate the optical efficiency of the LFR system. P. Boito [224] carried out the LFR system optimisation in terms of the focal length, positioning, and width of the mirrors and performed cost analysis.

N. Kincaid et al. [225] investigated the effect of the solar field optical efficiency on the whole plant thermal efficiency. The ray-tracing algorithm and incidence angle modifier coefficients were used to evaluate the collector performance. The results show that the solar irradiance and latitude position are the critical parameters for the plant site selection. E. Bellos et al. [226] analysed the analytical expression for determining the incidence angle modifier for the LFR system to minimize the optical losses and geometry optimization. A. Barbon et al. [227] evaluated the influence of the transversal and longitudinal parameters on the thermal performance of the LFR system without a longitudinal movement. The analysis was performed to study the effect of the receiver height, mirror width and mirror height on the amount of the thermal energy absorbed by a receiver tube.

P. Tsekouras et al. [228] determined the optical and thermal performance of the LFR system with a trapezoidal cavity receiver and evaluated the receiver thermal and optical performance. David R Mills et al. [229] investigated the conceptual design of the impact of compact linear Fresnel reflector receiver for the power generation system. The system analysed is the Fresnel mirror row directing solar irradiance towards two erected tower type receivers. A. Heimsath et al. [230] conducted the LFR receiver sensitivity analysis. The results show the dependence of the thermal losses on the receiver and secondary reflector specific geometry. R. Manikumar et al. [231] investigated the trapezoidal shape of the LFR receiver system. The thermal energy generated by the LFR system for heating of the working fluid was determined as a result of the numerical and experimental tests. R. Abbas et al. [232] evaluated the different shapes of the secondary reflector for the linear Fresnel technologies and their effect on the system optical performance. It was found that the efficiency of the LFR system with a secondary reflector was 23 % higher as compared to a parabolic trough collector.

5.2 Linear Fresnel Reflector Components

Fig 5.1 shows the main components of the LFR system in Almatret. The main components are the collector, receiver, support structure, and sun-tracking system assembly with piping and safety mechanism instrumentation. The LFR mirrors (primary reflectors) are almost plane in shape, and they are installed on the steel framework in rows and can be turned by step-motors to track the sun position. Several rows of mirrors concentrate solar radiation on the linear receiver mounted above the mirrors at a certain height. The LFR system has additional

components such as oil circulating pump, expansion tank and control instrumentation. The linear receiver captures the reflected solar radiations from Fresnel mirrors and converts this into thermal energy in heated heat transfer fluid, which flows from the absorber tubes. The sun-tracking system is electronically controlled to ensure the LFR focuses reflected solar radiation on the receiver. The receiver is made of a steel tube with the selective coating on its surface and surrounded by the evacuated glass tube.

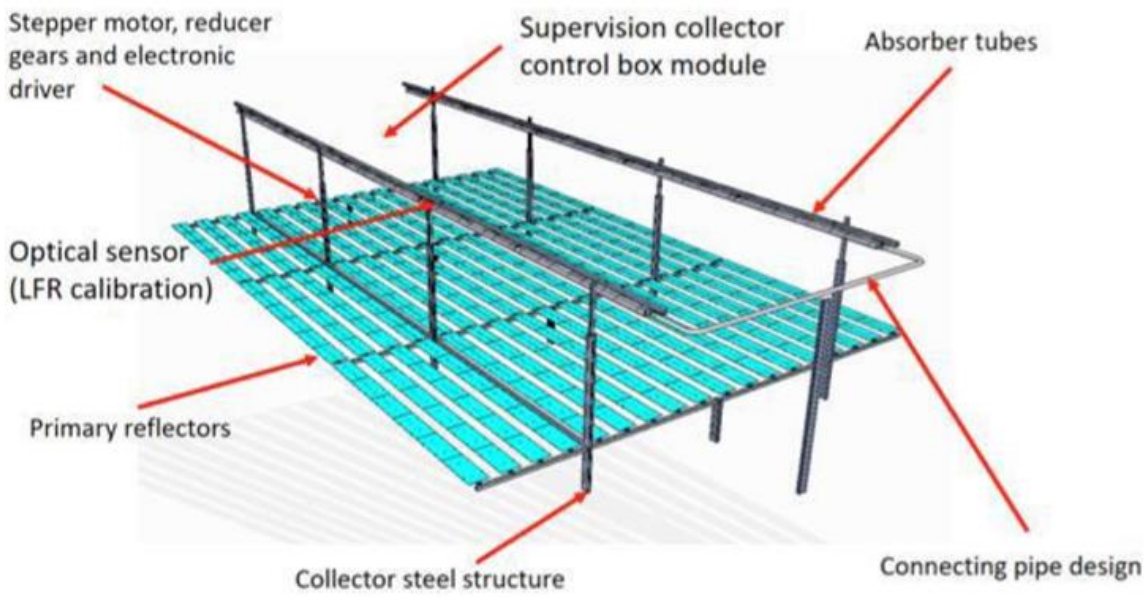

Figure 5.1 LFR system components [233]

Fig. 5.2 shows the HCEOI-12 receiver tube, used in the concentrated solar power plant system in Almatret. This receiver is produced by an Italian company and is designed only for oil as a heat transfer fluid. The outer glass cover has an antireflective ceramic-metallic material coating, according to ENEA standards. The receiver has high absorptance and low emittance at the operating temperature of the working fluid. The external surface of the receiver tube is made of borosilicate glass. The thermal expansion compensator maintains the vacuum between the metallic absorber tube and the external glass envelope. The maximum operating temperature of the fluid is 400 ^{o}C in such the tube. The steel tube thickness is 2 mm to minimize the corrosion effects and improve thermal performance. The HCEOI-12 has the tube getter in the vacuum annulus. Its function is to maintain a safe, efficient operation of the receiver tube

by absorbing the residual gases emitted by the glass and metal during a high-temperature process, increasing the receiver's life period.

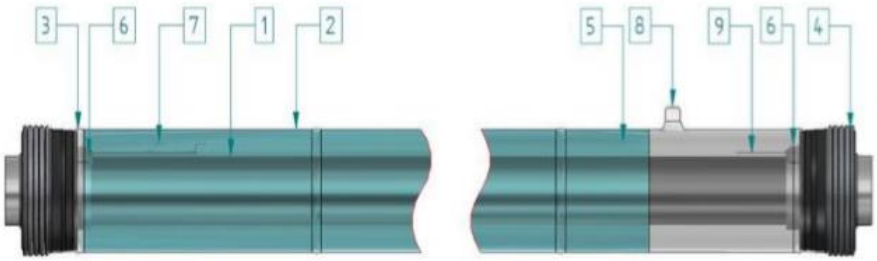

Figure 5.2 The sketch of the receiver tube [233]

1 - Stainless steel with the coating surface; 2 - Glass jacket with the anti-reflective coating surface; 3 -Glass-to-metal seals; 4 -Thermal expansion getter pills; 5 - Vacuum annulus; 6 -Nonevaporable getter pills; 7 - Barium getter; 8 - Pump nipple; 9 - Serial number

The solar field in Almatert is designed for a smaller thermal output and has only two receiver tube rows. In this study, a different configuration of the solar field is considered for the generation of higher thermal power output to run a larger ORC system than in Almatert, though it is based on using the same components. Fig. 5.3 shows the schematic of the solar field under investigation. The solar field collector is arranged as three parallel loops. Each loop consists of the modules that contain the series of the Fresnel mirrors. There are nine modules in each loop. The area of each module is 7.94 m^2 and calculated using the linear Fresnel mirror length and width. The loop area is 71.46 m^2 the overall aperture area of the solar collector is 214.38 m^2. There is a 0.3 m space between each module, and the actual footprint (ground) area of the LFR solar field system is 285.84 m^2. Table 5.1 shows the essential parameters of the Linear Fresnel collector.

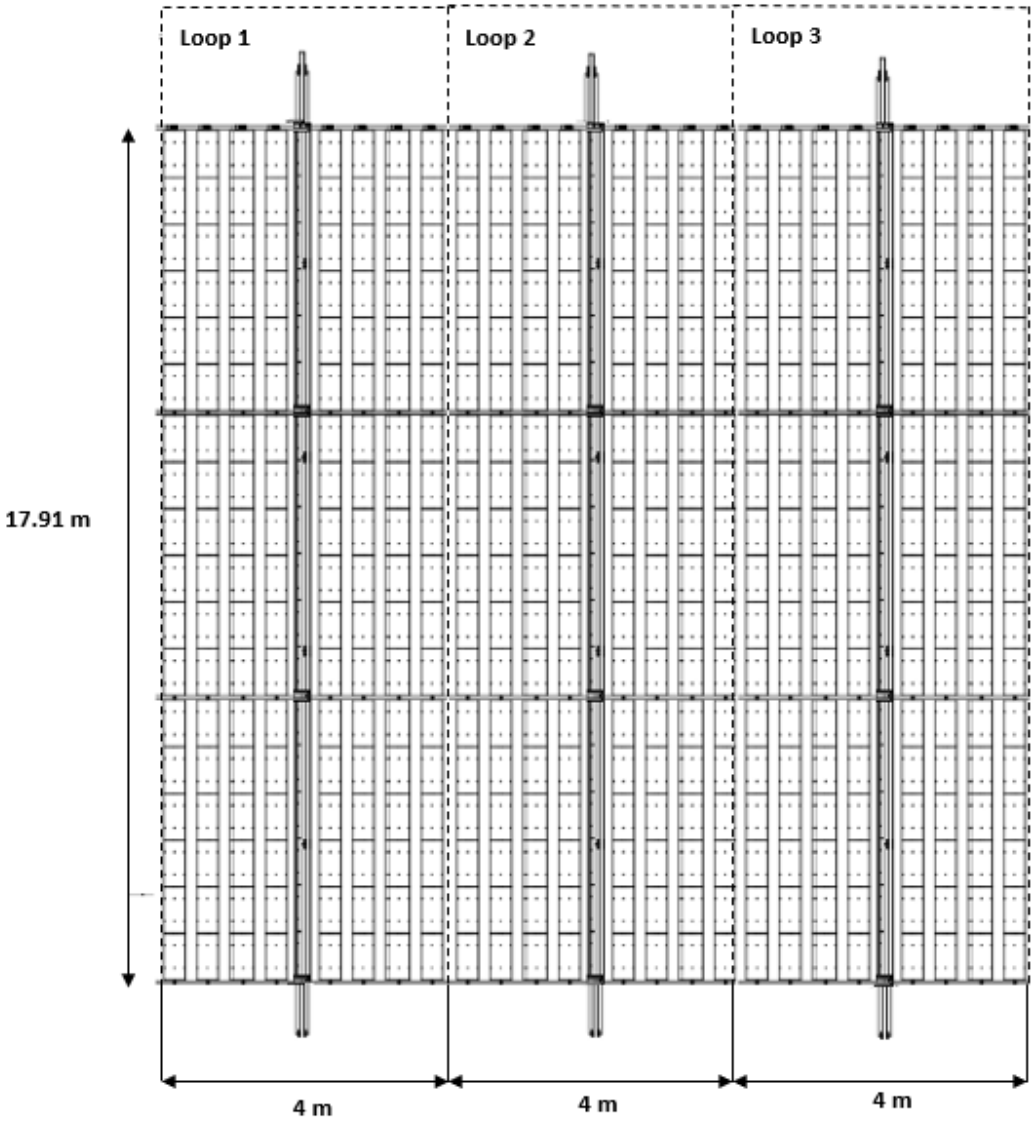

Figure 5.3 The 3-loop configuration of the LFR field

Table 5.1 Dimensions of the LFR solar field

Number of loops	3
Number of modules in each loop	9
Number of Fresnel mirrors in each module	18
The separate mirror width	0.443 m
The total length of the LFR	17.91 m
Total width of LFR	12 m
Module area	7.94 m^2
Single loop aperture area	71.46 m^2
Overall loop aperture area	214.38 m^2
The footprint area of the collector	285.84 m^2

The receiver tubes are equipped with secondary reflectors to maximise the catchment of solar thermal energy received by the primary reflectors, see Fig. 5.4. This figure also shows some of the dimensions of the receiver tube.

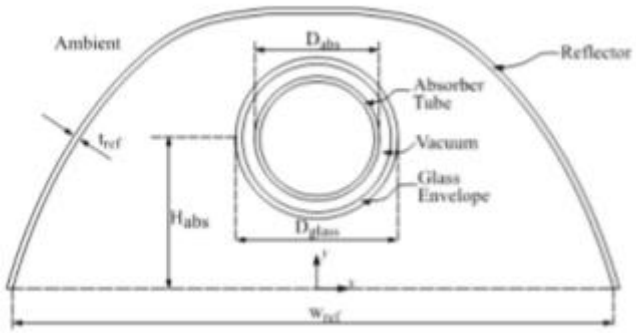

Figure 5.4 Receiver tube and secondary reflector configuration

Tables 5.2, 5.3 and 5.4, present some receiver characteristics, its core component including the absorber tube and the absorber tube glass envelope. Tables 5.5 and 5.5 show characteristics of the secondary reflector and Therminol-62, which is the heat transfer fluid in the receiver.

Table 5.2 Characteristics of the receiver

Receiver weight	28 Kg
Heat transfer fluid	Therminol-62
Enclosure pressure	1 x 10^{-4} mbar
Lifetime	25 years
Stability of coating	The coating is stable in vacuum at 600 ^{o}C

Table 5.3 Characteristics of the absorber tube of the receiver

Material	Austenitic stainless-steel tube electric-wedded longitudinally
Steel tube unit length	4060 mm
Steel tube thickness	2 mm
Steel tube outer diameter (D_{abs})	70 mm
Absorptance ($\alpha_{p,abs}$)	0.965
Emissivity ($\varepsilon_{p,abs}$)	0.085
Thermal conductivity ($K_{p,abs}$)	18.45 W/m-K

Table 5.4 Characteristics of the glass envelope of the receiver

Material	Borosilicate
Glass tube length	3900 mm
Glass tube thickness	3 mm
Glass tube outer diameter ($D_{g,\ in}$)	125 mm
Glass tube inner diameter ($D_{g,\ out}$)	121 mm
Glass cover absorptance (α_g)	0.02
Glass cover emissivity (ε_g)	0.86
Glass cover transmittance (τ_g)	0.965
Glass cover thermal conductivity (K_g)	1.4 W/m-K

Table 5.5 Characteristics of the secondary reflector of the receiver

Material	Coated aluminium
Opening width (w_{ref})	0.15 m
Reflectivity (ρ_{sr})	0.90
Emissivity (ε_{sr})	0.105
Absorptance (α_{sr})	0.03

Table 5.6 Properties of Therminol-62

Composition	Isopropyl biphenyl mixture
Appearance	Water-white liquid
Maximum bulk temperature	325°C
Normal Boiling Point	333 °C
Minimum use temperature	-23 °C
Heat of Vaporization	263.9 kJ/kg
Liquid Density (25°C)	951.1 kg/m^3
Pseudocritical temperature	487 °C
Pseudocritical pressure	15 Bar
Pseudocritical density	269.4 kg/m^3

5.3 Modelling of the operation of the solar field

Fig. 5.5 shows the heat transfer mechanisms in a receiver tube. Q_{inc} is the incident heat due to the concentrated solar radiation, Qabs is the heat absorbed by a steel pipe then passed to the heat transfer fluid through the heat conduction and convection mechanisms (Q_{CDP} and Q_{CVI}). The convection heat transfer also takes place between the outer surface of the glass envelope and air (Q_{CVE}). The heat is also lost to the environment through conduction in the glass cover (Q_{CDe}) and radiation (Q_{RDe}). Also, heat is lost through the radiative mechanism between the glass cover of the receiver and surface of the secondary reflector (Q_r).

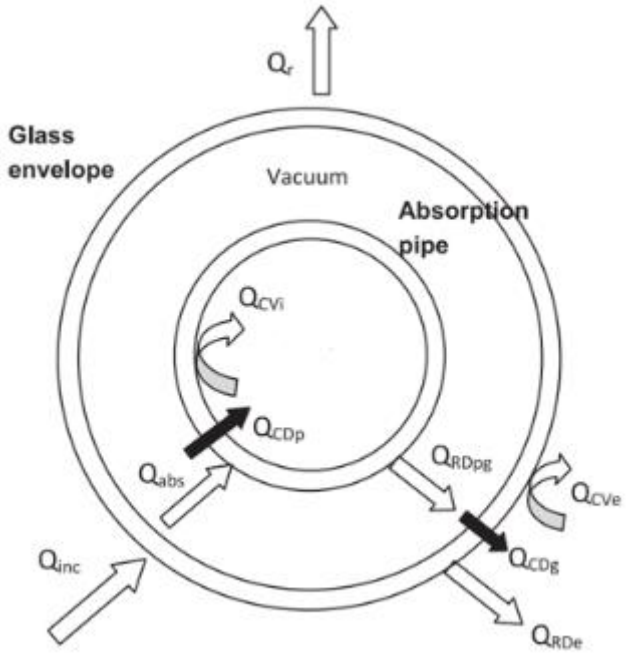

Figure 5.5 Heat transfer mechanisms in the receiver tube [234]

A. Parikh et al. [235] investigated the temperature distribution on an LFR assembly under DNI 1000 W/m^2 at the ambient temperature of 25 ^{o}C with the inner absorber tube wall temperature set to 400 ^{o}C. The results were obtained, and the simulation model indicated that the secondary reflector surface temperature varied between 60 ^{o}C and 120 ^{o}C, and the glass envelope temperature range was from 130 ^{o}C to 170 ^{o}C even at low solar concentration and wind conditions. Duffie et al. [236] carried out the optical and thermal investigation of the LFR system trapezoidal receiver case. The simulation results showed that the receiver heat losses varied from 181.2 W/m to 986 W/m in the receiver temperature range between 150 ^{o}C to 375 ^{o}C.

In this study, the value of Q_{inc} was defined using optical simulations of the LFR system with the deployment of the LightTools software based on the Monte-Carlo ray-tracing method (see Fig. 5.6. In this optical systems modelling software, it is necessary to describe the geometry of the LFR field, as shown in Fig. 5.7 and 5.9 and then for a certain instance of time to fix the position of the primary reflecting mirrors concerning the sun rays, to reflect the operation of sun-tracking mechanism (Fig. 5.6 shows mirrors in the initial arbitrary position).

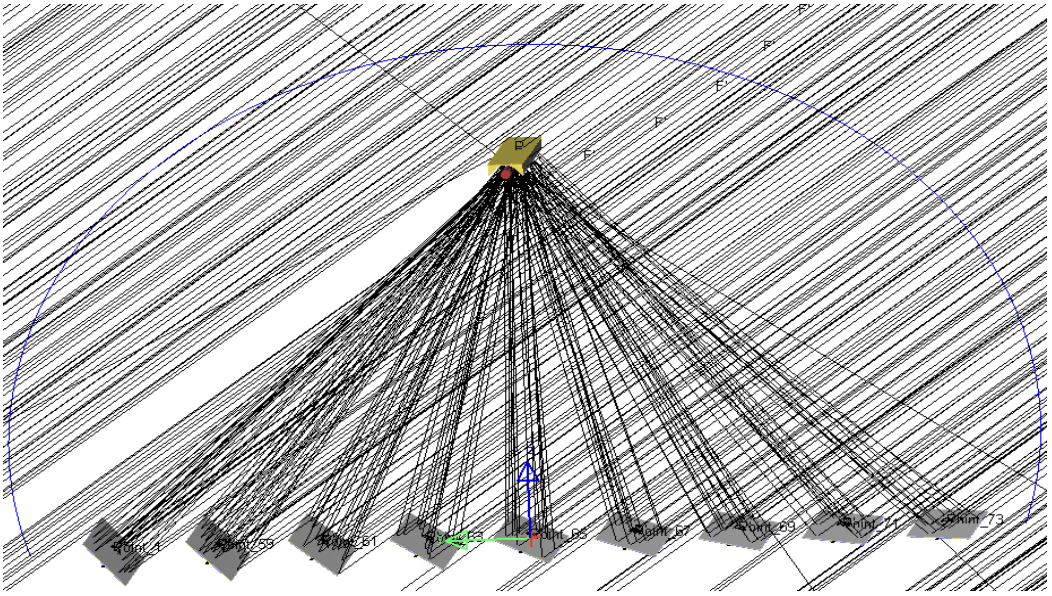

Figure 5.6 Modelling of the LFR module in the LighTools software

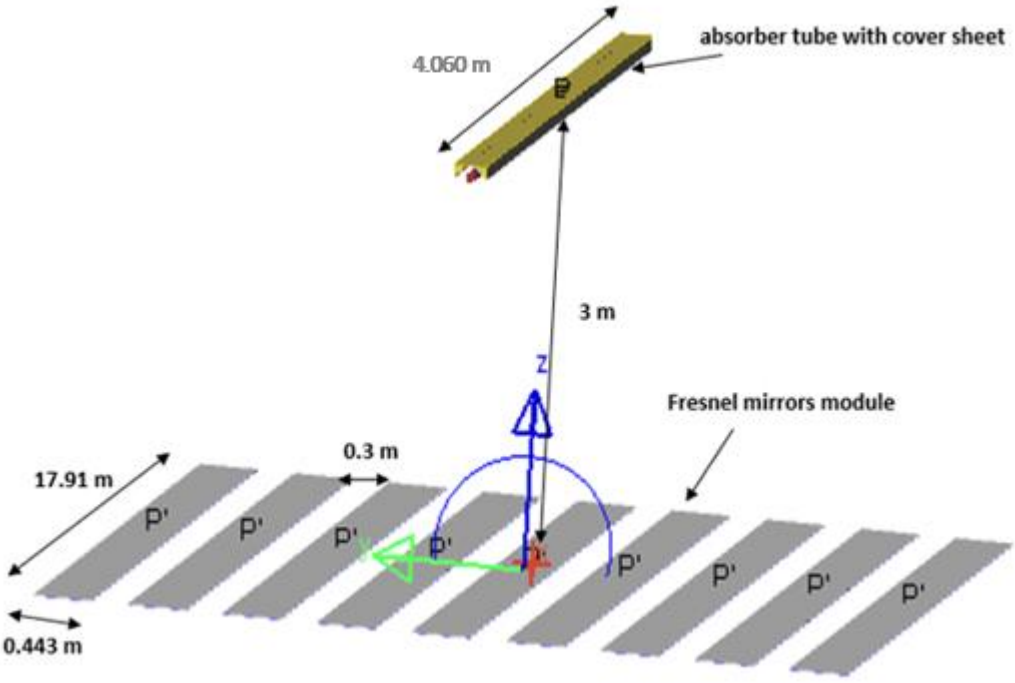

Figure 5.7 The design of the LFR module for the LighTools simulations

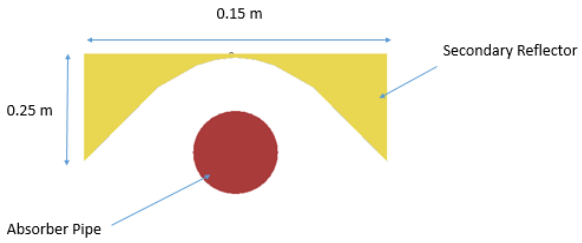

Figure 5.8 The diagram of the secondary reflector with the absorber tube for the LighTools simulations

Here the receiver tube is located at a 3 m height from the mirrors, and there are nine modules of primary reflectors in the loop with a distance 0.3 m between them. There are eighteen Fresnel mirrors in each module. The module area is 7.94 $m^{2,}$ and the loop area is 71.40 m^2.

For modelling purposes, it is also necessary to have information on Global Horizontal and Direct Normal Irradiance for the instance of time at which the simulation is performed at the site of plant installation. For example, Fig 5.13 shows the annual variation of the GHI in Almatret

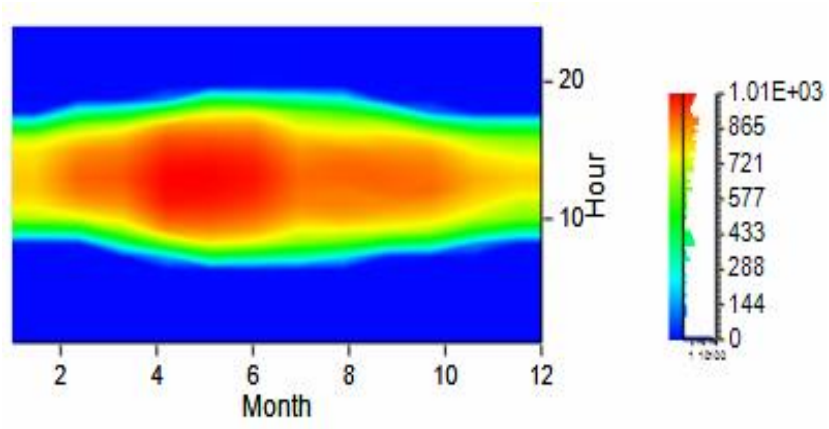

Figure 5.9 Global Horizontal Irradiance in Almatret (W/m^2).

The amount of solar energy concentrated on the receiver by the solar field depends on its orientation at the installation site, and the ray-tracing algorithm implemented to drive the step-motors of the sun-tracking system. Figure 5.10 shows the schematic used to develop the algorithm for the sun-tracking mechanism for Fresnel mirrors [237]. Table 5.7 presents a description of the angles used in Fig. 5.10.

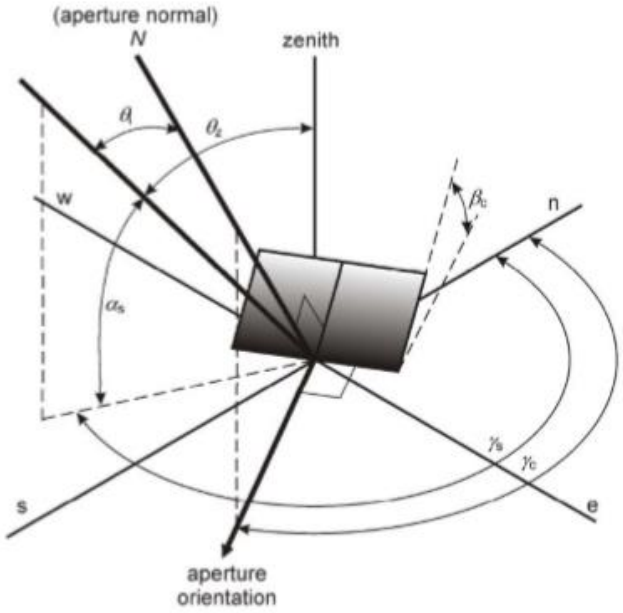

Figure 5.10 Schematic used for the development of the algorithm for the sun-tracking mechanism for Fresnel mirrors [237]

Table 5.7 Solar angles identification

The angle of incidence (θ_i)	The angle between the straight line to sun and collector normal
Collector axis tilt (β_c)	The between the collector surface and a horizontal plane $0 \leq \beta_c \leq 360^o$
Collector azimuth angle (γ_c)	The angle between north and the collector aperture orientation
Zenith angle (θ_z)	It is the complementary angle $(\theta_z) = 90 - \alpha_s$
Solar elevation angle (α_s)	It is the angle between a horizontal plane and a straight line to the sun
Solar azimuth angle (γ_s)	It is the angle between the solar projection position and north vertical on a horizontal plane $0 \leq \gamma_s \leq 360^o$

In this study, positions of the fresnel mirrors are used as a function of time (or sun's elevation and azimuth angles), which are implemented in the sun-tracking mechanism at the plant in Almatret. The electronic unit determines the collector's axis tilt (β_c) as a function of coordinates of the plant's site, day of the year and current time.

The LRF field modelling in LighTools software produces information on the heat flux on the glass cover surface from the primary mirrors and the secondary reflector, making it possible to find the heart rate incident on the receiver.

The heat energy gained by the HTF is determined in accordance with [236]:

$$\mathbf{Q_{gain} = (q_{averagefluxreceiver}\, A_w - Q_{loss})\, \eta_{opt,p}\, IAM} \qquad \mathbf{(5.1)}$$

The value of the optical efficiency of the receiver is determined as a product of the glass envelope transmissivity (τ_g), absorber tube absorptivity (α_p) and mirrors (ρ_{mi}) reflectivity.

$$\mathbf{\eta_{opt,p} = \tau_g\ \alpha_p\ \rho_{mi}} \qquad \mathbf{(5.2)}$$

In this study, the values of the above coefficients were used, which are equal to that in the real plant in Almatret. The mirror reflectivity factor is 0.72, and the calculated optical efficiency of the receiver is 0.67.

The simplified optical efficiency of the LFR system is the ratio of the amount of thermal energy absorbed by the HTF in the absorber tube to the product of the DNI value and the aperture area of the reflector:

$$\eta = \frac{\mathbf{Q_{abs}}}{\mathbf{A_{SC}} DNI} \qquad \mathbf{(5.3)}$$

The total thermal losses are defined as the sum of the convective heat losses to the environment, radiative heat losses from the receiver to the second reflector and radiative losses from the receiver to the environment.

$$\mathbf{Q_{loss} = Q_{cve} + Q_r + Q_{RDe}} \qquad \mathbf{(5.4)}$$

The convective heat transfer (Q_{CVE}) to the environment is calculated as

$$\mathbf{Q_{cve} = h_g A_{g,o}\, (T_{g,o} - T_o)} \qquad \mathbf{(5.5)}$$

where h_g is the heat transfer coefficient, the value of which depends on wind conditions; $A_{g,o}$ is the heat transfer area from the glass cover; $T_{g,o}$ is the glass temperature; T_0 is the ambient temperature.

The radiative heat transfer between the glass envelope and the secondary reflector is determined as

$$\mathbf{Q_r} = \frac{\sigma\left(\mathbf{T_{g,out}^4} - \mathbf{T_{sr,in}^4}\right)}{\left(\frac{1-\varepsilon_g}{A_{g,out}\varepsilon_g} + \frac{2}{A_{g,out}} + \frac{1-\varepsilon_{sr}}{A_{sr,in}\varepsilon_{sr}}\right)} \quad \textbf{(5.6)}$$

The radiative heat transfer between the outer surface of the glass envelope and the environment is defined as

$$\mathbf{Q_{RDe}} = \frac{\sigma\left(\mathbf{T_{g,out}^4} - \mathbf{T_{env}^4}\right)}{\left(\frac{1-\varepsilon_g}{A_{g,out}\varepsilon_g} + \frac{2}{A_{g,out}}\right)} \quad \textbf{(5.7)}$$

where σ is the Stephan-Boltzmann constant, equal to 5.67 x 10^{-8} W/m^2-K^4.

The IAM coefficients are calculated as the polynomial functions In the case of the transverse plane, the equation is

$$\mathbf{IAM_T = C_0 + C_1\,\phi_T + C_2\,\phi^2_T + C_3\,\phi^3_T + C_4\,\phi^2_T} \quad \textbf{(5.8)}$$

where ϕ_T is indicating the transversal incidence angle.

In the case of the longitudinal plane the equation is

$$\mathbf{IAM_L = C_0 + C_1\,\phi_L + C_2\,\phi^2_L + C_3\,\phi^3_L + C_4\,\phi^4_L} \quad \textbf{(5.9)}$$

where ϕ_L is indicating the longitudinal angle.

Tables 5.8 and 5.9 shows values of constant coefficients for the above polynomial functions.

Table 5.8 Transversal IAM coefficients [227]

C_0	1.007
C_1	2.256^{-09}
C_2	-4.479^{-07}
C_3	2.802^{-05}
C_4	-7.134^{-04}

Table 5.9 Longitudinal IAM coefficients.

C_0	1.000
C_1	9.996^{-10}
C_2	-1.869^{-07}
C_3	1.274^{-05}
C_4	-4.927^{-04}

The total IAM coefficient is determined as

$$\mathbf{IAM = IAM_T \times IAM_L} \qquad \mathbf{(5.10)}$$

5.4 Results and Discussions

Fig. 5.11 and 5.12 shows variations of the sun's elevation in the sky its azimuth angle during the day in Almatret on 7 July.

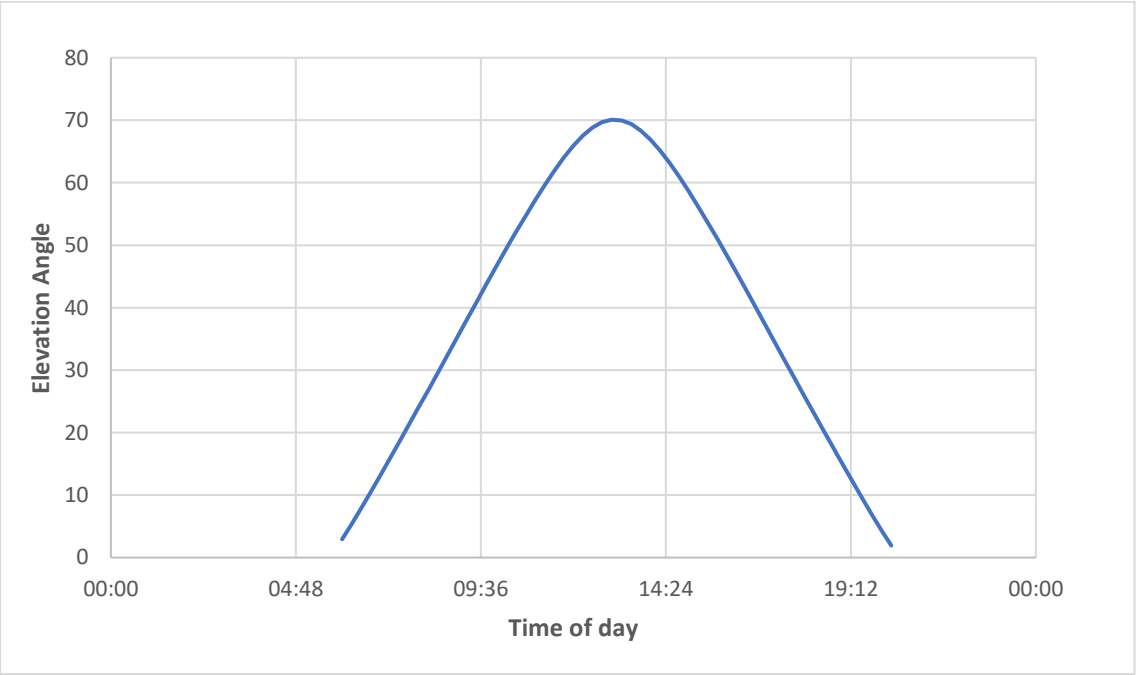

Figure 5.11 Sun elevation angle during the day in Almatret on 7 July

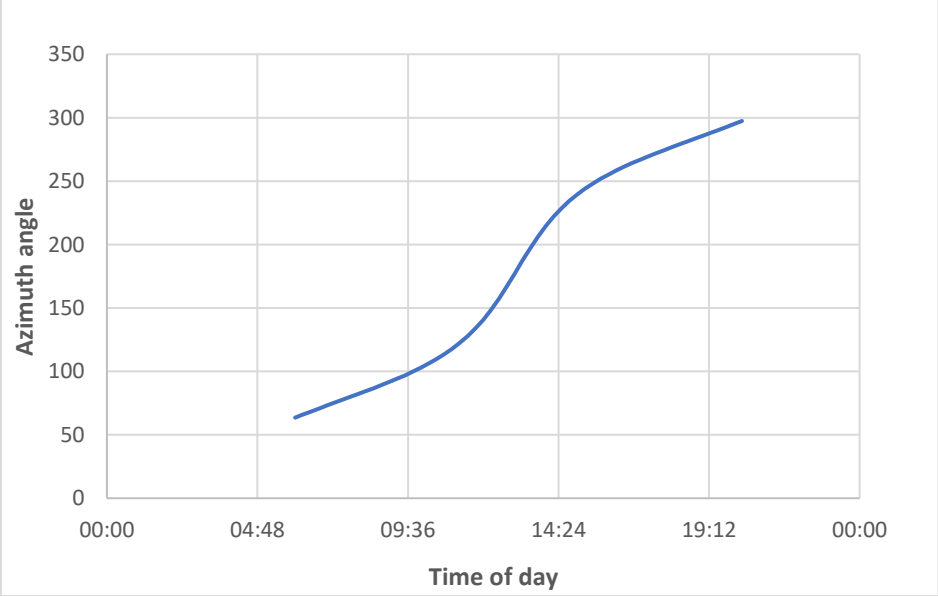

Figure 5.12 Sun azimuth angle variation during the day in Almatret on 7 July

Fig. 5.13 shows graphics of variation of the calculated GHI and DNI and DHI in the Almatret in July. This information was used as one of the input parameters in LightTools modelling of the LFR system. The maximum value of the DNI is 900 W/m^2, and it is achieved at 13.30.

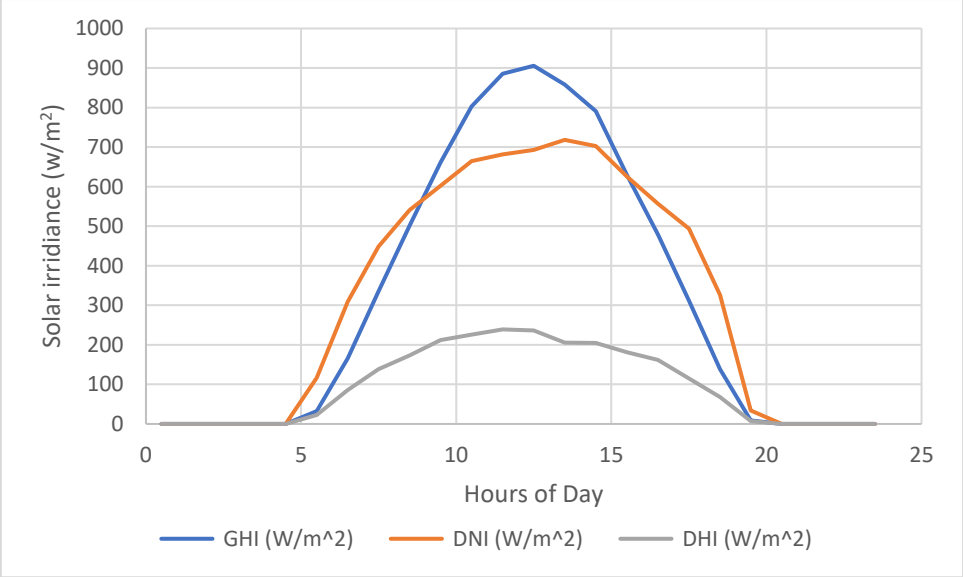

Figure 5.13 GHI and DNI variations in July

Fig. 5.14 shows the ray-tracing simulations results to determine the values of longitudinal and transverse components of IAM for the linear Fresnel reflector system. The higher value of the incidence angle causes the reduction of the IAM coefficients.

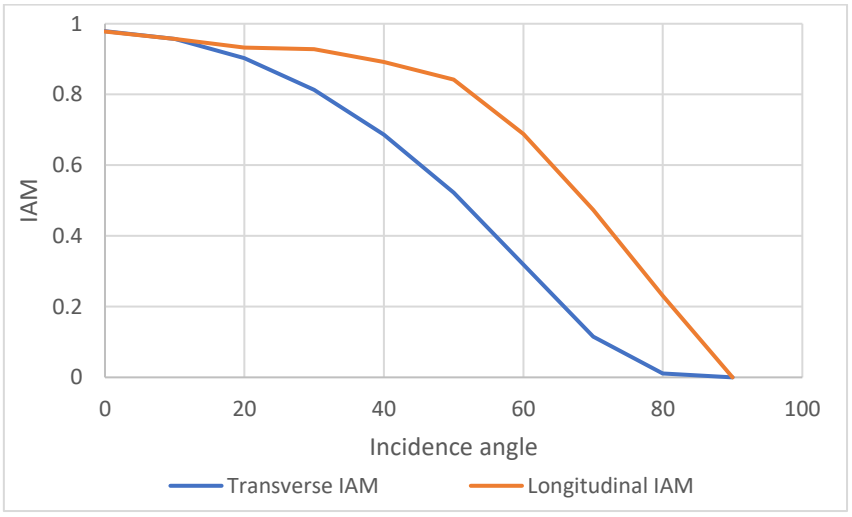

Figure 5.14 IAM coefficients at different values of incidence angle

Figure 5.15 shows the example of heat flux on the absorber tube due to solar irradiance concentration by the primary mirrors and secondary reflector on the upper part of the tube, corresponding to the early hours of operation. Due to the low level of solar irradiance at the beginning of the operation, the heat flux value is also very low (see the colour map).

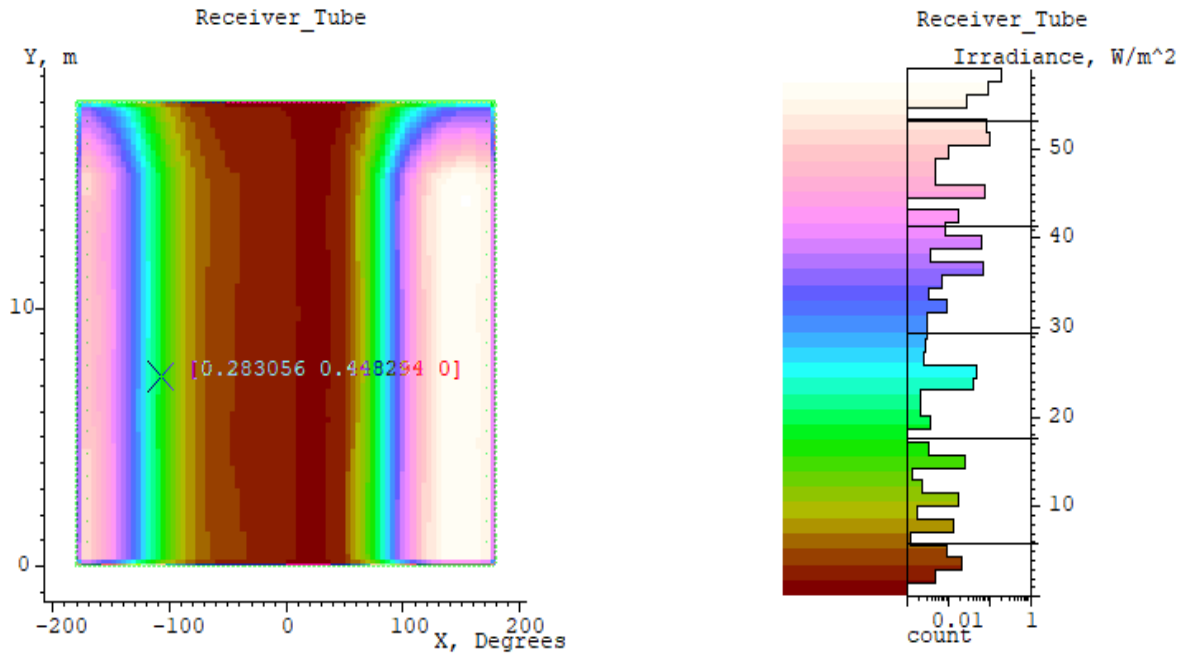

Figure 5.15 The colour scheme of the concentrated heat flux on the receiver tube at the beginning of operation of the LFR system

Information on the heat fluxes then can be used to estimate the thermal state of components of the receiver tube and the secondary collector. The thermal losses (Q_{loss}) of the solar collector are calculated using Equation 5.5, and these are 7.872 kW during the peak time of day (at 1:00 PM). There is a convective heat transfer (Q_{CVE}) between the outer surface of the glass and the environment. The heat transfer coefficient value considered to be 100 W/m^2-K for the case of moderate wind. The convective heat transfer (Q_{CVE}) was calculated to be 7.66 kW. The radiant heat transfer losses (Q_r) between the glass envelope and the secondary reflector was determined to be 9.783 W. There are also the radiant heat transfer losses (Q_{RDe}) between the glass envelope and the outer surface and the environment. The outside ambient temperature is considered to be 25 ^oC, and these heat losses were defined as are 11.450 W. Fig. 5.16 shows the calculated

total magnitude of heat losses from the receiver to the ambient and the secondary reflector using the simulation results for the LFR with the deployment of LightTools software.

Fig. 5.17 presents results on the determination of variation of heat absorption rate of the heat transfer fluid after taking into account the optical efficiency of the receiver and heat losses to the environment. The maximum thermal power transferred to the HTF (Therminol-62) is about 108 kW during the peak hour. These results then can be used in the calculation of other main parts of the SORC.

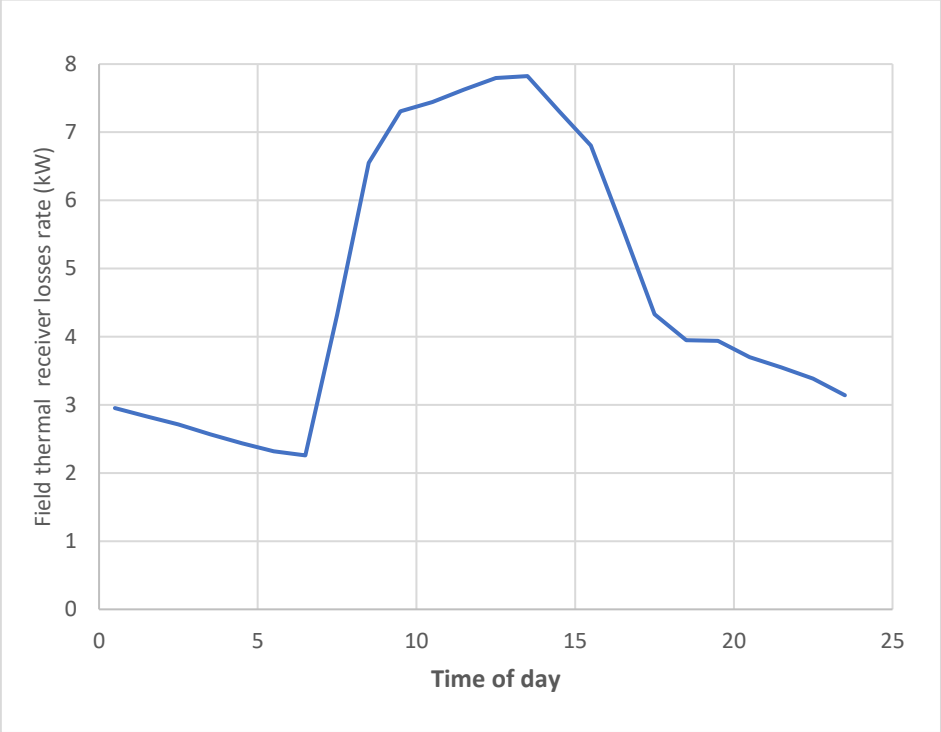

Figure 5.16 Variation of the thermal losses rate from the receiver during a day

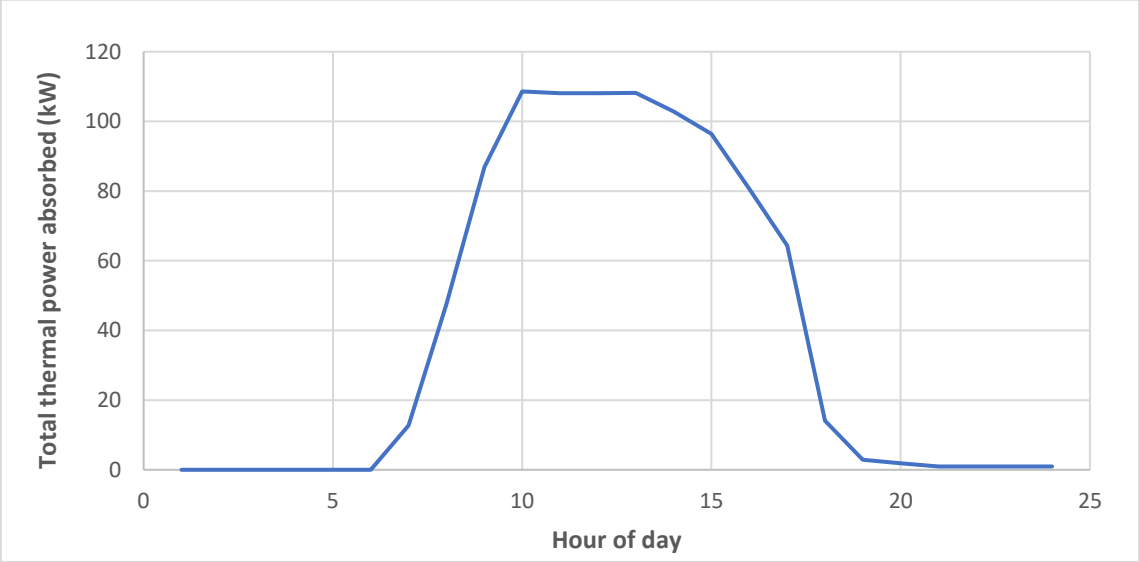

Figure 5.17 Variation in the amount of the thermal power absorbed by the HTF during the day

5.5 Conclusions

The thermal performance of the LFR receiver using the Therminol-62 HTF has not been investigated in the literature. The theoretical model for the description of the operation of the LFR was developed. The model is based on the application of LighTools software for optical modelling of the solar field based on the Monte-Carlo ray-tracing method. For the given configuration of the solar field of certain dimensions, the software allows to carry out heat flux calculations on the receiver surface due to solar energy concentration by the primary mirrors and secondary reflector of the solar field.

The data on the heat fluxes are then used to determine the thermal state of parts of the receiver, making it possible to estimate the heat losses in the system and determine the heat absorbed by the HTF of the solar field.

The used mathematical model calculates the thermal losses, which include the convective heat transfer (Q_{CVE}) losses, radiant heat transfer losses (Q_r) between the glass envelope and the secondary reflector and the (Q_{RDe}) between the outer surface of the glass envelope and the environment. These losses increase with the solar irradiance value. The thermal energy of the LFR increases if the IAM coefficient high value.

Chapter 6: Modelling of the annual performance of the SORC with thermal storage

This chapter describes the results of the modelling of the SORC with thermal storage. The thermal storage is designed to provide thermal energy for the operation of ORC with maximum power for 4 hours. In the SORC system, after the solar field starts to generate the maximum thermal power necessary for the ORC operation with maximum power output, the remaining generated thermal power is used to charge the thermal storage. The thermal storage medium is Therminol 62, and the working fluid for the ORC is NOVEC^{TM}649.

6.1 Introduction

Einav et al. [238] investigated a flat plate solar (FPC) collector developed at the national physical laboratory of Mali to run the Organic Rankine Cycle. The area of the collector was 100 m^2 to deliver 6 kW output power in remote locations. Kiceniuk et al. [239] studied the Parabolic dish collector (PDC) to operate the Organic Rankine Cycle power system using toluene as the working fluid and heat transfer fluid at Pasadena CA-USA. The PDC system collector area was 116.9 m^2, and the system generated 30-kW power output. Fenton et al. [240] designed a parabolic trough collector (PTC) at Willard NM-USA location. The PTC power system used mineral oil as a heat transfer fluid and HCFC-113 as the working fluid of the ORC. The PTC area was 1276 $m^{2,}$ and the system produced 19 kW of power with a direct thermocline thermal energy storage system. Moustafa et al. [241] investigated a parabolic dish collector (PDC) with an area of 1100 m^2 to operate an ORC power system in Kuwait. The solar field used synthetic oil and transferred the heat energy to toluene (the power cycle working fluid). The PDC power system included a thermocline direct thermal energy storage system and generated power up to 70 kW. Simonnot et al. [242] designed a parabolic trough collector (PTC) with an area of 1176 m^2 to operate ORC in France. The PTC power plant included a thermocline direct storage system and used Therminol as the heat transfer fluid and FC75 as the working fluid of the ORC to generated 100 kW output power. Barutti et al. [243] investigated the parabolic trough collector (PTC) in Perth, Australia. The PTC power system generated 35 kW of power by using Therminol as the heat transfer fluid and C_8F_{16} as the working fluid. Kane et al. [244] proposed a linear Fresnel collector (LFC) with an area of 100

m^2 using water in the tubes of collector and HCFC-134a as the working fluid of the ORC to generate 15 kW of power. Saitoh et al. [245] proposed a compound parabolic collector (CPC) with an area of 5.75 m^2 using water as the heat transfer fluid and HCFC-113 as the ORC working fluid. The CPC system generated power up to 1 kW with the use of the buffer thermal storage system. Canada et al. [246] designed a large plant with a PTC area equal to 10340 m^2 to operate the ORC. The mineral oil was used in the solar field and n-pentane as the working fluid of the ORC to generate power of 1 MW. Kohlenbach et al. [247] investigated a PTC with an area of 132 m^2 to operate the ORC power system. The system used the mineral oil in the solar field and HFE7100 in the power cycle to generate power of 6 kW. Galvez et al. [248] designed a PTC system to operate the ORC with 5 kW power using the Therminol in the solar field and SES36 as a working fluid. Wang et al. [249] investigated the flat plate collector (FPC) using HCFC-245fa as the working fluid and heat transfer fluid. The FPC power system was located in China, and its power was up to 13 kW. Wang et al. [250] also designed the evacuated tube collector (ETC) with an area of 44 m^2 using the HCFC-245fa as both heat transfer and working fluids. The ETC solar field powered the ORC system to generate power of 1.7 kW. Electratherm et al. [251] designed a PTC with an area of 216 m^2 using water in the solar field and R245fa as the working fluid in the ORC. The 18 KW of power was generated by the PTC power system, which was located in Cyprus. N. Soukpoe et al. [252] investigated the solar central tower (SCT) power system with an area of 180 m^2 using mineral oil in the solar field and HCFC-245fa as the working fluid. The SCT Rankine power system used a two-tank thermal storage system and generated 10 kW of output power. Qrosz et al. [253] investigated the PTC with an area of 75 m^2 to operate the ORC power system. The PTC used the Glycol in the solar field and HCFC-245fa as the working fluid for the ORC to generate the output power of 3 kW. Chambers et al. [254] analyzed the PTC with an area of 1051 m^2 using water in the solar field and HCFC-245fa as the working fluid in the ORC. The PTC power system generated the output power of 50 kW with a buffer thermal storage system. Goswami et al. [255] investigated the PTC power system using the phase change material (PCM) storage system. The PTC power cycle used the water in the solar field and HCFC-245fa as the working fluid to generate the output power of 50 kW. Rieu et al. [256] investigated the PTC with an area of 550 m^2 using water as the heat transfer fluid in the solar field and HCFC-245fa as the working fluid. The PTC power system was equipped with the Thermocline storage system and generated

the power of 10 kW. They also proposed the PTC with an area of 6159 m^2 and air as the working fluid and a sensible bed storage system to generate the power of 3 MW. The NREL described the project based on the LFC with an area of 9780 m^2 in Italy using mineral oil to generate an output power of 1 MW. NREL's other project was in the USA and based on the PTC with an area of 656 m^2. The PTC power system used the water in the solar field and Isobutane working fluid [257]. Georges et al. [258] investigated the PTC with an area of 78 m^2 using synthetic oil in the solar field and HCFC-245fa as the working fluid in the ORC to produce the power of 3 kW. Baral et al. [259] investigated the ETC to operate the power cycle using water in the solar field and HCFC-245fa as the working fluid in the ORC to generate the power output of 1.5 kW.

This Chapter describes the modelling of a SORC with the Therminol-62 heat transfer fluid in the solar field and NOVEC as the working fluid in the cycle. Such a system was not considered previously in the open literature, and the objective is to determine its performance over different annual seasons and the effect of the thermal storage system on the SORC performance. The dimensions of the LFR field are the same as for the Almatret power system discussed in Chapter 5. The thermal storage with the two-tank configuration was included in the power plant. The simulations were performed using the System Advisor Model software.

6.2 Solar Organic Rankine Cycle (SORC) system model description

Fig. 6.1 shows the SORC system schematic diagram with the solar field, which was modelled in Chapter 5. The schematic shows four loops, demonstrating that the model can be easily adapted for a new configuration of the solar field, but in this chapter, the same three-loop configuration was used as in Chapter 5. Fossil fuel back-up boiler was not modelled since its operation depends on the solar radiations random variation during the day. The ORC model is the same which was used previously (without regenerative heating), but it uses a new working fluid – NOVEC ^{TM}649 (as in the plant in Almatret).

NOVEC^{TM}649 belongs to the ketone family and is called the ethyl isopropyl ketone. NOVEC has a wide range of applications in various ORCs. It has excellent thermal stability and non-corrosive for ORC components. It is environmentally friendly and has low toxicity, is non-

flammable. This working fluid has low global warming potential and a zero ozone depletion. Table 6.1 shows the properties of NOVEC as the working fluid.

Table 6.1 Properties of the NOVEC^{TM}649 [260]

Chemical formula	$C_6H_{12}O$
Molecular weight	316.04 g/mol
Boiling point at 1 ATM.	49 ^oC
Freezing point	< -100 ^oC
Critical temperature	169 ^oC
Critical pressure	1.87 MPa
Kinematic viscosity	0.42 CST
Specific heat	1103 J/kg-K
Thermal conductivity	0.059 W/m-K

Table 6.2 shows the dimensions and operating parameters of the LFR solar field.

Table 6.2 Dimensions and operating parameters of the LFR solar field

Parameters	**Value**
Overall loop aperture area	214.38 m^2
The ground coverage area of the collector	285.84 m^2
Height of receiver	3 m
Working fluid	Therminol - 62
Maximum mass flow rate	0.205 kg/sec
Inlet temperature	67 ^oC
Outlet temperature	280 ^oC
Specific heat capacity	2.44 kJ/kg-K

The solar field outlet temperature of the Therminol 62 is 280 ^oC. The storage system of the SORC has hot and cold tanks (see Fig. 6.2). In the case of the charging of the hot storage tank

system, the mass flow of fluid in the LFR system approaches 0.410 kg/sec. The control valve system distributes equal fractions of the fluid towards the thermal storage system and ORC plant. A portion of the solar field thermal energy is transferred to the heat transfer fluid stream between cold and hot storage tanks. The Therminol-62 fluid is also used as a thermal storage medium.

The storage tank system thermal capacity is assumed to be four hours (corresponds to the plant technical specification in Almatret). The volume of tanks was calculated to have the necessary thermal capacity. The specific heat capacity of Therminol 62 at 280 ^{o}C is 2.44 kJ/kgK. The heat exchanger for transferring the heat from the solar field and thermal storage tanks was calculated using the NTU method, which was used in Chapters 3 and 4.

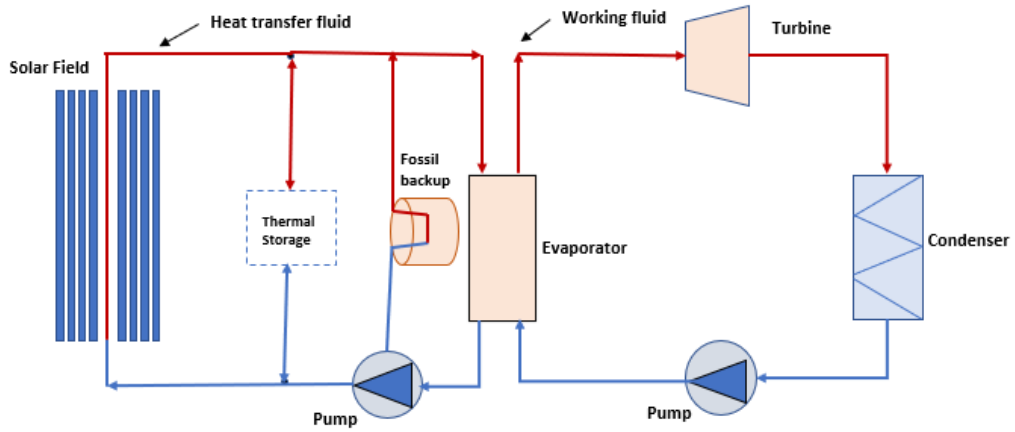

Figure 6.1 Schematic diagram of the SORC with thermal storage system

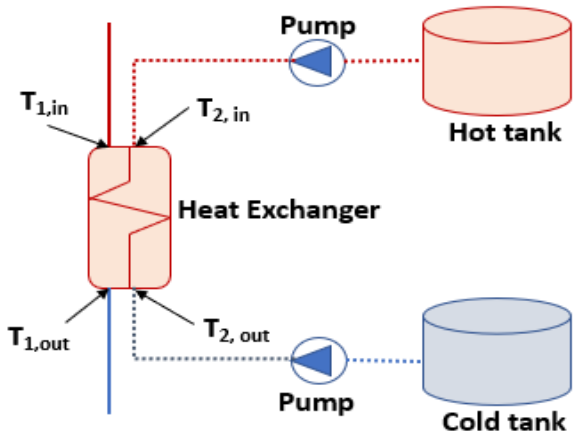

Figure 6.2 Thermal storage system of the plant

The heat exchanger transfers the heat from the solar field to the thermal storage. As highlighted above, the thermal storage system and solar field use the Therminol-62 fluid. The solar field Therminol-62 has a higher temperature. It is used to transfer the heat to a lower temperature Therminol-62 in the storage. A counter-flow heat exchanger is used for transferring heat between two streams of Therminol-62. The thermal characteristics of the hot and cold fluids are listed in Table 6.5.

Table 6.3 Parameters of the hot and cold Therminol-62 in the heat exchanger

Parameters	**Value**
Heat exchanger hot fluid inlet temperature ($T_{1,in}$)	280 ^{o}C
Heat exchanger cold fluid outlet temperature ($T_{1,out}$)	67 ^{o}C
Heat exchanger cold fluid inlet temperature ($T_{2,\ in}$)	40 ^{o}C
Heat exchanger cold fluid outlet temperature ($T_{2,\ out}$)	173.5 ^{o}C
Specific heat of hot fluid (C_h)	2.44 kJ/kg-K
Specific heat of cold fluid (C_c)	1.99 kJ/kg-K
The mass flow rate of hot fluid ($\dot{m}_h$)	0.205 kg/sec
The mass flow rate of hot fluid ($\dot{m}_c$)	0.300 kg/sec

The storage tank system thermal capacity is determined as a product of load hours and a ratio of the turbine power output at design conditions (W_{des}) and conversion efficiency of the power cycle (η_{des}):

$$\boldsymbol{C = \frac{w_{des}}{\eta_{des}} * T_{load}} \qquad \textbf{(6.1)}$$

There are two types of thermal storage systems. If the heat transfer solar field fluid and storage fluid are different, the system is known as indirect storage. In this case, the heat exchanger derating parameter μ_h has a value of less than one. A direct thermal storage system used in the

current model. The solar field and storage system use the same type of fluid (Therminol-62). The fluid set temperature in the hot tank ($T_{S, OUT}$) is 250 ^oC, and the cold tank set temperature ($T_{S, IN}$) is 40 ^oC. The cold tank fluid is transferred to the hot tank via a heat exchanger. The Therminol-62 flowing from the solar field fluid (HTF) has a density (ρ_{HTF}) of 830 kg/m^3 and specific heat (C_{HTF}) of 2.440 kJ/kgK. The derataing parameter for a direct system is 1. The storage volume of the fluid tanks is calculated as

$$\boldsymbol{V_T = \frac{C*10e^6*3600}{\rho_{HTF}*C_{HTF}*\mu_h*1000\,(T_{S,OUT}-T_{S,IN})}} \quad \textbf{(6.2)}$$

The height (H) of the storage tank is assuming to 5 m. The storage system is made as a 2-tank system (number of pairs N_p =1) - cold tank and hot tanks. The diameter (D) of the tank is calculated by using the following expression

$$\boldsymbol{D = 2\sqrt{\frac{V_T}{H*\pi*N_P}}} \quad \textbf{(6.3)}$$

The minimum fluid volume in the storage tank (V_{min}) depends on the minimum storage height (H_{min}) of the fluid and the storage volume (V_T) and height (H) of the storage tank. The minimum storage height of the tank is assumed to be 1 m. The minimum storage volume of the tank (V_{min}) is calculated as

$$\boldsymbol{V_{min} = V_T\frac{H_{min}}{H_T}} \quad \textbf{(6.4)}$$

The heat loss factor of the storage tank system depends on the height (H), diameter (D), number of pairs (in this case, N_P =1), average fluid temperature (T_{ave}), and loss coefficient of the tank (C_{loss}). The temperatures of the hot and cold fluids at inlets of the tanks are 280^o and 40^o, respectively. The average fluid temperature is calculated as

$$\boldsymbol{T_{ave} = \frac{T_{h,tank}+T_{c,tank}}{2}} \quad \textbf{(6.5)}$$

The heat loss coefficient (C_{loss}) of the tank is assumed to be 0.2 W/m^2-K. The amount of heat lost (H_{loss}) by a tank storage system is calculated as

$$\boldsymbol{H_{Loss} = \left(H*\pi*D+\pi*\left(\frac{D}{2}\right)^2\right)N_p*(T_{ave}-20)*C_{Loss}} \quad \textbf{(6.6)}$$

Fig. 6.3 shows the schematic of the ORC plant used in the Thermolib model and P-h diagram of the cycle, which was used for the calculation of the mass flow rate of NOVEC in the cycle, specific heat input and rejection and specific power output from the turbine and work input for the pump.

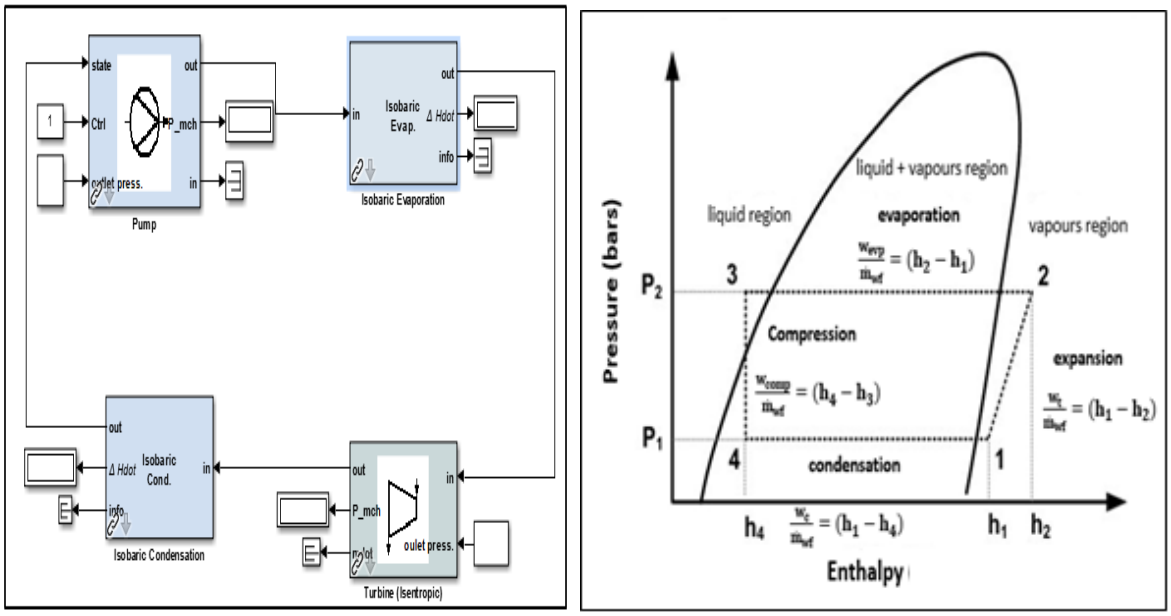

Figure 6.3 The schematic of the ORC in Thermolib and its P-h diagram

6.3 Results and discussion

Table 6.4 shows the ORC system's performance results on 7 July, for instance, when the highest level of thermal energy is supplied to the ORC (46.432 kW) and when the power of the turbine is 6.856 kW. The mass flow rate *(m_{wf})* of NOVEC is 0.1 kg/sec. The thermal efficiency of the Rankine cycle is 14 %. In this mode of operation, the ORC works from about 9.30 to 16.30, see Fig. 6.4. During this period, the solar field produces more thermal energy than required for the ORC to generate the maximum power (see Fig. 5.17), and that surplus is used to charge the thermal storage. This accumulated thermal storage is then used to run ORC from about 19.30 to 11.30 (see Fig. 6.5).

The thermal capacity (C) of the storage system is 571.42 kW. The storage volume (V_T) of the fluid tanks is 5.03 m^3 using the diameter (D) of the tank is 0.798 m. The minimum storage volume of the tank (V_{min}) is 1.006 m^3. The average fluid temperature is 173.5^o in the hot tank.

The amount of heat losses (H_{loss}) by the storage system is 399.974 W. The effectiveness (ϵ) of the heat exchanger is 0.746. The number of transfer units (*NTU*) of the counterflow heat exchanger is 2.13.

Table 6.4 Performance of components of the Rankine cycle

Parameter	**Value**
Heat input in the evaporator (at 15 bar and 450 K)	46.432 kW
Turbine power output (exit at 1 bar and 400 K)	6.856 kW
Heat rejection rate (at 1 bar and 281 K)	22.138 kW
Pump power input (inlet at 15 bar and 280 K)	0.32 kW

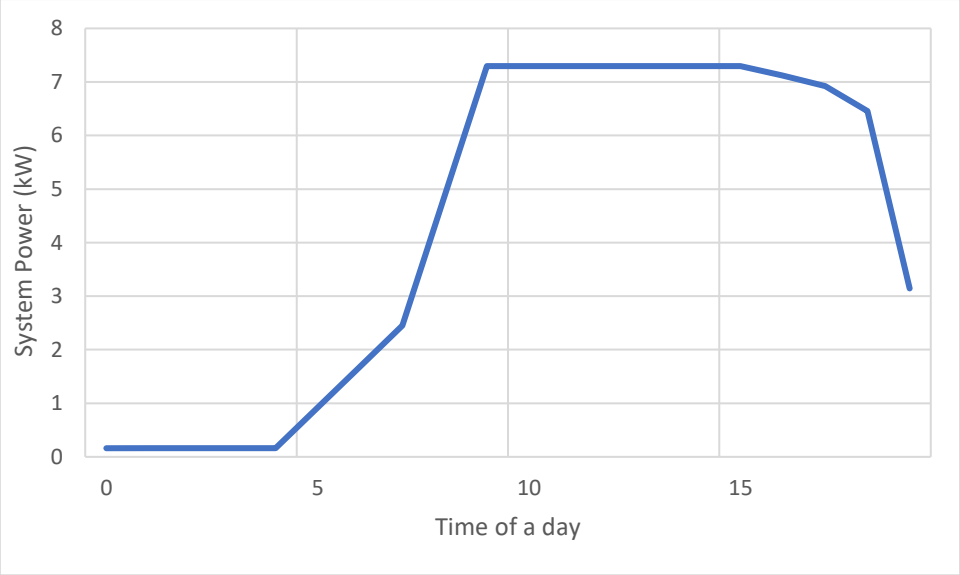

Fig. 6.4 ORC power generation during a day in July without the thermal storage (with the excess of the thermal energy generated by the solar field being dissipated)

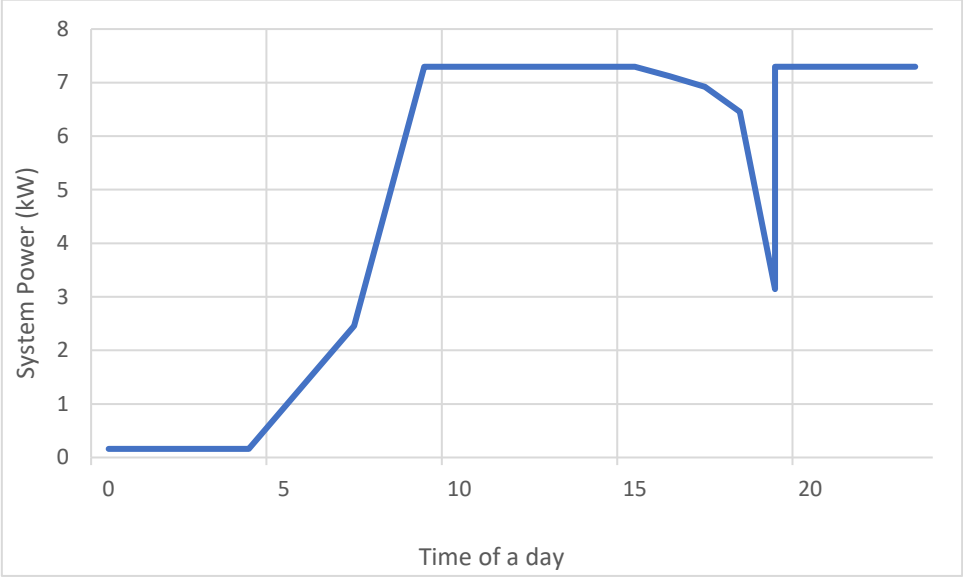

Figure 6.5 ORC power generation during a day in July with the thermal storage

The SORC plant was designed using the System Advisor Model (SAM). The dimensions of the LFR is the same as for the Almatret plant (described in Chapter 5). The actual annual weather data file was imported to the SAM for the plant site in Almatret. The data file with Therminol-62 fluid properties was also imported to the fluid library in SAM software. The simulations described in Section 6.2, were performed for 12 months, taking into account statistical data on the average solar irradiation in Almatert (see Fig. 5.13). Fig. 6.6 shows the annual performance of the SORC with thermal storage. It can be seen that the highest power output was observed in July with 2160 kWh of energy produced by the ORC. The lowest amount of plant thermal power is observed in January, and this is an example of the month in which the thermal storage is not engaged in the plant operation.

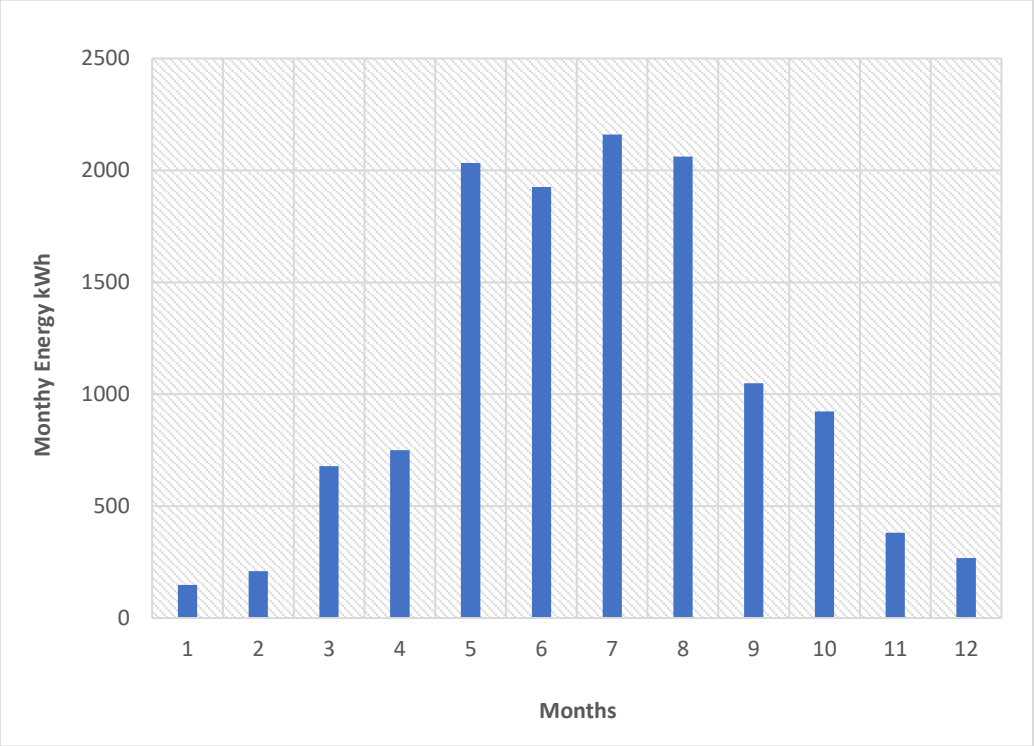

Figure 6.4 Annual energy generation by the SORC with the thermal storage

6.4 Conclusions

The performance of the SORC with solar field and thermal storage was modelled. The new working fluid was implemented for the ORC, which is NOVEC. It has not been investigated in the literature. The thermal storage was charged only in the case in which the solar field generates more thermal energy than it is necessary for the ORC operation at its maximum power output mode using Therminol-62 HTF. The one-axis tracking system of LFR utilizing the maximum solar irradiance during a day. The Therminol-62 has good results in LFR solar field to operate the Rankine power cycle. The thermodynamic and simulation analysis shows the LFR field aperture area of 214.38 m^2 with a receiver tube at 3 m high above the Fresnel mirror surface to generate a maximum 7.2 kW output ORC plant power during a peak hour of the July month. The annual performance of the SORC was estimated in terms of generated energy. In the winter months and early spring and late autumn, the solar field does not generate excess heat, which is necessary to engage thermal storage.

Chapter 7: Conclusions and Recommendations for future work

This research was focused on the development of modelling tools for analysis of various configurations of solar thermal power systems and their main components, which could be used in the development of a small solar plant being built in Almatret, Spain, as a part of the EU funded project.

7.1 Conclusions

- An overview of publications and technologies in the field of solar power and heat production were carried out. The literature review revealed that power plants on the basis of ORC turbines with the utilisation of solar energy with low- and medium-temperature heat transfer fluids are becoming a very attractive proposition for micro- and small-scale power production. Despite a large number of publications in this area, there is still a shortage of mathematical models for the simulation of the operation of the whole Solar Organic Rankine Cycle plants and their components, which could make it possible to use various configurations of the plants and their main parts and working fluids of the ORC and HTFs of the solar field.

- The mathematical model of a simple ORC and ORC with regenerative heating was developed in the MATLAB/Simulink, and Thermolib environments and their operations were simulated on various organic working fluids to ensure that the model predictions are correct and it can be used as a part of the whole SORC plant modelling. Results obtained demonstrate that for the range of tested working fluids, the cycle efficiency is improved by about 0.5-1.5% when the regeneration of the heat in the cycle is used, and this option should be very carefully analysed since the cost of an additional heat exchanger increases the capital cost of the ORC plant. The ORC model was tested using R245fa, ethanol, iso-propane, iso-pentane, methanol, HCFC-32, and HCFC-R134a as working fluids which provided thermal efficiencies of 14.8%. 17.04%,

14.9%, 17.23%, 17.23 %, 17.61%, 18.17% and 15.33% respectively when critical operating parameters of these fluids were used.

- The SORC model with a simple HCFC–134a ORC plant coupled with non-concentrating solar collectors with water as HTF was developed in MATLAB/Simulink and Thermolib environments. The actual weather data imported from the Meteonorm standard database for the geographical location, corresponding to Almatret (Spain), was used. The solar collector without a tracking system had a surface area of 600 m2. The model also includes the calculation of local solar irradiance incident on the surface of the collector. The model results demonstrate that the maximum amount of thermal energy produced is 71 kW at 1:00 PM on 2 July. Additionally, the calculation of heat exchanger for transferring the heat for the solar field to the ORC by deploying NTU method is the part of the developed SORC model. The obtained turbine power is about 7.6 kW, and the thermal efficiency value in the ORC plant is 13.16 %. The mathematical model of the ORC cycle was enhanced by the code for optimisation of operational parameters of the ORC using GA method. The SORC system is generating 7.58 kW output power with optimum values of the design variable.

- The Linear Fresnel Reflector (LFR) solar field simulation model was developed in the LighTools software, which uses the Monte-Carlo method for ray-tracing. The solar field designed model consists of three loops (rows) with a total area of 214.38 m2. Therminol-62 is used as the heat transfer fluid of the system, which is heated to 280 oC. The theoretical model takes into account the real location (Almatret) and orientation of the primary reflecting and secondary mirrors and their optical properties, along with the optical properties of the absorption receiver. The model also takes into account the heat losses from the absorption receivers due to infrared radiation, convective and conduction heat losses. The results are showing the receiver tube gain (Qgain) 115.98 kW energy on 7 July. The calculated thermal losses from the receiver tube are 7.681 kW. The actual thermal energy generated by the solar field is 106.25 kW.

- The SORC model, consisting of the LFR model in LightTools and the ORC plant with the thermal storage, was developed. NOVEC is used as the working fluid in the PRC, and Therminol-62 is used as the heat transfer fluid in the solar field. The thermal storage system is made as to the two-tank system (hot and cold HTF tanks) and accumulates the thermal energy in the form of heated Therminol 62 to 250 ^{o}C, which is sufficient to run the ORC for 4 hours. The thermal storage is charged when the solar field starts to generate the heat more than it is necessary for the ORC to generate its power output at the maximum level (6.85 kW at the efficiency of 14%). The annual performance of the SORC was estimated in terms of generated energy. The highest power output was observed in July with 2160 kWh of energy produced by the ORC. The lowest amount is observed in January, and this is also an example of the month, in which the thermal storage is not engaged in the operation of the plant. In winter months and early spring and late autumn, the solar field does not generate excess heat, which is necessary to engage the thermal storage.

- The above-developed modelling tools can be used to analyse configurations of SORC plants that need to be built.

7.2 Recommendations for future work

Simulation tools developed in this work can be further developed to make them more generic for designing the SORC systems. Important areas to consider for further development are as follows:

- The mathematical model, which describes the ORC expander operation, should be developed and included in the overall mathematical model of the SORC system into account its physical dimensions. Using such a model, it would be possible to optimise dimensions of the expander;

- Similarly, detailed models should be developed for heat exchangers used in the SORC system;

- The optimisation code should be introduced to find dimensions of the solar field at the given geographical location to provide the maximum thermal power output. The optimisation code should be for different types of the solar field: the LFR, solar plate collectors and evacuated tube collectors.

- A more detailed mathematical model of the thermocline thermal storage tank should be developed to take into account the features of its operation during the modelling of the whole plant;

- The mathematical models for different types of thermal storage systems should be developed, such as phase change materials based or fixed bed solid material type.

REFERENCES

[1] World Population Prospects: The 2017 Revision - United Nations Population Division.

[2] BP energy economics, 2018 edition of BP's Energy Outlook.

[3] Corinne Le Quere et al., Global Carbon Budget, 2017.

[4] IPCC, Global Warming Special Report, 2018.

[5] Gaia M, Thirty years of organic Rankine cycle development. In: First international seminar on ORC power systems, Delft TU-Technical University, The Netherlands, September 2012, 22–23 (Key-note presentation).

[6] Rankine WJM, A manual of the steam engine and other prime movers. Richard Griffin, London (Publishers to the University of Glasgow), 1859.

[7] Takahisa Yamamoto a, Tomohiko Furuhata b, Norio Arai b, Koichi Mori, Design and testing of the Organic Rankine Cycle. Department of Chemical Engineering, Nagoya University, Chikusa-Ku, 2000, Nagoya, Japan 464-8603.

[8] E. Galloni, G. Fontana, S. Staccone (2015) Design and experimental analysis of a mini organic Rankine Cycle) power plant based on R245fa working fluid. DiCem, the University of Cassino and Southern Latium, Italy, 2015, Energy 90, pp. 768-775.

[9] Wenhao Pu a, Chen Yue, Experimental study on Organic Rankine cycle for low-grade thermal energy recovery. 2016, Applied Thermal Engineering 94, pp. 221–227.

[10] Gary J. Zyhowskia, Andrew P. Brownb, Abdennacer Achaichiab, HFC-245fa Working Fluid in Organic Rankine Cycle - A Safe and Economic Way to Generate Electricity from Waste Heat. Honeywell, Buffalo, New York, USA, 2010.

[11] Lemmon, E. W., Huber, M. L., McLinden, M. O.: NIST Standard Reference Database 23: Reference Fluid Thermodynamic and Transport Properties-REFPROP, Version 9.1.,National Institute of Standards and Technology, Standard Reference Data Program, Gaithersburg (2013)

[12] Tachanche, B.F.; Low-Grade Heat Conversion into Power Using Small Scale Organic Rankine Cycles, Doctoral Thesis, University of Athens, 2010.

[13] Bao, J., Zhao, L.: A review of working fluid and expander selections for Organic Rankine Cycle. Renewable and Sustainable Energy Reviews, 2013, Vol. 24, issue C, 325-342

[14] Badr, O., O'Callaghan, P. W., Hussein, M., Probert, S. D.: Multi-vane Expanders as Prime Movers for Low-Grade Energy Organic Rankine Cycle Engines. Applied Energy Volume 16, Issue 2, 1984, Pages 129-146.
[15] Chen, Yang, et al. 'Theoretical Research of Carbon Dioxide Power Cycle Application in Automobile Industry to Reduce Vehicle's Fuel Consumption.' Applied Thermal Engineering, Vol. 25, no. 14–15, 2005, pp. 2041–2053.
[16] Bianchi, M., Pascale, A.: Bottoming Cycles for Electric Energy Generation: Parametric Investigation of Available and Innovative Solutions for the Exploitation of Low and Medium Temperature Heat Sources. Applied Energy Volume 88, Issue 5, May 2011, Pages 1500-1509.
[17] Mago, P. J., Chamra, L. M., Srinivasan, K., Somayaji, C.: An Examination of Regenerative Organic Rankine Cycles Using Dry Fluids. Applied Thermal Engineering,2008, 28, 998-1007.
[18] Gu, Z., Sato, H.: Performance of Supercritical Cycles for Geothermal Binary Design. Energy Conversion and Management 43(7), 2002, 961-971.
[19] Sauret, E., Rowlands, A. S.: Candidate Radial-Inflow Turbines and High-Density Working Fluids for Geothermal Power Systems. Energy 36(7), 2011, 4460-4467.
[20] Fiaschi, D., Manfredi, G., Maraschiello, F.: Thermo-fluid dynamic preliminary design of turbo-expanders for ORC cycles. Applied Energy 97, 2012, 601-608.
[21] Kang, S.: Design and Preliminary Tests of ORC (Organic Rankine Cycle) with the two-stage radial turbine. Energy 96, 2016, 142-154.
[22] Hung, T.-C.: Waste Heat Recovery of Organic Rankine Cycle Using Dry Fluids. Energy Conversion and Management, 2001, 42(5), 539-553.
[23] Dai, Y., Wang, J., Gao, L.: Parametric Optimisation and Comparative Study of Organic Rankine Cycle (ORC) for Low-Grade Waste Heat Recovery. Energy Conversion and Management 50(3), 2009, 576-582.
[24] Saleh, B., Koglbauer, G., Wendland, M., Fisher, J.: Working Fluids for Low-Temperature Organic Rankine Cycles. Energy 32(7), 2007, 1210-1221.
[25] Quoilin S. Sustainable energy conversion using organic Rankine cycles for waste heat recovery and solar applications, 2011, PhD thesis. University of Liege, Belgium.
[26] U Drescher, D. Bruggemann Fluid selection for the organic Rankine cycle (ORC) in biomass power and heat plants, Applied Thermal Engineering, 2007, pp. 223-228.

[27] R Rayegan, YX. Tao's procedure to select working fluids for solar organic Rankine cycles (ORCs) Renewable Energy, 36 (2) (2011), pp. 659-670.
[28] Cayer, E., Galanis, N., Nesreddine, H.: Parametric Study and Optimisation of a Transcritical Power Cycle Using a Low-Temperature Heat Source. Applied Energy 87, 2010, 1349-1367.
[29] Hung, T. C., Shai, T. Y., Wang, S. K.: A review of Organic Rankine cycles (ORCs) for the recovery of low-grade waste heat. Energy 22(7), 1997, 661-667.
[30] Pasetti, M., Invernizzi, C., Iora, P.: Thermal Stability of Working Fluids for Organic Rankine Cycles: An Improved Survey Method and Experimental Results for Cyclopentane, Isopentane, and n-Butane. Applied Thermal Engineering 73(1), 2015, 764-774.
[31] Drescher, U., Bruggemann, D.: Fluid Selection for the Organic Rankine Cycle (ORC) in Biomass Power and Heat Plants. Applied Thermal Engineering 27(1), 2007, 223-228.
[32] Invernizzi, C. M., Bonalumi, D.: 5- Thermal Stability of Organic Fluids for Organic Rankine Cycle Systems. In: Organic Rankine Cycle (ORC) Power Systems. 2017, 121-151.
[33] Heberle, F., Preißinger, M., Bruggemann, D.: Zeotropic Mixtures as Working Fluids in Organic Rankine Cycles for Low-Enthalpy Geothermal Resources. Renewable Energy 37(1), 2012, 364-370.
[34] Emily Spayde, Pedro J. Mago, Heejin Cho, Performance Evaluation of a Solar-Powered Regenerative Organic Rankine Cycle in Different Climate Condition, Energies 2017, 10, 94; doi:10.3390/en10010094.
[35] Huan Xi, Ming Jia, Li Chao Xu, Ya-Ling He, Parametric optimization of regenerative organic Rankine cycle (ORC) for low-grade waste heat recovery using genetic algorithm, Energy Volume 58, 1 September 2013, Pages 473-482
[36] Enslin J, Rankine Cycle Efficiency Increase by the Regenerative Recovery of Historically Rejected Heat_rev2. 2019, Bioenergetics 7: 155. doi: 10.4172/2167-7662.1000155
[37] A.Mahmoudi, M.Fazli, M.R.Morad, A recent review of waste heat recovery by Organic Rankine Cycle, Applied Thermal Engineering 143, 2018, 660–675.
[38] Pikra, G. and Rohmah, N. Comparison of Single and Double Stage Regenerative Organic Rankine Cycle for Medium Grade Heat Source Through Energy and Exergy Estimation. Int. Journal of Renewable Energy Development, 2019, 8(2), 141-148, doi.org/ijred.8.2.141-148

[39] Peris, B., Navarro-Esbrí, J., Molés, F., Martí, J., Mota-Babiloni, A.: Experimental Characterisation of an Organic Rankine Cycle (ORC) for micro-scale CHP applications. Applied Thermal Engineering 79, 2015, 1-8.
[40] Wang, X. D., Zhao, L., Wang, J. L., Zhang, W. Z., Zhao, X. Z., Wu, W.: Performance Evaluation of a Low-Temperature Solar Organic Rankine Cycle System utilizing R245fa, 2009, Solar Energy.
[41] L. Li, Y.T. Ge, S.A. Tassou, Experimental Study on a Small-scale R245fa Organic Rankine Cycle System for Low-grade Thermal Energy Recovery, Energy Procedia, Volume 105, 2017, Pages 1827-1832, ISSN 1876-6102, https://doi.org/10.1016/j.egypro.2017.03.531.
[42] Eunkoo Yun, Dokyun Kim, Sang Youl Yoon, Kyung Chun Kim, Experimental investigation of an organic Rankine cycle with multiple expanders used in parallel, Applied Energy, Volume 145, 2015, Pages 246-254, ISSN 0306-2619, https://doi.org/10.1016/j.apenergy.2015.02.022.
[43] Quoilin, S., Lemort, V., Lebrun, J.: Experimental Study and Modeling of an Organic Rankine Cycle using Scroll Expander. Applied Energy 87(4), 2010, 1260-1268.
[44] Navarro-Esbri, J., Molés, F., Peris, B., Mota-Babiloni, A., Kontomaris, K.: Experimental Study of an Organic Rankine Cycle with HFO-1336mzz-Z as a low global-warming potential working fluid for micro-scale low-temperature applications, 2017. Energy 133, 79-89.
[45] Eyerer, S., Wieland, C., Vandersickel, A., Spliethoff, H.: Experimental Study of an ORC (Organic Rankine Cycle) and analysis of R1233zd-E as a Drop-in Replacement for R245fa for low-temperature heat utilization. 2016, Energy 103, 660-671.
[46] M. Bianchi, L. Branchini, A. De Pascale, V. Orlandini, S. Ottaviano, M. Pinelli, P.R. Spina, A. Suman, Experimental Performance of a Micro-ORC Energy System for Low-Grade Heat Recovery, Energy Procedia, Volume 129, 2017, Pages 899-906, ISSN 1876-6102, https://doi.org/10.1016/j.egypro.2017.09.096.
[47] Muhammad, U., Imran, M., Lee, D., Park, B.: Design and Experimental Investigation of a 1kW organic Rankine cycle system using R245fa as the working fluid for low-grade waste heat recovery from steam. 2015, Energy Conversion and Management 103, 1089-1100.
[48] Vanslambrouck B. The Organic Rankine Cycle: a current market overview. In: Proceedings of the international symposium on waste heat recovery by Organic Rankine Cycle, 2009.

[49] Ohman H. Implementation and evaluation of a low-temperature waste heat recovery power cycle using NH_3 in an Organic Rankine Cycle, Energy, 2012, doi: 10.1016/j.energy.2012.02.074.
[50] Gaia M. Turboden ORC Systems "Electricity Generation from Enhanced Geothermal Systems," Strasbourg, 2006.
[51] A. Schuster, S. Karellas, E. Kakaras, H. Spliethoff, Energetic, and economic investigation of Organic Rankine Cycle applications, 2008 Applied Thermal Engineering, pp. 1809-1817.
[52] P. Petr and G. Raabe, Evaluation of R-1234ze(Z) as a drop-in replacement for R-245fa in Organic Rankine Cycles – From thermophysical properties to cycle performance, 2015, *Energy*, Vol. 93, pp. 266-274.
[53] M. Bianchi, A. Pascale, Bottoming cycles for electric energy generation: Parametric investigation of available and innovative solutions for the exploitation of low and medium temperature heat sources, 2011, Applied Energy Volume 88, Issue 5, Pages 1500-1509.
[54] B. F. Tchanche, G. Papadakis, G. Lambrinos, and A. Frangoudakis, Fluid selection for a low-temperature solar organic Rankine cycle, 2009, Applied Thermal Engineering, vol. 29, pp., 2468-2476.
[55] Sprouse, C. III, and Depcik, C. Review of Organic Rankine Cycles for Internal Combustion Engine Exhaust Waste Hear Recovery, 2013, Applied Thermal Engineering 51, 711- 722.
[56] F. Ferrara, A. Gimelli, A. Luongo, Small-scale concentrated solar power (CSP) plant. 2013, Energy Procedia 45, pp 217 – 226.
[57] Saleh B, Koglbauer G, Wendland M, Fischer J., Working fluids for low-temperature organic Rankine cycles, 2007, Energy, 32:1210–21.
[58] R. Rayegan and Y. X. Tao, A procedure to select working fluids for solar organic Rankine cycles (ORCs), 2011, Renewable Energy, vol. 36, pp. 659-670.
[59] X. D. Wang and L. Zhao, Analysis of zeotropic mixtures used in low-temperature solar Rankine cycles for power generation, 2009, Solar Energy, vol. 83, pp. 605-613.
[60] A. M. Delgado-Torres and L Garcaí-Rodrgíuez, Analysis and optimization of the low-temperature solar organic Rankine cycle (ORC), 2010, Energy Conversion and Management, vol. 51, pp. 2846-2856.

[61] Edwin S. R. Escalante; João A. de Carvalho Junior; José A. P. Balestieri., Effect of working fluids on organic Rankine cycle for the recovery of low-grade waste heat, 2018, The 12th Latin-American congress on electricity generation and transmission.
[62] Lakew, A.A., Bolland, O., Working fluids for a low-temperature heat source, 2010, Appl. Therm. Eng., 30, 1262–1268.
[63] Drescher U, Bruggemann D., Fluid selection for the organic Rankine cycle (ORC) in biomass power and heat plants, 2007. Applied Thermal Engineering;27: 223–8.
[64] Shang Jun, Z., Huaixin, W., Tao, G.: Performance Comparison and Parametric Optimisation of Subcritical Organic Rankine Cycle (ORC) and Transcritical Power 224 Cycle System or Low-Temperature Geothermal Power Generation, 2011, Applied Energy 88(8), 2740-2754.
[65] Lakew, A., Bolland, O.: Working Fluids for Low-Temperature Heat Sources, 2010, Applied Thermal Engineering 30(10), 1262-1268.
[66] Dai, Y., Wang, J., Gao, L.: Parametric Optimisation and Comparative Study of Organic Rankine Cycle (ORC) for Low-Grade Waste Heat Recovery. 2009, Energy Conversion and Management 50(3), 576-582.
[67] Zhang, T., Zhu, T., An, W., Song, X., Liu, L., Liu, H.: Unsteady Analysis of a Bottoming Organic Rankine Cycle for Exhaust Heat Recovery from an Internal Combustion 225 Engine using Monte Carlo Simulation. 2016, Energy Conversion and Management 124, 357368.
[68] Liu, B.-T., Chien, K.-H., Wang, C.-C.: Effect of Working Fluids on Organic Rankine Cycle for Waste Heat Recovery. 2004, Energy 29(8), 1207-1217.
[69] Hung, T. C., Shai, T. Y., Wang, S. K.: A review of Organic Rankine cycles (ORCs) for the recovery of low-grade waste heat. 1997, Energy 22(7), 661-667.
[70] Larjola, J.: Electricity from Industrial Waste Heat using High-Speed Organic Rankine Cycle (ORC). 1995, International Journal of Production Economics 41, 227-235
[71] Baik, Y.-J., Kim, M., Chang, K.-C., Lee, Y.-S., Yoon, H.-K.: Power Enhancement Potential of a Mixture Transcritical Cycle for A Low-Temperature Geothermal Power Generation. 2012, Energy 47(1), 70-76.
[72] Chen, Y., Lunchqvist, P., Platell, P.: Theoretical Research of Carbon Dioxide Power Cycle Application in Automobile Industry to Reduce Vehicle's Fuel Consumption. 2005, Applied Thermal Engineering 25(14-15), 2041-2053.

[73] Papadopoulos, A., Stijepovic, M., Linke, P.: On the systematic design and selection of optimal working fluids for Organic Rankine Cycles. 2010, Applied Thermal Engineering 30, 760-769.
[74] B. Gozdur, A.: Pumping Work in the Organic Rankine Cycle. 2013, Applied Thermal Engineering 51(1-2), 781-786.
[75] Subbiah, S., Natarajan, R.: Thermodynamic Analysis of Binary-Fluid Rankine Cycles for Geothermal Power Plants. 1988, Energy Conversion and Management 28(1), 47-52.
[76] Yang, F., Zhang, H., Song, S., Bei, C., Wang, H., Wang, E.: Thermo economic Multi-Objective Optimisation of an Organic Rankine cycle for Exhaust Waste Heat Recovery of a Diesel Engine. 2015, Energy 93(2), 2208-2228.
[77] Helvaci, H. U.: Thermodynamic Modelling and Analysis of a Solar Organic Rankine Cycle Employing Thermo fluids. 2017, Energy Conversion and Management 138, 493-510.
[78] P.J. Linstrom and W.G. Mallard, Eds., May 2019 ‘‘NIST Chemistry WebBook, NIST Standard Reference Database Number 69’’ National Institute of Standards and Technology, Gaithersburg MD, 20899, https://doi.org/10.18434/T4D303.
[79] Xi, H., Li, M.-J., Xu, C., He, Y.-L.: Parametric optimization of regenerative organic Rankine cycle (ORC) for low-grade waste heat recovery using genetic algorithm. 2013, Energy 58, 473-482.
[80] Pierobon, L., Nguyen, T-V., Larsen, U., Haglind, F., & Elmegaard, B. Multi-objective optimization of organic Rankine cycles for waste heat recovery: Application in an offshore platform. 20132, Energy, 58, 538-549.
[81] Kai, Z., Mi, Z., Yabo, W., Zhili, S., Shengchun, L., Jinghong, N.: Parametric Optimisation of Low-Temperature ORC System. 2015, Energy Procedia 75, 1596-1602.
[82] Sadeghi, M., Nemati, A., Ghavimi, A., Yari, M.: Thermodynamic analysis and multi-objective optimization of various ORC (organic Rankine cycle) configurations using zeotropic mixtures. 2016, Energy 109, 791-802.
[83] Tartiere, T., Astolfi, m.: A World Overview of the Organic Rankine Cycle Market. 2017, Energy Procedia 129, 2-9.
[84] X. D. Wang, L. Zhao, J. L. Wang, W. Z. Zhang, X. Z. Zhao, and W. Wu, 2010 "Performance evaluation of a low-temperature solar Rankine cycle system utilizing R245fa," Solar Energy, vol. 84, pp. 353-364.

[85] Agustín M. Delgado-Torres, LourdesGarcía-Rodríguez, ,Analysis and optimization of the low-temperature solar organic Rankine cycle (ORC), 2010, Energy Conversion and Management 51(12), 2846-2856.

[86] S. Quoilin, M. Orosz, H. Hemond, and V. Lemort, Performance and design optimization of a low-cost solar organic Rankine cycle for remote power generation, 2011, Solar Energy, vol. 85, no. 5, pp. 955-966.

[87] Amir Farzaneh, Maysam Mohammadi, Zaki Ahmad and Intesar Ahmad. Aluminium Alloys in Solar Power − Benefits and Limitations, Aluminium Alloys - New Trends in Fabrication and Applications, Zaki Ahmad, IntechOpen, December 5th 2012 DOI: 10.5772/54721.

[88] Chopra K, Tyagi VV, Pandey AK, Sari A. Global advancement on experimental and thermal analysis of evacuated tube collector with and without heat pipe systems and possible applications. Appl Energy 15-Oct-2018;228:351e89. Elsevier.

[89] Urban F, Geall S, Wang Y. Solar PV and solar water heaters in China: different pathways to low carbon energy. Renew Sustain Energy Rev 2016;64:531e42.

[90] Qiu S, Ruth M, Ghosh S. Evacuated tube collectors: a notable driver behind the solar water heater industry in China,. Renew Sustain Energy Rev Jul. 2015;47: 580e8.

[91] Urban F, Geall S, Wang Y. Solar PV and solar water heaters in China: different pathways to low carbon energy. Renew Sustain Energy Rev 2016;64:531e42.

[92] Werner Weiss, Monika Spörk-Dür, Solar Heat World Wide, AEE - Institute for Sustainable Technologies 8200 Gleisdorf, Austria, 2 0 1 8 E D I T I O N.

[93] Wu YT, Liu SW, Xiong YX, Ma CF, Ding YL, Experimental study on the heat transfer characteristics of a low melting point salt in a parabolic trough solar collector system. 2015, Applied Thermal Eng; 89:748–54.

[94] Rovira A, Barbero R, Montes MJ, Abbas R, Varela F, Analysis and comparison of Integrated Solar Combined Cycles using parabolic troughs and linear Fresnel reflectors as concentrating systems. 2016, Applied Energy 162:990–1000.

[95] Wu YT, Liu SW, Xiong YX, Ma CF, Ding YL, Experimental study on the heat transfer characteristics of a low melting point salt in a parabolic trough solar collector system. 2015, Applied Thermal Eng; 89:748–54.

[96] Abbas R, Montes MJ, Piera M, Martínez-Val JM., Solar radiation concentration features in Linear Fresnel Reflector arrays, 2012, Energy Convers Manage 54:133–44.

[97] Rovira A, Barbero R, Montes MJ, Abbas R, Varela F, Analysis and comparison of Integrated Solar Combined Cycles using parabolic troughs and linear Fresnel reflectors as concentrating systems. 2016, Applied Energy 162:990–1000.
[98] Fabian Feldhoff, June 28, 2012, '' SFERA Summer School, Linear Fresnel Collectors''.
[99] Purohit, I., Purohit, P., Shekhar, S., Evaluating the potential of concentrating solar power generation in North-western India, 2013, Energy Policy 62, 157-175.
[100] Collado, F.J., Guallar, J., A review of optimized design layouts for solar power tower plants with campo code. Renew. 2013, Sustain. Energy Rev. 20, 142-154.
[101] Sampaio PGV, González MOA, Photovoltaic solar energy conceptual framework. 2017, Renew Sustain Energy Rev;74:590–601.
[102] Sharma V, Nayak JK, Kedare SB. Effects of shading and blocking in linear Fresnel reflector field. 2015, Solar Energy;113:114–38.
[103] Li J, Pei G, Li Y, Wang D, Energetic and energetic investigation of an organic Rankine cycle at different heat source temperatures. 2012, Energy 38:85–95.
[104] Tian, Y., Zhao, C.Y., A review of solar collectors and thermal energy storage in solar thermal applications. 2013, Applied. Energy 104, 538e553.
[105] Zhang, H.L., Baeyens, J., Degreve, J., Caceres, G. Concentrated solar power plants: review and design methodology. 2013, Renew. Sustain. Energy Rev. 22, 466-481.
[106] Fabian Feldhoff, June 28, 2012, '' SFERA Summer School, Linear Fresnel Collectors''.
[107] Zhu, G., Wendelin, T., Wagner,M.J., Kutscher, C., History, current state, and future of linear Fresnel concentrating solar collectors. 2014, Solar Energy 103, 639-652.
[108] M. J. Proctor, W. Yu, R. D. Kirkpatrick, and B. R. Young, Dynamic modelling and validation of a commercial-scale geothermal organic Rankine cycle power plant, 2016, Geothermic, vol. 61, pp. 63-74.
[109] National Renewable Energy Laboratory, "U.S. Solar Radiation Resource Maps: Atlas of the Solar Radiation Data Manual for Flat-Plate and Concentrating Collectors", http://rredc.nrel.gov/solar/pubs/redbook/PDFs/CA.PDF
[110] Zanis Jesko,2008, ''Classification of Solar Collector' 'Latvia University of Agriculture, Faculty of Engineering.
[111] G. Zhu, T. Wendelin, M. J. Wagner, and C. Kutscher, "History, current state, and future of linear Fresnel concentrating solar collectors, 2014, Sol. Energy, vol. 103, pp. 639–652.

[112] Sen, P. K., K. Ashutosh, K. Bhuwanesh, Z. Engineer, S. Hegde, P. V. Sen, and P. Davies., 2013, Linear Fresnel Mirror Solar Concentrator with tracking, Procedia Eng., Vol. 56, pp. 613–618.
[113] Patnode M. A., "Simulation and Performance Evaluation of Parabolic Trough Solar Power Plants," 2006, M.S. Thesis University of Wisconsin, Madison.
[114] "Linear Fresnel Reflector based Solar System: Operation and Maintenance Manual," 2014, Ministry of New and Renewable Energy, Government of India.
[115] F. Burkholder and C. F. Kutscher, Heat loss testing of Schott's 2008 PTR70 parabolic trough receiver, 2009, NREL Technical Report.
[116] Sen, P. K., K. Ashutosh, K. Bhuwanesh, Z. Engineer, S. Hegde, P. V. Sen, and P. Davies., 2013, Linear Fresnel Mirror Solar Concentrator with tracking, Procedia Eng., Vol. 56, pp. 613–618.
[117] Dostucok, I., Selbas, R., Sencan, A., Experimental Investigation of a Linear Fresnel, 2014, J. of Thermal Science and Technology, vol. 34, pp. 77–83.
[118] K. S. Reddy and K. R. Kumar, Estimation of convective and radiative heat losses from an inverted trapezoidal cavity receiver of solar linear Fresnel reflector system, 2014, Int. J. Therm. Sci., Vol. 80, no. 1, pp. 48–57.
[119] Elmaanaoui Youssef, Saifaoui Dennoun, Preliminary Assessment of an Organic Rankine Cycle Power Plant Derived by Linear Fresnel Reflector, 2018, International Journal of Renewable Research, Vol.8, No.4.
[120] G. Mokhtar, B. Boussad, and S. Noureddine, A linear Fresnel reflector as a solar system for heating water: Theoretical and experimental study, 2016, Case Stud. Therm. Eng., Vol. 8, pp. 176–186.
[121] J. He, Z. Qiu, Q. Li, and Y. Zhang, "Optical design of linear Fresnel reflector solar concentrators, 2012, Energy Procedia, vol. 14, no. 2011, pp., 1960–1966.
[122] R. Abbas, M. J. Montes, M. Piera, and J. M. Martínez-Val, "Solar radiation concentration features in Linear Fresnel Reflector arrays, 2012, Energy Convers. Manag., Vol. 54, no. 1, pp. 133–144.
[123] F. Huang, L. Li, and W. Huang, Optical performance of an azimuth tracking linear Fresnel solar concentrator, 2014, Sol. Energy, Vol. 108, pp. 1–12.

[124] S. Song, J. Ma, Z. Zhan, Y. Dai, Optical Analysis and Optimization of the Linear Fresnel Collector's Mirror Field, 2015, International Forum on Energy, Environment Science and Materials, 2015.
[125] V. Sharma, J. K. Nayak, S. B. Kedare, Effects of shading and blocking in linear Fresnel reflector field,2015, Solar Energy, Vol. 113, pp. 114-138.
[126] S. Benyakhlef A. A. Mers, O. Merrion, A. Bouatem, N. Boutammachte, S. E. Alj, H. Ajdad, Z. Erregueragui, E. Zemmouri., Impact of heliostat curvature on the optical performance of Linear Fresnel solar concentrators, 2016, Renew. Energy, Vol. 89, pp. 463–474.
[127] Silvi, C., The pioneering work on linear Fresnel reflector concentrators in Italy, 2009, 15th Solar PACES International Symposium.
[128] M. Haagen, C. Zahler, E. Zimmermann, and M. M. R. Al-najami, "Solar process steam for the pharmaceutical industry in Jordan, 2015, Energy Procedia, Vol. 70, pp. 621–625.
[129] F. J. Pino, R. Caro, F. Rosa, and J. Guerra, "Experimental validation of an optical and thermal model of a linear Fresnel collector system," 2013, Appl. Therm. Eng., Vol. 50, no. 2, pp. 1463–1471.
[130] Purohit, I. Purohit, P. 2017. The technical and economic potential of concentrating solar thermal power generation in India.2017, Renewable and Sustainable Energy Reviews, 78, pp. 648–667
[131] Soteris A.Kalogirou, A detailed thermal model of a parabolic trough collector receiver, Energy Volume 48, Issue 1, December 2012, Pages 298-306.
[132] Fahad A. Al-Sulaiman, Exergy analysis of parabolic trough solar collectors integrated with combined steam and organic Rankine cycles, Energy Conversion and Management, Volume 77, January 2014, Pages 441-449.
[133] L.L.Vant-Hull, Central tower concentrating solar power (CSP) systems, Concentrating Solar Power Technology Principles, Developments and Applications Woodhead Publishing Series in Energy 2012, Pages 240-283.
[134] K.Vignarooban, Xinhai Xu, A.Arvay, K.Hsu, A.M.Kannan, Heat transfer fluids for concentrating solar power systems – A review, Applied Energy Volume 146, 15 May 2015, Pages 383-396.

[135] Chao Xu, Zhifeng Wang, Xin Li, Feihu Sun, Energy and exergy analysis of solar power tower plants, Applied Thermal Engineering Volume 31, Issues 17–18, December 2011, Pages 3904-3913.
[136] Solar PACES. CSP projects around the world. Available from ⟨http://www. Solar pages. org/CSP-technology/CSP-projects-around-the-world⟩; 2016 [Last accessed on 07 May 2016].
[137] Ioan Sarbu, Calin Sebarchievici, Solar Heating, and Cooling Systems Fundamentals, Experiments and Applications, 2017, Pages 29-97.
[138] R. Loni, A.B.Kasaeian, E.Askari, Asli-Ardeh, B.Ghobadian, W.G.Le Roux, Performance study of a solar-assisted organic Rankine cycle using a dish-mounted rectangular-cavity tubular solar receiver, 2016, Applied Thermal Engineering Volume 108, Pages 1298-1309.
[139] Mohammad Javidmehr, Fatemeh Joda, Amin Mohammadi, Thermodynamic and economic analyses and optimization of a multi-generation system composed by compressed air storage, solar dish collector, micro gas turbine, organic Rankine cycle, and desalination system,2018, Energy Conversion and Management Volume 168, Pages 467-481.
[140] Pavlovic, S. R., et al.: Daily Performance of a Solar Dish Collector THERMAL SCIENCE: The Year 2019, Vol. 23, No. 3B, pp. 2107-2115.
[141] Aggrey Mwesigye, Zhongjie Huan, Josua P.Meyer, Thermal performance and entropy generation analysis of a high concentration ratio parabolic trough solar collector with Cu-Therminol®VP-1 nanofluid, Energy Conversion and Management Volume 120, 15 July 2016, Pages 449-465.
[142] S.K.Tyag, Shengwei Wang, M.K.Singhal, S.C.Kaushik, S.R.Park, Exergy analysis and parametric study of concentrating type solar collectors, International Journal of Thermal Sciences Volume 46, Issue 12, December 2007, Pages 1304-1310.
[143] Jie Zhu, Ziwei Chen, Optical design of compact linear Fresnel reflector systems, Solar Energy Materials and Solar Cells Volume 176, March 2018, Pages 239-250.
[144] Evangelos Bellos, Christos Tzivanidis, Angelos Papadopoulos, Daily, the monthly and yearly performance of a linear Fresnel reflector, 2018, Solar Energy 173 517–529.
[145] Rabbani, M., Ratlamwala, T.A.H. & Dincer, I. Development of a New Heliostat Field-Based Integrated Solar Energy System for Cogeneration. 2018, *Arab J Sci Eng* 43, 1267–1277.

[146] T.C.Hung, T.Y.ShaiS, K.Wang, A review of organic Rankine cycles (ORCs) for the recovery of low-grade waste heat. Energy Volume 22, Issue 7, July 1997, Pages 661-667 https://doi.org/10.1016/S0360-5442(96)00165-X
[147] Tzu-Chen Hung Waste heat recovery of organic Rankine cycle using dry fluids Energy Conversion and Management 42 (2001) 539-553
[148] Lecompte S, Huisseune H, van den Broek M, Vanslambrouck B, De Paepe M, Review of organic Rankine cycle (ORC) architectures for waste heat recovery Renewable and Sustainable Energy Reviews Volume 47, July 2015, Pages 448-461.
[149] Liu B-T, Chien K-H, Wang C-C, Effect of working fluids on organic Rankine cycle for waste heat recovery Energy Volume 29, Issue 8, June 2004, Pages 1207-1217 https://doi.org/10.1016/j.energy.2004.01.004
[150] M. Ibarra, A. Rovira, D. Alarcón-Padilla, J. Blanco, Performance of a five kWe organic Rankine cycle at part-load operation Appl Energy, 120 (2014), pp. 147-158
[151] Arnaud Landelle, Nicolas Tauveron, Philippe Haberschill, Rémi Revellin, Stéphane Colasson, Organic Rankine cycle design and performance comparison based on an experimental database, Applied Energy 204 (2017) 1172–1187.
[152] Jinjiang Bao, Li Zhao, A review of working fluid and expander selections for organic Rankine cycle, Renewable and Sustainable Energy Reviews 24 (2013) 325–342 https://doi.org/10.1016/j.rser.2013.03.040
[153] S. Lecompte, B. Ameel, D. Ziviani, M. van den Broek, M. De Paepe, Exergy analysis of zeotropic mixtures as working fluids in Organic Rankine Cycles, Energy Conversion and Management 85 (2014) 727–739
[154] Kiyarash Rahbar, Saad Mahmoud, Raya K. Al-Dadah, Nima Moazami, Sayed A. Mirhadizadeh, Review of organic Rankine cycle for small-scale applications, Energy Conversion and Management 134 (2017) 135–155
[155] Wenqiang Sun, Xiaoyu Yue, Yanhui Wang, Exergy efficiency analysis of ORC (Organic Rankine Cycle) and ORC-based combined cycles driven by low-temperature waste heat, Energy Conversion and Management 135 (2017) 63–73
[156] Seok Hun Kang, Design and experimental study of ORC (organic Rankine cycle) and radial turbine using R245fa working fluid, Energy 41 (2012) 514 – 524

[157] Irene Garcia-Saez a, Juan Mendez, Carlos Ortiz, Drazen Loncar, Jose A. Becerra, Ricardo Chacartegui, Energy and economic assessment of solar Organic Rankine Cycle for combined heat and power generation in residential applications, Renewable Energy 140 (2019) 461 – 476 https://doi.org/10.1016/j.renene.2019.03.033

[158] Alireza Javanshir, Nenad Saranac, Zahra Razzaghpanah, Thermodynamic analysis of a regenerative organic Rankine cycle using dry fluids, Applied Thermal Engineering,123(2017)852–864

[159] Thomas Tartière, Marco Astolfi, A World Overview of the Organic Rankine Cycle Market, IV International Seminar on ORC Power Systems, ORC 2017 13-15 September 2017, Milano, Italy

[160] Maoqing Li, Jiangfeng Wang, Weifeng He, Lin Gao, Bo Wang, Shaolin Ma, Yiping Dai, Construction and preliminary test of a low-temperature regenerative Organic Rankine Cycle (ORC) using R123, Renewable Energy 57 (2013) 216 – 222.

[161] R. Rayegan and Y. X. Tao, A procedure to select working fluids for solar organic Rankine cycles (ORCs), 2001, Renewable Energy, vol. 36, pp. 659-670.

[162] G. Li, "Organic Rankine cycle performance evaluation and thermo-economic assessment with various applications part I: Energy and exergy performance evaluation," Renewable and Sustainable Energy Reviews, 2016, vol. 53, pp. 477 - 499.

[163] B. F. Tchanche, M. Petrissans, and G. Papadakis, 2014 "Heat resources and organic Rankine cycle machines," Renewable and Sustainable Energy Reviews, vol. 39, pp. 1185-1199, 11. 50.

[164] S. A. Kalogirou, "Solar thermal collectors and applications," Progress in Energy and Combustion Science''.

[165] Y. Feng, Y. Zhang, B. Li, J. Yang, and Y. Shi, 2015 "Sensitivity analysis and thermo-economic comparison of ORCs (organic Rankine cycles) for low-temperature waste heat recovery," Energy, vol. 82, pp. 664-677.

[166] Liu, B.T.; Chien, K.H.; Wang, C.C. Effect of Working Fluids on Organic Rankine Cycle for Waste Heat Recovery; Energy 2004, 29, 1207-1217.

[167] M. Yari and S. M. S. Mahmoudi, 2010, "Utilization of waste heat from GT-MHR for power generation in organic Rankine cycles," Applied Thermal Engineering, vol. 30, pp. 366-375.

[168] P. J. Mago, A. Hueffed, and L. M. Chamra, 2010 "Analysis and optimization of the use of CHP–ORC systems for small commercial buildings," Energy and Buildings, vol. 42, pp. 1491-1498.

[169] F. Fang, L. Wei, J. Liu, J. Zhang, and G. Hou, 2012 "Complementary configuration and operation of a CCHP-ORC system," Energy, vol. 46, pp. 211-220.

[170] I. H. Aljundi, 2011, "Effect of dry hydrocarbons and critical point temperature on the efficiencies of organic Rankine cycle," Renewable Energy, vol. 36, pp. 1196-1202.

[171] Anna Bryszewska-Mazurek, Tymoteusz Świeboda & Wojciech Mazurek (2011) Performance Analysis of a Solar-Powered Organic Rankine Cycle Engine, Journal of the Air & Waste Management Association, 61:1, 3-6, DOI: 10.3155/1047-3289.61.1.3

[172] F. Heberle and D. Brüggemann, 2016, "Thermo-Economic Analysis of Zeotropic Mixtures and Pure Working Fluids in Organic Rankine Cycles for Waste Heat Recovery," Energies, vol. 9, p. 226.

[173] M. Imran, B.-S. Park, H.-J. Kim, D.-H. Lee, and M. Usman, 2015, "Economic assessment of greenhouse gas reduction through low-grade waste heat recovery using organic Rankine cycle (ORC)," Journal of Mechanical Science and Technology, vol. 29, pp. 835-843.

[174] V. L. Le, M. Feidt, A. Kheiri, and S. Pelloux-Prayer,2014 "Performance optimization of low-temperature power generation by supercritical ORCs (organic Rankine cycles) using low GWP (global warming potential) working fluids," Energy, vol. 67, pp. 513-526.

[176] Bamgbopa, Musbaudeen O. Modeling and performance evaluation of an organic Rankine cycle (ORC) with R245FA as the working fluid. MSc Thesis, 2012, Middle East Technical University.

[177] Eric W. Lemmon, Mark O. McLinden and Daniel G. Friend, "Thermophysical Properties of Fluid Systems" in NIST Chemistry WebBook, NIST Standard Reference Database Number 69, Eds. P.J. Linstrom and W.G. Mallard, National Institute of Standards and Technology, Gaithersburg MD, 20899, https://doi.org/10.18434/T4D303, (retrieved October 23, 2020).

[178] Haynes, W.M. (ed.). CRC Handbook of Chemistry and Physics. 95th Edition. CRC Press LLC, Boca Raton: FL 2014-2015, p. 3-246

[179] Haynes, W.M. (ed.). CRC Handbook of Chemistry and Physics. 95th Edition. CRC Press LLC, Boca Raton: FL 2014-2015, p. 3-330

[180] O'Neil, M.J. (ed.). The Merck Index - An Encyclopedia of Chemicals, Drugs, and Biologicals. 13th Edition, Whitehouse Station, NJ: Merck and Co., Inc., 2001., p. 1397

[181] O'Neil, M.J. (ed.). The Merck Index - An Encyclopedia of Chemicals, Drugs, and Biologicals. Cambridge, UK: Royal Society of Chemistry, 2013., p. 1106

[182] O'Neil, M.J. (ed.). The Merck Index - An Encyclopedia of Chemicals, Drugs, and Biologicals. Cambridge, UK: Royal Society of Chemistry, 2013., p. 871

[183] C.N. Markides, The role of pumped and waste heat technologies in a high efficiency sustainable energy future for the UK, Appl. Thermal Eng. 53 (2) (2013) 197–209.

[184] A. Ramos, I. Guarracino, A. Mellor, D. Alonso-Álvarez, P.R.N. Childs, N.J. Ekins Daukes, C.N. Markides, Solar-Thermal and Hybrid Photovoltaic-Thermal Systems for Renewable Heating, Grantham Institute Briefing Paper, May 2017, Available from: https://www.imperial.ac.uk/grantham/publications/

[185] Petrollese, M.; Cocco, D. Robust optimization for the preliminary design of solar organic Rankine cycle (ORC) systems. Energy Convers. Manag. 2019, 184, 338–349.

[186] Casartelli, D.; Binotti, M.; Silva, P.; Macchi, E.; Roccaro, E.; Passera, T. Power Block Off-design Control Strategies for Indirect Solar ORC Cycles. Energy Procedia 2015, 69, 1220–1230.

[187] Wang, X.; Zhao, L.; Wang, J.; Zhang, W.; Zhao, X.; Wu, W.2010, ‘’Performance evaluation of a low-temperature solar Rankine cycle system utilizing R245fa’’. Sol. Energy, 2010, 84, 353– 364.

[188] Declaye, S.; Quoilin, S.; Guillaume, L.; Lemort, V. Experimental study on an open drive scroll expander integrated into an ORC (Organic Rankine Cycle) system with R245fa as working fluid. Energy, 2013, 55, 173–183.

[189] Yamamoto T, Furuhata T, Arai N, Mori K. Design and testing of the organic Rankine cycle. Energy 2001; 26:239–51.

[190] F. Velez, F. Chejne, A. Quijano, Thermodynamic analysis of R134a in an Organic Rankine cycle for power generation from low-temperature sources, DYNA 81 (2014) 153-159.

[191] Suresh Baral and Kyung Chun Kim, ‘‘Simulation, Validation and Economic Analysis of Solar Powered Organic Rankine Cycle for Electricity Generation’’ Journal of Clean Energy Technologies, January 2015, Vol. 3, No. 1.

[192] Emily Spayde1 and Pedro J. Mago, ‘‘Evaluation of a solar-powered organic Rankine cycle using dry organic working fluids’’. Department of Mechanical Engineering, Mississippi State University, Mississippi, March 2015, MS 39759, USA.

[193] Adweek Odhiambo George, Imran Ali Shah, Xiang Gou, ‘‘Energy analysis of Organic Rankine Cycle for a residential apartment using solar energy based on Aspen Plus’’ April 2017. Environmental Science International Journal of Current Advanced Research

[194] Jesko, Z., Classification of solar collectors. In: Proceedings of the 7th International Scientific Conference in Engineering for Rural Development, Jelgava, 2008, Latvia, pp. 22–27.

[195] Chakkraphan Thawonngamyingsakul, Tanongkiat Kiatsiriroat, ‘‘Potential of a Solar Organic Rankine Cycle with Evacuated-Tube Solar Collectors as Heat Source for Power Generation in Thailand’’ 2012, Energy and science technology, vol 4, no 2.

[196] M. Idris Alhamid, Nasruddin, Nyayu Aisyah, and Sholahudin, ‘‘Characteristics of Evacuated Tubular Solar Thermal Collector as Input Energy for Cooling System at Universities Indonesia’’, AIP Conference Proceedings 1826, 020016 (2017);

[197] Tchanche Fankam Bertrand, George Papadakis, Gregory Lambrinos, Antonios Frangoudakis. Fluid selection for a low-temperature solar organic Rankine cycle. Applied Thermal Engineering, Elsevier, 2009, 29 (11-12), pp.2468.

[198] R. Rayegan and Y. X. Tao, “A procedure to select working fluids for solar organic Rankine cycles (ORCs),” Renewable Energy, 2011, vol. 36, pp. 659-670.

[199] He Y, Mei D, Tao W, Yang W, Liu H. Simulation of the parabolic trough solar energy generation system with Organic Rankine Cycle. APPL ENERG 2012-09-01; 97:630-41.

[200] Santiago R.E., João A.C. Jr.., Antonio P.B., Effect of working fluids on organic Rankine cycle for the recovery of low-grade waste heat, 2017, Proceedings of the 12th Latin American Congress on Electricity Generation and Transmission –CLAGTEE, Mar del Plata, Argentina

[201] Tchanche Fankam Bertrand, George Papadakis, Gregory Lambrinos, Antonios Frangoudakis. Fluid selection for a low-temperature solar organic Rankine cycle. Applied Thermal Engineering, Elsevier, 2009, 29 (11-12), pp.2468.

[202] Oyewunmi, O., Taleb, A., Haslam, A. and Markides, C., On the use of SAFT-VR Mie for assessing large-glide fluorocarbon working-fluid mixtures in organic Rankine cycles, Applied Energy Vol.163, pp 263-282, 1 February 2016.

[203] S. Sobhansarbandi, P.M. Martinez, A. Papadimitratos, A. Zakhidovc, F. Hassanipour, Evacuated tube solar collector with multifunctional absorber layers, Solar Energy Vol. 146 pp 342–350, 2017.

[204] Furukawa, G.T.; McCoskey, R.E.; Reilly, M.L., Heat capacity, heats of fusion and vaporization, and vapour pressure of tetrafluoroethylene, J. Res.**,** 1953, NBS 51, 69-72.

[205] Global Meteorological Database Version 7 Software and Data for Engineers, Planners and Education Meteonorm V7.3.0.26247, Meteotest AG, Bern, Switzerland www. meteonorm.com

[206] ESTIF/Nielsen, Recommendation: Converting solar thermal collector area into installed capacity, 2004.

[207] S. Mokhatab, J. Mak, J. Valappil, D. Wood, Handbook of Liquefied Natural Gas 1st Edition, 2014, Pages 229-257. https://doi.org/10.1016/B978-0-12-404585-9.00005-2

[208] M. Feidt, H. Semmari, First optimization approach of a solar Organic Rankine Cycle, 2020, ISTE Open Science.

[209] J. Sun, W. Lib, Operation optimization of an organic Rankine cycle (ORC) heat recovery power plant, Applied Thermal Engineering, 2011, pp. 2032-2041.

[210] J. F. Wang, Z. Yan, M. Wang, S. Ma, Y. Dai, Thermodynamic analysis and optimization of an (organic Rankine cycle) ORC using a low-grade heat source, Energy Volume 49, 1 January 2013, Pages 356 365

[211] Y. Feng, Y. Zhang, B. Li, J. Yang, Y. Shi, Comparison between regenerative organic Rankine cycle (RORC) and basic organic Rankine cycle (BORC) based on thermo-economic multi-objective optimization considering exergy efficiency and levelized energy cost *(LEC)*, Energy Conversion and Management, Volume 96, 15 May 2015, Pages 58-71.

[212] L. Zhai, G. Xu, J. Wen, Y. Quan, J. Fu, H. Wu, T. Li, An improved modelling for low-grade organic Rankine cycle coupled with optimization design of the radial-inflow turbine, Energy Conversion and Management, Volume 153, 1 December 2017, Pages 60-70

[213] A. M. S. Zalzala and P. J. Fleming, Genetic Algorithms in Engineering Systems. UK: Institution of Electrical Engineers, 1997.

[214] K. Kraitong, "Mathematical Modelling and Optimisation of Stirling Engines for Power Production," PhD Thesis, University of Northumbria, 2012.

[215] R. L. Haupt and S. E. Haupt, Practical Genetic Algorithms, 2nd ed. USA: John Wiley & Sons, Inc., 2004.

[216] B. Belgasim, "Theoretical and Experimental Investigation of the Dynamic Solar Water Desalination Unit," PhD Thesis, Northumbria University, 2013.

[217] Khaled Hossin, Dynamic Modelling and Thermo-Economic Optimization of a Small-Scale Hybrid Solar/Biomass Organic Rankine Cycle Power System, PhD. Thesis, Northumbria University, 2016.
[218] Guoqiang Xu, Gu Song, Xiaoxun Zhu, Wei Gao, Haiwang Li, Yongkai Quan, Performance evaluation of a direct vapour generation supercritical ORC system driven by linear Fresnel reflector solar concentrator, Applied Thermal Engineering 80 (2015) 196 – 204 http://dx.doi.org/10.1016/j.applthermaleng.2014.12.071
[219] Jia Hea, Zhongzhu Qiub, Qiming Lia, Yi Zhanga, Optical Design of Linear Fresnel Reflector Solar Concentrators, Energy Procedia 14 (2012) 1960 – 1966.
[220] G. Zhu, T. Wendelin, J. Wagner, C. Kutscher, History, current state, and future of linear Fresnel concentrating solar collectors. Solar Energy 103 (2014) 639–652
[221] R. Abbas, J. Munoz-Anton, M. Valdes, J.M. Martinez, High concentration linear Fresnel reflectors, Energy Conversion, and Management 72 (2013) 60–68.
[222] R. Grena, P. Tarquini, Solar linear Fresnel collector using molten nitrates as heat transfer fluid, Energy 36 (2011) 1048-1056.
[223] F. Yanga, D. Itskhokinea, S. Benmarrazea, M. Benmarrazea, A. Hoferb, F. Lecatc, A. Ferrierec, Acceptance testing procedure for Linear Fresnel Reflector solar systems in utility-scale solar thermal power plants, Energy Procedia 69 (2015) 1479 – 1487.
[224] P. Boito, R. Grena, Optimization of the geometry of Fresnel linear collectors, Solar Energy, Volume 135, October 2016, Pages 479-486.
[225] N. Kincaid, G. Mungas, N. Kramer, M. Wagner, G. Zhu, An optical performance comparison of three concentrating solar power collector designs in linear Fresnel, parabolic trough, and central receiver, Applied Energy Volume 231, 1 December 2018, Pages 1109-1121
[226] E. Bellos, C. zivanidis, Development of analytical expressions for the incident angle modifiers of a linear Fresnel reflector, Solar Energy, Volume 173, October 2018, Pages 769-779.
[227] A.Barbon, N.Barbon, L.Bayon, J.A.Sanchez, Parametric study of the small scale linear Fresnel reflector, Renewable Energy, Volume 116, Part A, 2018, Pages 64-74
[228] P. Tsekouras, C. Tzivanidis, K. Antonopoulos, Optical and thermal investigation of a linear Fresnel collector with trapezoidal cavity receiver, Applied Thermal Engineering 135 (2018) 379–388.

[229] David R. Mills, G. L. Morrison, Compact Linear Fresnel Reflector Solar Thermal Power Plants, Solar Energy Vol. 68, No. 3, pp. 263–283, 2000.
[230] A. Heimsatha, F. Cuevas, A. Hofera, P. Nitza, W.J. Platzera, Linear Fresnel collector receiver heat loss and temperatures, Energy Procedia 49 (2014) 386 – 397.
[231] R. Manikumar, A.V. Arasu, Heat loss characteristics study of a trapezoidal cavity absorber with and without a plate for a linear Fresnel reflector solar concentrator system, Renewable Energy Volume 63, March 2014, Pages 98-108.
[232] R. Abbas, A.Sebastián, M.J.Montes, M.Valdes, Optical features of linear Fresnel collectors with different secondary reflector technologies, Applied Energy, Volume 232, 15 December 2018, Pages 386-397
[233] Mahkamov, Khamid, Pili, Piero, Manca, Roberto, Leroux, Arthur, Mintsa, Andre-Charles, Lynn, Kevin, Mullen, David, Halimic, Elvedin, Bartolini, Carlo, Pirro, Matteo, Costa Pereira, Carolina, Cabeza, Luis F., de Gracia Cuesto, Alvaro, Kenisarin, Murat and Makhkamova, Irina (2018) Development of a small solar thermal power plant for heat and power supply to domestic and small business buildings. In: ASME 2018 Power and Energy Conference, 24th - 28th June 2018, Florida, USA
[234] F.J. Pino, R. Caro, F. Rosa, J. Guerra, Experimental validation of an optical and thermal model of a linear Fresnel collector system, Applied Thermal Engineering 50 (2013) 1463-1471.
[235] (Incropera, Frank P., and DeWitt, David P. "Fundamentals of Heat and Mass Transfer," 5th edition, New York: John Wiley and Sons, Inc., 2002)
[236] Duffie, John A., and Beckman, William A., "Solar Engineering of Thermal Processes " 3rd edition, New York: John Wiley and Sons, Inc., 2006
[237] Jan Fabian Feldhoff, Linear Fresnel Collectors A Technology Overview, SFERA Summer School 2012 June 28, 2012, Almería, Spain
[238] Einav, A., 2004. Solar energy research and development achievements in Israel and their practical significance. Journal of Solar Energy Engineering 126 (3), 921.
[239] Kiceniuk, T., 1985. Development of an Organic Rankine-Cycle Power Module for a Small Community.
[240] Fenton, D.L., Abernathy, G.H., Krivokapich, G.A., Otts, J.V.,1984. Operation and evaluation of the Willard solar thermal power irrigation system. Solar Energy 32 (6), 735e751.

[241] Moustafa, S., Hoefler, W., El-Mansy, H., Kamal, A., Jarrar, D., Hoppman, H., Zewen, H., 1984. Design specifications and application of a 100 kW (700 kW) cogeneration solar power plant. Solar Energy 32 (2), 263-269

[242] Simonnot, G., Louche, A., Decanini, Y., 1987. Three years of exploitation of the 100 kWe Ajaccio solar power plant. In: Proceedings of the ISES Solar World Congress, pp. 1588-1592.

[243] Barutti, A., Pedrick, W.G., Angelino, G., Gaia, M., Macchi, E., 1984.Ansaldosolar thermal and photovoltaic plants located at Ballajura, Western Australia. In: Proceedings of the 8th Solar World Congress 1983, Biennial Congress of the International Solar Energy Society, vol. 3, pp. 1572-1576.

[244] Kane, M., Larrain, D., Favrat, D., Allani, Y., 2003. Small hybrid solar power system. Energy 28 (14), 1427-1443.

[245] Saitoh, T., Yamada, N., Wakashima, S., 2007. Solar Rankine cycle system using scroll expander. Journal of Environmental Engineering 2 (4), 708-719.

[246] Canada, S., Cohen, G., Cable, R., Brosseau, D., Price, H., 2005b. Parabolic Trough Organic Rankine Cycle Solar Power Plant NREL CP/-550-37077. Denver, CO.

[247] Kalogirou, S.A., 2004. Solar thermal collectors and applications. Progress in Energy and Combustion Science 30 (3), 231 – 295.

[248] Galvez, J.B., 2010. Powersol: Mechanical Power Generation Based on Solar Thermodynamic Engines - Final Report.

[249] Wang, X.D., Zhao, L., Wang, J.L., Zhang, W.Z., Zhao, X.Z., Wu, W., March 2010.Performance evaluation of a low-temperature solar Rankine cycle system utilizing R245fa. Solar Energy 84 (3), 353-364.

[250] Wang, X.D., Zhao, L., Wang, J.L., 2011. Experimental investigation on the low-temperature solar Rankine cycle system using R245fa. Energy Conversation and Management 52(2),946-952.

[251] Electratherm METU NCC Solar ORC Report. Electratherm Website, 2010.

[252] N. soukpoe, K.E., Azoumah, K.Y., Clerc, E., Zmuda, J., Gaye, M., Seshie, Y.M., Kenda Nitedem, S.E., 2014. CSP4Africa: development d'un piloted économiquement viable d'une mini-CSP pour la production electricity pour mini-réseau en Afrique.

[253] Orosz, M.S., 2012. Thermo-solar and Photovoltaic Hybridization for Small Scale Distributed Generation: Application for Powering Rural Health Massachusetts Institute of Technology.

[254] Chambers, T., Raush, J., Russo, B., 2014. Installation and operation of parabolic trough organic Rankine cycle solar thermal power plant in south Louisiana. Energy Procedia 49, 1107-1116.

[255] Goswami, D.Y., Stefaakos, E., Rahman, M.M., Aydin, S., Reedy, R., 2013. Design, Construction, and Operation of CSP Solar Thermal Power Plants in Florida.

[256] Rieu, V., September2012.A10 kW solar power plant for rural electrification. In: Proceedings of Solar PACES 2012.Ait-Baha CSP Pilot Plant - Technical Datasheet.

[257] NREL,2013. "Distributed Generation Renewable Energy Estimate of Costs (Online).Available: http://www.nrel.gov/analysis/tech_lcoe_re_cost_est.html.NREL - CSP Projects Review.

[258] Georges, E., Declaye, S., Dumont, O., Quoilin, S., Lemort, V., 2013. Design of a small-scale organic Rankine cycle engine used in a solar power plant. International Journal of Low Carbon Technologies 8 (Suppl. 1), 1 - 8.

[259] Baral, S., Kim, D., Yun, E., Kim, K., 2015. Experimental and thermo-economic analysis of small-scale solar organic Rankine cycle (SORC) system. Entropy 17 (4), 2039 - 2061.

[260] Forrest, Eric, Buongiorno, Jacopo, McKrell, Thomas, & Hu, Lin-Wen (2009). Pool boiling performance of Novec^{TM} 649 engineered fluid. Boiling 2009: 7 ECI International conference on boiling heat transfer, Brazil

[261] Apricus.com. 2021. *Apricus eco-energy*. [online] Available at: <https://www.apricus.com/> [Accessed 9 February 2021].

APPENDICES

Appendix 1. Global Temperature Increase

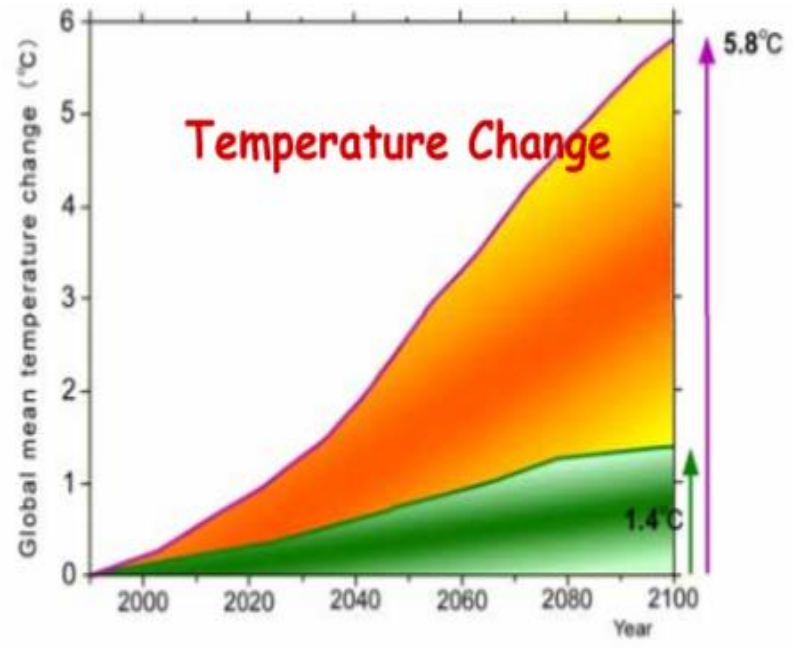

Appendix 2. Increase in Seal Level

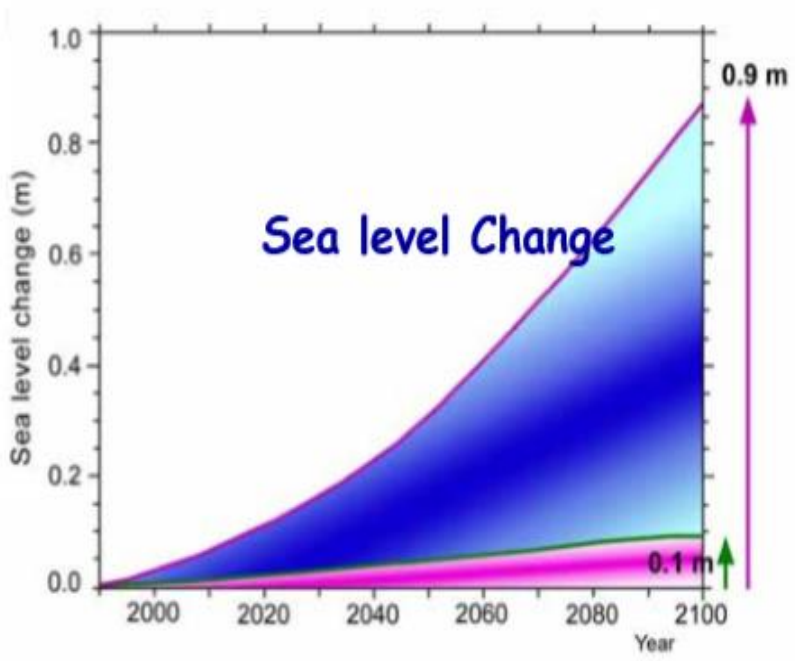

Appendix 3. World Population Growth Rates

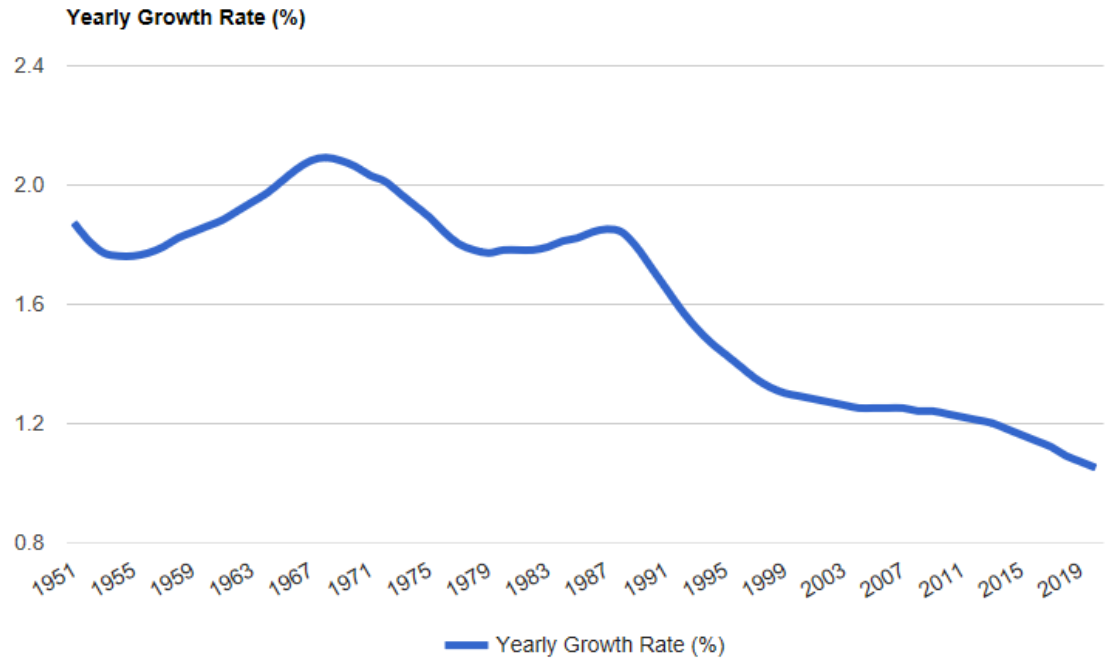

Appendix 4. Thermophysical properties of the refrigerant HCFC-245fa

Temperature (K)	Pressure (bar)	Density (mol/l)	Enthalpy (kJ/kg)	Entropy (J/g-K)	Cp (J/g-K)	Therm. Cond. (W/m-K)
280	36	10.408	210.13	1.0275	1.2946	0.09714
282	36	10.371	212.73	1.0367	1.298	0.09652
284	36	10.334	215.33	1.0459	1.3015	0.0959
286	36	10.297	217.93	1.055	1.3051	0.09529
288	36	10.259	220.55	1.0641	1.3087	0.09468
290	36	10.221	223.17	1.0732	1.3123	0.09407
292	36	10.183	225.8	1.0822	1.316	0.09346
294	36	10.145	228.43	1.0912	1.3197	0.09285
296	36	10.107	231.08	1.1002	1.3235	0.09225

298	36	10.068	233.73	1.1091	1.3274	0.09165
300	36	10.029	236.38	1.118	1.3313	0.09105
302	36	9.9898	239.05	1.1269	1.3353	0.09046
304	36	9.9504	241.73	1.1357	1.3393	0.08986
306	36	9.9108	244.41	1.1445	1.3434	0.08927
308	36	9.8708	247.1	1.1533	1.3476	0.08868
310	36	9.8307	249.8	1.162	1.3518	0.08809
312	36	9.7902	252.51	1.1707	1.3561	0.08751
314	36	9.7495	255.22	1.1794	1.3604	0.08692
316	36	9.7084	257.95	1.188	1.3648	0.08634
318	36	9.667	260.68	1.1967	1.3693	0.08576
320	36	9.6254	263.43	1.2053	1.3739	0.08518
322	36	9.5833	266.18	1.2138	1.3786	0.0846
324	36	9.541	268.94	1.2224	1.3833	0.08402
326	36	9.4983	271.71	1.2309	1.3881	0.08344
328	36	9.4552	274.49	1.2394	1.3931	0.08287
330	36	9.4117	277.28	1.2479	1.3981	0.08229
332	36	9.3678	280.09	1.2564	1.4032	0.08172
334	36	9.3235	282.9	1.2648	1.4084	0.08114
336	36	9.2787	285.72	1.2732	1.4137	0.08057
338	36	9.2335	288.55	1.2816	1.4192	0.08
340	36	9.1879	291.4	1.29	1.4247	0.07943
342	36	9.1417	294.25	1.2984	1.4304	0.07885
344	36	9.095	297.12	1.3068	1.4363	0.07828

346	36	9.0478	300	1.3151	1.4422	0.07771
348	36	9	302.89	1.3234	1.4484	0.07714
350	36	8.9517	305.79	1.3318	1.4547	0.07656
352	36	8.9027	308.71	1.3401	1.4611	0.07599
354	36	8.8531	311.63	1.3484	1.4678	0.07542
356	36	8.8028	314.58	1.3566	1.4747	0.07484
358	36	8.7518	317.53	1.3649	1.4818	0.07427
360	36	8.7001	320.5	1.3732	1.4891	0.07369
362	36	8.6476	323.49	1.3815	1.4966	0.07311
364	36	8.5943	326.49	1.3897	1.5045	0.07253
366	36	8.5401	329.51	1.398	1.5126	0.07195
368	36	8.485	332.54	1.4063	1.5211	0.07137
370	36	8.429	335.59	1.4145	1.5299	0.07078
372	36	8.3719	338.66	1.4228	1.539	0.07019
374	36	8.3137	341.75	1.4311	1.5486	0.0696
376	36	8.2544	344.86	1.4394	1.5587	0.069
378	36	8.1938	347.98	1.4477	1.5692	0.06841
380	36	8.132	351.13	1.456	1.5803	0.0678
382	36	8.0687	354.31	1.4643	1.5921	0.0672
384	36	8.0039	357.5	1.4727	1.6045	0.06659
386	36	7.9375	360.72	1.481	1.6178	0.06597
388	36	7.8693	363.97	1.4894	1.6319	0.06535
390	36	7.7992	367.25	1.4979	1.647	0.06472
392	36	7.727	370.56	1.5063	1.6634	0.06409

394	36	7.6525	373.91	1.5148	1.681	0.06344
396	36	7.5755	377.29	1.5234	1.7003	0.06279
398	36	7.4956	380.71	1.532	1.7215	0.06213
400	36	7.4127	384.18	1.5407	1.7449	0.06147
402	36	7.3262	387.69	1.5495	1.771	0.06079
404	36	7.2356	391.26	1.5583	1.8006	0.0601
406	36	7.1405	394.9	1.5673	1.8343	0.0594
408	36	7.0399	398.6	1.5764	1.8734	0.05868
410	36	6.9329	402.39	1.5857	1.9197	0.05795
412	36	6.8182	406.29	1.5951	1.9755	0.0572
414	36	6.6939	410.31	1.6049	2.045	0.05644
416	36	6.5572	414.48	1.6149	2.1347	0.05567
418	36	6.404	418.87	1.6254	2.2566	0.0549
420	36	6.2274	423.54	1.6366	2.4356	0.05414
422	36	6.0138	428.68	1.6488	2.7324	0.05348
424	36	5.7309	434.68	1.663	3.3569	0.05317
426	36	5.2439	443.2	1.683	6.0792	0.05494
426.63	36	4.8767	448.58	1.6957	14.029	0.06015

Appendix 5. Thermolib command to generate the energy and mass balance of the ORC model

The following command used in Thermolib/MATLAB workspace of the ORC model in excel sheet.

SModelBalance_out = th_ExportBalance (SModelBalance, 'BalanceResults.xls', 'BalanceResults.txt')

In case to store the results in the working directory of the MATLAB, then the following command will use

SModelBalance_out = th_ExportBalance (SModelBalance, [], 'BalanceResults.txt')

Appendix 6. Solar Declination Yearly

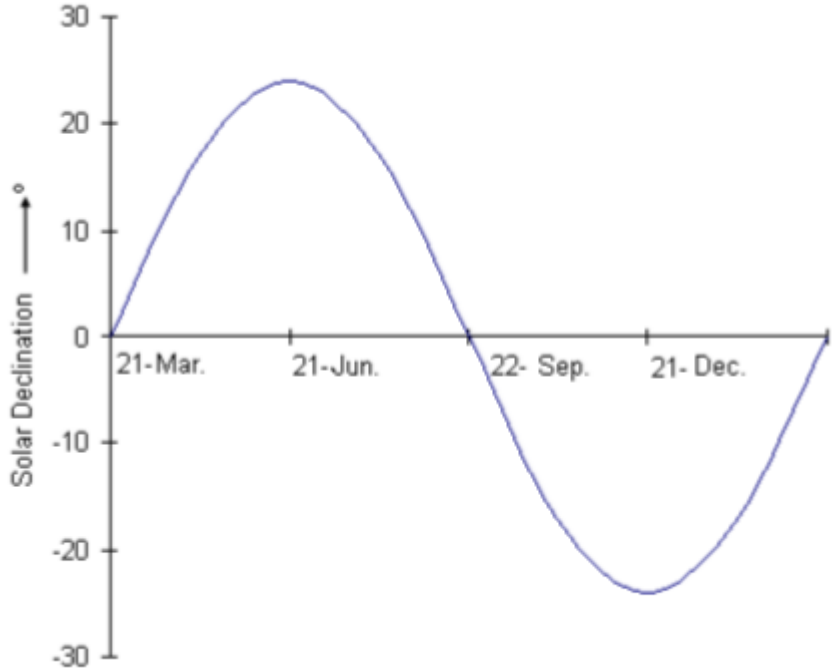

Appendix 7. Genetic Algorithm Code

Design Variables

```
%************************************************************************
%GA.m
%************************************************************************

global Tc
global Qin
global Mc
global Pa
global Mv
```

Input Data GA_LPST

```
%*******************************************
%inputdata_GA_LPST.m
%*******************************************
global popsize
%*******************************************
```

```
%GA parameters
%popsize=input('population size =');
popsize=80;              % set population size
mutrate=.2;             % set mutation rate
selection=0.5;          % fraction of population kept
maxit=50;                % max number of generations
%***********************************************************************
%%**********************************************************************
*
%geometric data
%disp ('Choose optimal engine parameters and define upper and lower
bounds')
%diameter of displacer piston, m
%M_vded=input('Dead volume is optimal engine parameter : enter 1 if not
enter 0');
M_vded=1;
%M_d1=input('Dead volume is optimal engine parameter : enter 1 if not enter
0');
M_d1=1;
%M_d2=input('Dead volume is optimal engine parameter : enter 1 if not enter
0');
M_d2=1;
%M_P2=input('Dead volume is optimal engine parameter : enter 1 if not enter
0');
M_P2=1;

M=[M_vded M_d1 M_d2 M_P2];

npar=sum(M);
%disp ('define value of engine parameter and also upper and lower bounds of
optimal engine parameters')
var_hi=zeros(1,npar);
var_lo=zeros(1,npar);
sign=zeros(1,npar);
if M_vded==0
    %vded=input('dead volume[m3]');
    %vded = 0.008;
elseif M_vded==1
    var_hi(1,1)=1272000;        % upper bound
    sign(1,npar)=1;
    var_lo(1,1)=1172000;        % lower bound
end
if M_d1==0
    d1=input('internal diameter[m]');
    %d1 = 0.025;
elseif M_d1==1
    %var_hi(1,sum(sign)+1)=input('internal diameter-upper bound[m]');
    var_hi(1,sum(sign)+1)=12;         % upper bound
    %var_lo(1,sum(sign)+1)=input('internal diameter-lower bound[m]');
    var_lo(1,sum(sign)+1)=6;         % lower bound
    sign(1,sum(sign)+1)=1;
end
if M_d2==0
    d2=input('external diameter[m]');
    %d1 = 0.025;
elseif M_d2==1
```

```
    %var_hi(1,sum(sign)+1)=input('external diameter-upper bound[m]');
    var_hi(1,sum(sign)+1)=8;        % upper bound
    %var_lo(1,sum(sign)+1)=input('external diameter-lower bound[m]');
    var_lo(1,sum(sign)+1)=4;        % lower bound
    sign(1,sum(sign)+1)=1;
end
if M_P2==0
    P2=input('external pressure[Pa]');
    %d1 = 0.025;
elseif M_P2==1
    %var_hi(1,sum(sign)+1)=input('external pressure-upper bound[Pa]');
    var_hi(1,sum(sign)+1)=40;        % upper bound
    %var_lo(1,sum(sign)+1)=input('external pressure-lower bound[Pa]');
    var_lo(1,sum(sign)+1)=30;        % lower bound
    sign(1,sum(sign)+1)=1;
end
```

LPST_Modelling

```
function [m]=LPST_modelling(vded,d1,d2,P2)

simparameter(vded,d1,d2,P2)
simout= sim('R134fa_Final_Opt');
m=max(-Mv.signals.values);

end
```

Objective_Function_LPST

```
function ff=objective_function_LPST(x)

global popsize

for i=1:1:popsize
    %inputdata_GA
    vded=x(i,1);
    d1=x(i,2);
    d2=x(i,3);
    P2=x(i,4);
    [m]=LPST_modelling(vded,d1,d2,P2);
    fprintf('m= %9.5f  \n\n',m);
    Dm(i)=m;
end
ff = [Dm];
ff=ff';
end
```

Sim_Paramters

```
function vv=simparameter(vded,d1,d2,P2)

global Tc;
Tc=vded;
```

```
global Qin;
Qin=d1;

global Mc;
Mc=d2;

global Ma
Ma=P2;

end
```